Spectroscopic Investigations of Azobenzene Based Self-assembled Monolayers on Gold, SiO_2, and Water

Dissertation

in fulfillment of the requirements for the degree of
"Dr. rer. nat."
of the Faculty of Mathematics and Natural Sciences
at Christian-Albrechts-University Kiel

submittted by
Saira Riaz

Kiel, 2017
Institute of Physical Chemistry

First Referee:	Prof. Dr. Gernot Friedrichs
Second Referee:	Prof. Dr. Friedrichs Temps
Day of oral examination:	26. 09. 2017
Approved for publication:	05. 10. 2017

Signed Prof. Dr. Natascha Oppelt, Dean

Declaration

I hereby declare that the work presented in this thesis is original and my own without any help except the guidance of my supervisor Prof. Dr. Gernot Friedrichs. All the references are cited properly.

This is my first dissertation and the work has neither been used as a whole nor in parts in any other dissertation, and it has niether been published nor submitted for publication.

The dissertation complies to the Rules of Good Scientific Practice as proposed by the German Research Foundation (DFG).

(Place) (Date) (Saira Riaz)

Abstract

This study was concerned with the investigation of photo-induced molecular switching processes of azobenzene based self-assembled monolayers (SAMs) on surfaces.

The rational design of such surfaces, which often hold the potential for practical application, require a thorough understanding of the factors that control surface assembly into highly ordered architectures as well as photoswitching efficiency. The latter is often limited by steric hindrance, i.e., the lack of free volume in the molecular monolayer. This work further aimed at a demonstration of the capability of Sum Frequency Generation spectroscopy (SFG) to investigate diverse functionalized surfaces including reflective gold and transparent quartz substrates as well as monolayers at water-air interfaces.

SFG analysis of Azobenzene (AB) like 4-(11-Mercapto-undecanoxy)-4'-methylazobenzene (MeAB-OC11S), 4-(10-Mercapto-decanoxy)-4'-methylazobenzene (MeAB-OC10S) on 100 nm Au (111), (E)-12c-[4-(4-Methyl/CN phenyldiazenyl)phenyl]ethynyl-$4,8,12$-tri-octyl-$4,8,12$-triazatriangulene, (Me/CN-Azo-8-TATA) on quartz and Azobenzenecholesterol/ Dipalmitoylphosphatidylcholine (Azo-Chol/ DPPC) on water was used to confirm the formation of self-assembled monolayers (SAMs) on the substrate, to depict the morphology of these SAMs and to check their photoisomerizing ability. Characteristic spectra confirmed the adsorption of molecules on the surfaces with vibrational signatures of different CH units. In particular, resonances of CH_2 (d^+, d^-, d^+_{FR}) and CH_3 (r^+, r^-, r^+_{FR}) and CH_{aromatic} have been identified in SFG spectra of pure and mixed monolayers. The observed amplitude ratios of the d^+/r^+ and r^+/r^- bonds confirm the presence of gauche defects in the mixed monolayer, where fitting of the spectra indicate the loss of structural order of the monolayers on dilution with coligand alkylthiol molecules.

Pure and mixed monolayers of AB thiols/ thiol on gold were used to investigate the photoisomerization efficiency as a function of the degree of surface dilution. The SFG signals of CH_3 or CN SFG marker group at the phenyl group of azobenzene was used as direct measure of *trans* / *cis* isomerization of azobenzene functionalized SAMs. Moreover, different thiols with various chain lengths were

used as co-ligands to get insight into steric hindrance effects. In case of gold, the non-resonant SFG background proved a challenging factor for spectrum acquisition and limited the reproducibility of these experiments. Nevertheless, it could be successfully shown that most of the investigated mixed monolayers exhibit photoswitching ability. An exception was a monolayer of MeAB-OC11S using hexadecanethiol as a co-ligand. Obviously, the long alkyl chain of the co-ligand induced strong steric hindrance and efficiently inhibited photoswitching. This result could also be confirmed by additional experiments by means of UV-Vis transmission spectroscopy. Moreover, thermal back-isomerization from the *cis* to *trans*-state with time constants in the order of 5 min to 50 min have been observed.

In addition to the systematic studies on gold, explorative SFG measurements have been performed with many different molecular systems including TATA functionalized quartz surfaces. Intense SFG signatures have been observed showing high degree of surface functionalization and molecular order. However, photoisomerization of TATA based SAMs was sensitive to aging of the sample and laser damage.

Finally, both the changes of surface pressure as well as SFG characteristics have been analyzed for Azobenzene-Cholesterol/ Dipalmitoylphosphatidylcholine (AB-Chol/DPPC) monolayers on water. Switching these layers to the *cis*-state of AB-Chol caused an increase in surface pressure going along with better aligned alkyl chains of DPPC, hence consistent with a higher spatial demand of the *cis*-state.

Zusammenfassung

In dieser Arbeit wurden photoinduzierte molekulare Schaltvorgänge von selbst-anordnenden Monolagen (SAMs) auf Azobenzolbasis untersucht. Die gezielte Herstellung von solchen funktionalisierten Oberflächen, die ein hohes Anwendungspotenzial aufweisen, erfordert ein detailliertes Verständnis der Faktoren, die einerseits die Bildung der hochgeordneten Schichten und andererseits deren Photoschaltbarkeit beeinflussen. Dabei wird die Effizienz der Photoschaltung oft durch sterische Effekte und das damit in Zusammenhang stehende fehlende freie Volumen in der molekularen Monolage bedingt. Ein weiteres Ziel der Arbeit war es, die Anwendbarkeit der Summenfrequenzerzeugungs-Spektroskopie (SFG) zur Untersuchung unterschiedlich funktionalisierter Oberflächen auf Gold, auf transparentem Quarz und an der Wasser-Luft-Grenzfläche zu demonstrieren.

Die Analyse des SFG-Spektren von Molekülen mit Azobenzol-Schalter (AB) wie beispielsweise 4-(11-Mercapto-Undecanoxy)-4'-Methylazobenzene (MeAB-OC11S), 4-(10-Mercapto-Decanoxy)-4'-Methylazobenzene (MeAB-OC10S) auf 100 nm $Au(111)$, E-12c-[4-(4-Methyl/CN- Phenyldiazenyl)-Phenyl]-ethynyl-4,8,12-Tri-Octyl-4,8,12-Triazatriangulen (Me/CN-Azo-8-TATA) auf Quarz und Azobenzol-Cholesterol/Dipalmitoylphosphatidylcholin (Azo-Chol/DPPC) auf Wasser erlaubte es, die Bildung von SAMs auf den Substraten zu verifizieren, deren Morphologie zu untersuchen und die Photoschalteffizienz zu quantifizieren. Charakteristische Spektren der SAMS zeigten eine ausgeprägte Schwingungsstruktur, die Beiträgen unterschiedlicher CH-Bindungen zugeordnet werden konnte. Insbesondere konnten in den Spektren von reinen und gemischten Monolagen die Resonanzen von CH_2-Gruppen (d^+, d^-, d^+_{FR}), von CH_3-Gruppen (r^+, r^-, r^+_{FR}) und von aromatischen CH-Schwingungen identifiziert werden. Die beobachteten Intensitätsverhältnisse der d^+/r^+ and r^+/r^- Signale wiesen auf mehr oder wenig ausgeprägte gauche-Defekte in den vorhandenen Alkylketten hin. Dabei kommt es insbesondere in gemischten SAMs mit zunehmender Verdünnung mit den als Co-Liganden verwendeten Alkylthiolen zum Verlust der strukturellen Ordnung der Monolage. Reine und gemischte Monolagen von AB-Alkylthiolen mit Alkylthiolen al Co-Liganden wurden ebenfalls verwendet, um die Photoschalteffizient auf Gold als Funktion des Verdünnungsgrades zu untersuchen. Dabei dienten die SFG-Signale zusätzlicher CH_3- oder CN-Gruppen am AB als SFG-Marker, die Rückschlüsse auf die *trans-cis*-Isomerisierung von AB gestatten. Darüber hinaus wurde untersucht, welchen Einfluss

Co-Liganden mit unterschiedlicher Kettenlänge und damit variabler sterischer Hemmung auf die Schalteffizienz ausüben. Im Falle von Goldsubstraten erwies sich das nicht-resonante Hintergrundsignal im SFG-Spektren als schlecht reproduzierbar. Außerdem kam es sehr leicht zur Laserablation der Oberfläche, was die Interpretation der gemessenen Spektren zusätzlich erschwerte. Trotzdem gelang es, für die meisten untersuchten gemischten Monoschichten eine Photoschaltfähigkeit nachzuweisen. Eine Ausnahme bildeten die Monoschicht von MeAB-OC11S mit Hexadecanethiol als Co-Ligand. Offensichtlich übte in diesem Fall die lange Alkylkette des Co-Liganden einen so großen sterischen Effekt aus, dass die Schicht nicht mehr geschaltet werden konnte. Dieser Befund konnte durch zusätzliche Experimente mit sehr dünnen funktionalisierten Goldschichten bestätigt werden, die mit UV-Vis-Spektroskopie in Transmission vermessen werden konnten. Mittels UV-Vis konnte auch die thermische Rück-Isomerisierung von *cis*- zu *trans*-AB zeitlich verfolgt werden, die mit Zeitkonstanten im Bereich von 5 min bis 50 min erfolgte. Zusätzlich zu den systematischen Studien an den funktionalisierten Goldsubstraten wurden explorative SFG-Messungen an zahlreichen weiteren molekularen Systemen durchgeführt, einschließlich TATA-funktionalisierte Quarzoberflächen. Diese lieferten ebenfalls intensive SFG-Signaturen, die auf eine hohe Funktionalisierungsdichte und eine hohe strukturelle Ordnung der Schicht schließen lassen. Allerdings erwiesen sich die TATA-basierten SAMs als recht empfindlich gegenüber einer Alterung der Probe und es kam auch hier sehr leicht zu Laserablationseffekten. Schließlich wurden noch kombinierte SFG- und Oberflächendruck-Messungen an Azobenzol-Cholesterol/Dipalmitoylphosphatidylcholin (Azo-Chol/DPPC)-Monoschichten auf Wasser durchgeführt. Die Schaltung der AB-Einheit zum *cis*-Isomer führte zu einer Erhöhung des Oberflächendrucks, die mit besser ausgerichteten Alkylketten im DPPC einherging. Dieses Ergebnis steht im Einklang mit dem erwarteten höheren Flächenbedarf des *cis*-Isomers.

Acknowledgements

Few words are not enough to acknowledge all the people who supported my work and continually encouraged me throughout the writing of this dissertation. Without their time, attention, encouragement, thoughtful feedback and patience, I would not have been able to achieve this endeavor. However, I will try my best to extend great appreciation to everyone who helped me scientifically and emotionally during the whole PhD period.

Above all I would like to express my special appreciation and thanks to my supervisor Prof. Dr. Gernot Friedrichs. He has been a tremendous mentor for me. His endless curiosity and enthusiasm in science and technology, his ability to construct clear physical pictures without getting lost in mathematics, and his availability to help his students and colleagues are among his many characteristics that I hope to emulate throughout my career. I always remain thankful to him that he provided me the opportunity to do my PhD under his kind supervision. He always encouraged me to grow as a research scientist. Being a scientist critical thinking is important. I understood from him the significance of 1%. For me if I achieve 99%, it is more than satisfactory but I learnt from him "why not 100%". I learnt from him how to be perfectionist as well as realistic. He helped and supported me throughout my PhD tenure, like father. He gave tremendous amount of time, help, encouragement, without these, it would not have possible to complete my PhD and dissertation.

I would like to thank Dr. Kristian Lass for teaching me in every detail how to use and maintain the sum-frequency vibrational spectroscopy setup. I was very lucky to have a room partner like him, I was able to obtain immediate help and support in my PhD work. He was supportive from day one. It was very easy to discuss the ideas and results. I learnt a lot from his guidance. Without him it would have been difficult to achieve this task. He was always ready to help within no times. His help made my life easy, without them it would have taken enormous time to solve software and hardware issues. I experienced his importance during his leave period.

I would like to thank my colleague Dr. Joscha Kleber who was a great source of help and support. He was the one to whom I could share my feelings. He was a source of moral support during my difficult times.

I am grateful to my fellow Ibrahim Sadiek for his advice, help, discussions, ideas, and friendship. I am thankful for his valuable suggestions which proved to be very helpful in reshaping the manuscript greatly. I would like to thank all the group members of Prof. Dr. Gernot Friedrichs for their support during my PhD time and I also would like to thank all members of Institute of Physical Chemistry who provided support on one way or other in successful completion of my PhD work.

A special thanks goes to Prof. Dr. F. Temps for the collaboration and great team work throughout this project.

This dissertation would not have been possible without funding from the Collaborative Research Center (SFB) 677 "Function by Switching" at Kiel University. Therefore, I am thankful for their generous support which helped me to carry out my PhD studies.

There are no proper words to say thanks to my husband Riaz without his continuous support and help I would not be in position to accomplish this. He was the one who experienced both my excitement and frustration these years and provided the greatest spiritual support. I definitely would not have come to this stage in my life without his help.

I thank my lovely daughters Mahrukh Riaz and Maheen Riaz who are the pride and joy of my life. I love them more than anything and I appreciate all their patience and support during my PhD studies. I would like to thank to my family members especially my parents who supported and helped me to pursue my goal. It is all due to their prayers and constant and untiring support to achieve my goals without their prayers and support in life I am nothing. I would also like to thank my father-in-law, mother-in-law sister-in-laws and brother in laws for their continuous support and encouragement.

Finally, I am thankful to almighty Allah: without his will I would have never found a right path. His mercy is with me throughout my life. I also offer my humblest thanks from the deepest core of my heart to the Holy prophet MUHAMMAD (peace be upon him) who is forever a torch of guidance and knowledge for humanity as a whole.

Abbreviations and Symbols

SFG: Sum frequency generation spectroscopy

BBSFG: Broadband SFG (BBSFG)

SAM: Self-assembled monolayer

AB: Azobenzene

C10S: Decanethiol

MeAB-OC11-Thiol: 4-(11-Mercapto-undecanoxy)-4'-methylazobenzene

Me-Azo-8-TATA: (E)-12c-[4-(4-Methylphenyldiazenyl)phenyl]ethynyl -4,8,12-tri-n-octyl-4, 8, 12 triazatriangulene

CN-Azo-8-TATA: (E)-12c-[4-(4-cyanophenyldiazenyl)phenyl]ethynyl-4, 8, 12- tri-n-octyl-4, 8, 12-triazatriangulene.

CN-Azo-8-TATA(propanol): (E)-12c-[4-(4-Cyanophenyldiazenyl)phenyl]ethynyl-4, 8, 12-tri-n-propanol-4, 8, 12-triazatriangulene

TATA: Triazatriangulene

TOTA: Trioxatriangulenium

Azo-chol-DPPC: Azobenzene-cholesterol-dipalmitoylphosphatidylcholine(DPPC)

IR: Infra Red Vis: Visible Ar: Aromatic

χ: Second order non-linear susceptibility

$\chi^{(2)}_{\mathrm{R}}$: Resonant susceptibility

$\chi^{(2)}_{\mathrm{NR}}$: Non-resonant susceptibility

δ: resonant phase

ε: non-resonant phase

A_{ω}: Amplitude of the observed vibration mode

Γ: damping constant that determines the linewidth

ω_{v}: Vibrational frequency

δ: Phase change

r^{+}: Symmetric stretching vibration modes of CH_3

r^{+}_{FR}: Fermi resonance symmetric stretching vibration modes of CH_3

r^{-}_{op} : Out of plane asymmetric stretching vibration modes of CH_3

r^{-}_{ip} : In plane asymmetric stretching vibration modes of CH_3

d^{+}: Symmetric stretching vibration modes of CH_2

d^{-}: Asymmetric stretching vibration modes of CH_2

CH_{aromatic}: Aromatic CH vibration mode

Π: Surface pressure

Table of contents

List of figures

List of tables

Chapter 1

Introduction

1.1 Motivation and Aim

With the rapid development of technology there is an ongoing trend to design, synthesize, and characterize molecular switches [1–4]. Photochromic molecules such as azobenzene(AB) are appealing candidates among molecular switches. They have found the applications in the field of nanotechnology [5–7], biotechnology [8–10], and material sciences [11–13]. Such molecules are used in devices for data storage [14–17], they offer high degree of control and compatibility with biological systems [18, 19], and are used as target drugs [20–22].

The focus of this thesis, as initiated by the Collaborative Research Center "Function by Switching" (SFB677), is to investigate the efficiency and photochemical dynamics of light-driven azobenzene (AB) based molecular switches in self-assembled monolayers (SAMs) on surfaces. Photoisomerization of molecular switches critically depends upon the substrate and on the local environment of the functional units attached to AB. Therefore, the influence of structural and electronic effects were systematically studied for SAMs on planar Au (111) / SiO_2 substrate as well as at the water-air interface. Systems comprising complementary monolayers were investigated by the sensitive and structure specific non-linear sum frequency generation (SFG) and UV-Vis spectroscopy. One of the aims was to study the effects of molecular structure on the morphology and switching efficiency of AB functionalized systems, secondly, to range the potential of SFG as a sensitive probe for structural order and electronic structure in pure and mixed self-assembled monolayers. Target systems

were chosen to gain information of specific factors affecting photoisomerization dynamics. Methyl (CH_3) and cyano (CN) groups attached to the AB unit were used as SFG markers to monitor the switching state of the SAMs. Both co-ligands with different chain lengths and alkyl linkers with even or odd number of carbon atoms have been used to study the overall structure, the available free volume, and possible even-odd effects. Moreover, alternative photoswitchable AB monolayer based on the TATA platform approach of Herges *et al.* [23, 24] and Cholesterol based SAMs have been investigated.

1.2 Self-assembled monolayers

Self-assembled monolayers (SAMs) are organic assemblies formed by the adsorption of molecular constituents from solution or gas phase on the solid or liquid surface [25, 26]. Anchoring molecular switches on surfaces open new prospectives for the control of their switching abilities and their integration into large assemblies. Such assemblies have successfully been used to change the surface properties. To investigate the switching behavior of the molecules self-assembled monolayers (SAMs) functionalized with long chain hydrocarbon are frequently used. In general SAMs architecture consist of three units (see Fig. 1.1):

1. a head group binding to the substrate,

2. an end group (tail group) that constitutes the outer surface of the film and,

3. a spacer that connects head and tail and has the effect of adjusting the intermolecular separation, molecular orientation and the degree of order in the monolayer. It acts as backbone or bridge for the molecule [27].

1.2.1 Self-assembled monolayers on solid substrate

There are a number of head groups that bind to specific metals, metal oxides, and semiconductors. Each class of self-assembled monolayers is characterized by a specific head group, typically covalently bonded to a specific type of substrate. Most widely studied systems are alkylthiolate monolayers on gold, alkylsilane monolayers on silica, and alkylphosphonic acids on oxide surfaces. The thiol head group that contains a hydrogen-sulfur (-SH) group is

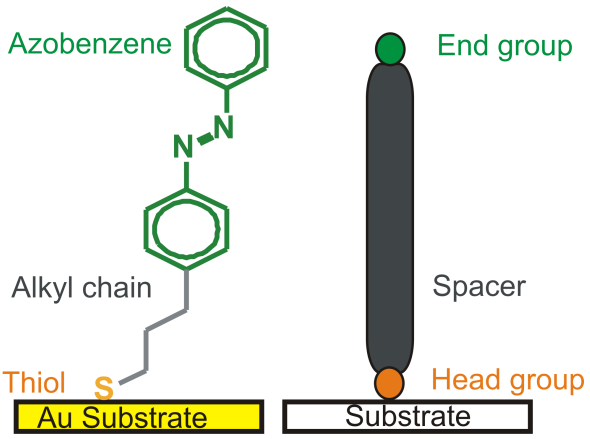

Fig. 1.1 Schematic of self-assembled monolayer architecture on solid surface. Commonly used spacers are alkyl chains or tripodal linkers, commonly used head groups are -S-, -SiO-, common substrates are Au, Ag, SiO_2.

one of the rather rare functionalities forming a strong interaction with noble metals [25, 28]. Therefore, it is possible to utilize the thiol molecules to generate well-defined organic monolayers with alterable chemical functionalities. Generally alkanethiols spontaneously assemble on noble metals i.e., gold [25]. They constitute a sulfur binding group for attachment to the noble metal surface, a spacer chain (typically made up of methylene groups $(CH_2)_n$, and a functional end group. The sulfur-gold bond and the interchain Van-der-Waals forces between the alkyl chains act as the main driving force for assembly of the alkanethiols on gold substrate.

It is assumed that formation of S-Au bond requires loss of hydrogen from the S-H groups [29]. Monolayers of thiols assemble spontaneously on the gold surface through breaking of the S-H bond and the thiolate $(R-S-)$ is then bound to gold surface by a covalent bond [25]. Actually sulfur-gold interaction is semi-covalent and has a strength of approximately 188 kJ / mol. However, nature of sulfur-gold bond allows the rearrangement of sulfur groups on the underlying surface and are still not completely understood. Nevertheless, CO, O_2, H_2O, and hydrocarbons can easily contaminate the gold surface, it should be stored in argon atmosphere or cleaned directly before the monolayer adsorption. Although sulfur compounds could also bind strongly to silver, copper, and platinum surfaces [26, 30]. Often gold surfaces are preferred because they are chemically inert [26].

The most common procedure for preparing SAMs of thiolates on gold is immersion of a clean gold substrate into a thiol solution for several hours or a day. The adsorption mechanism of alkanethiol SAMs have widely been investigated. Adsorption proceeds in two distinct

steps [31]. In the first step, a fast process that often takes only few minutes, the thiol is adsorbed and interacts with the gold surface. In second step, a relatively slow process lasting several hours, molecules organize themselves and reach equilibrium in the form of ordered SAM film. For low concentrations of the immersion solution and short immersion times (in case of adsorption from solution) [32, 33] or low exposure times (in case of adsorption in ultrahigh vacuum conditions) [34], the molecules are physisorbed with chains parallel to substrate [35]. Longer immersion times and high concentrations lead to chemisorption with the alkanethiol bound through the sulfur end group. Generally, the molecular density needs to be high enough to obtain an all-*trans* conformation of the alkyl chains. There are a lot of discussions about preferential adsorption sites for alkanethiol on gold. Historically, hollow sites (i.e., binding sites in between two or four gold atoms instead of binding sites on the top of gold atom), are generally considered the most energetically favored sites [36].

Self-assembled monolayers with a silicon head group are another class of SAMs and have been used to form monolayers on glass [37]. This is achieved through reaction of either trichlorosilane monomers or alkoxysilane monomers. Trichlorosilane monomers are highly reactive towards glass substrates but are also reactive towards water, silica gel, and other silane monomers in solution. Hence, this class of monomers is more problematic to synthesize and purify. The use of trialkoxysilane monomers overcomes many of these issues, but requires more difficult assembly conditions including multiple soak and annealing steps [38, 39]. Nevertheless, the resulting monolayers are proved to exhibit high degree of monomer cross-linking on the surface and this cross linking between monomers imparts some degree of instability. Often, the monolayer can be peeled away from surface and, therefore, these monolayers are more useful in short-term applications [40, 41].

1.2.2 Self-assembled monolayers on liquid substrates

A complete different method of achieving molecular assemblies with precisely layered structures is spreading an insoluble monolayer of amphiphilic molecules on the surface of a liquid (often aqueous) subphase in a shallow trough, known as a Langmuir trough. The monolayer can be highly compressed by applying lateral pressure. The monolayers (termed as Langmuir film) have an appropriate hydrophilic–hydrophobic balance. Such monolayers are formed from surfactants, polymers, proteins, steroids, lipids, and other compounds of biophysical nature. The Langmuir troughs are equipped with barriers (usually of Teflon) which can be used to compress monolayers in order that the area occupied by each amphiphile

molecule is varied. At the same time, changes in the surface pressure of the monolayer can be monitored in situ by using a surface balance. The conventional surface balance used is of Wilhelmy-type in which a thin rectangular plate of glass or filter paper is hung from a force sensor and bottom half of the plate is immersed in the subphase. The area occupied by a single amphiphile molecule can be calculated from the geometrical area of the surface occupied by Langmuir monolayer and the number of amphiphilic molecules in monolayer [42–44].

1.3 Molecular switches / Photoisomerization

Molecular switches are systems, either small molecules or supramolecular species, that can reversibly interconverted between (at least) two different isomeric forms under the influence of external stimuli [45]. A shift between the different states of a molecular switch implies an abrupt change in its properties including geometric, electronic, optical and electrical properties. Light energy, chemical energy or electrical energy can be used as external stimuli. Light induced isomerization is called photoisomerization and the molecule is termed as photoswitch. Photoswitches can be based on $trans \rightarrow cis$ isomerization [46–48] as well as open-closed ring transition [49, 50], ligand driven [51, 52] and/ or coordination involved spin state switching [53–56]. Mostly, *trans-cis* isomerization is induced by illumination with UV-light [57, 58] and this transformation is reversed either upon irradiation with visible light or thermal *trans-cis* isomerization occurs spontaneously in dark due to thermodynamic stability of the *trans* isomer [59–61]. Depending on the thermal stability of the photogenerated isomer, photochromic systems can be classified into two categories [4]:

1. P-type (photochemically reversible type); these systems do not revert to the initial isomer even at elevated temperatures (e.g., fulgides and diarylethenes) [62].

2. T-type (thermally reversible type); the photogenerated isomer thermally reverts to the initial form (e.g., azobenzenes, stilbenes or spiropyranes) [63].

Many diverse molecules such as azobenzene, stilbenes, spiropyranes, fulgides, diarylethenes, and chromenes have been investigated for molecular switching applications. Among these, azobenzene is mostly used for basic studies of molecular photoswitching process and optical switching applications.

1.4 Azobenzene based photoswitches

Azobenzene (AB) is an aromatic molecule possessing a diazene group –N=N– in conjugation with two phenyl substituents. It is a photochromic T-type system, which exhibits a reversible isomerisation process between its *trans* and *cis* isomers of different stability shown in Fig. 1.2. In the photoisomerization process, the photoreaction simply causes the rearrangement of the electronic and nuclear structure of the molecule without any bond breaking. However, *trans* isomer is planar whereas the *cis* isomer is a twisted non-planar molecule. Owing to different structure and symmetry both isomers have different properties. AB exhibits remarkable

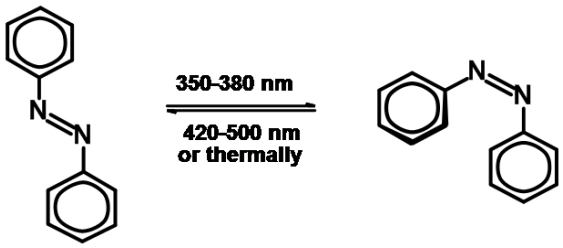

Fig. 1.2 Photoisomerization of azobenzene when irradiated with UV light. $trans-$form converted to $cis-$form using $320-380$ nm of light. Blue light of $\lambda > 420$ nm can be used to convert molecule to *trans* isomer. Alternatively, the molecule thermally relaxes to more stable *trans*-form.

photostability as negligible decomposition occurs even after prolonged irradiation and many switching cycles. The rate of thermal *cis-trans* back reaction heavily depends on chemical architecture of the system. In unsubstituted AB, net photoisomerization is significantly faster than thermal isomerization; therefore, the two processes are well-separated in time. It is well known that the appropriate modification of the substitution of the azobenzene core is one of the main factors that allows modulation of the thermal relaxation rate of azobenzene and, therefore, varies the overall response time of the photochromic molecular switch. For many applications thermal back isomerization is unwanted, hence, molecular systems with high backisomerization barriers, are preferred. Slow thermally back isomerising azobenzene derivatives are required for optically–controlled storage devices and are valuable photoactive materials for memory storage devices, where they exhibit a thermal relaxation time of microseconds [64]. However, for azobenzene-based photochromic switches that can be used in real-time information transmitting systems as well as optical oscillators, it is essential that the return to thermodynamically stable *trans*-form in dark occurs as fast as possible. In fact, the information is expected to be transmitted at the molecular scale with response times ultimately within the nanosecond or picosecond range. Even though,

some chromophores, such as spiropyranes [65], have already been proved to show very fast thermal back reactions, occurring on the order of hundreds of nanoseconds. However, a major advantage of azobenzene switches is that they are easy to synthesize.

1.4.1 Mechanism of photoisomerization

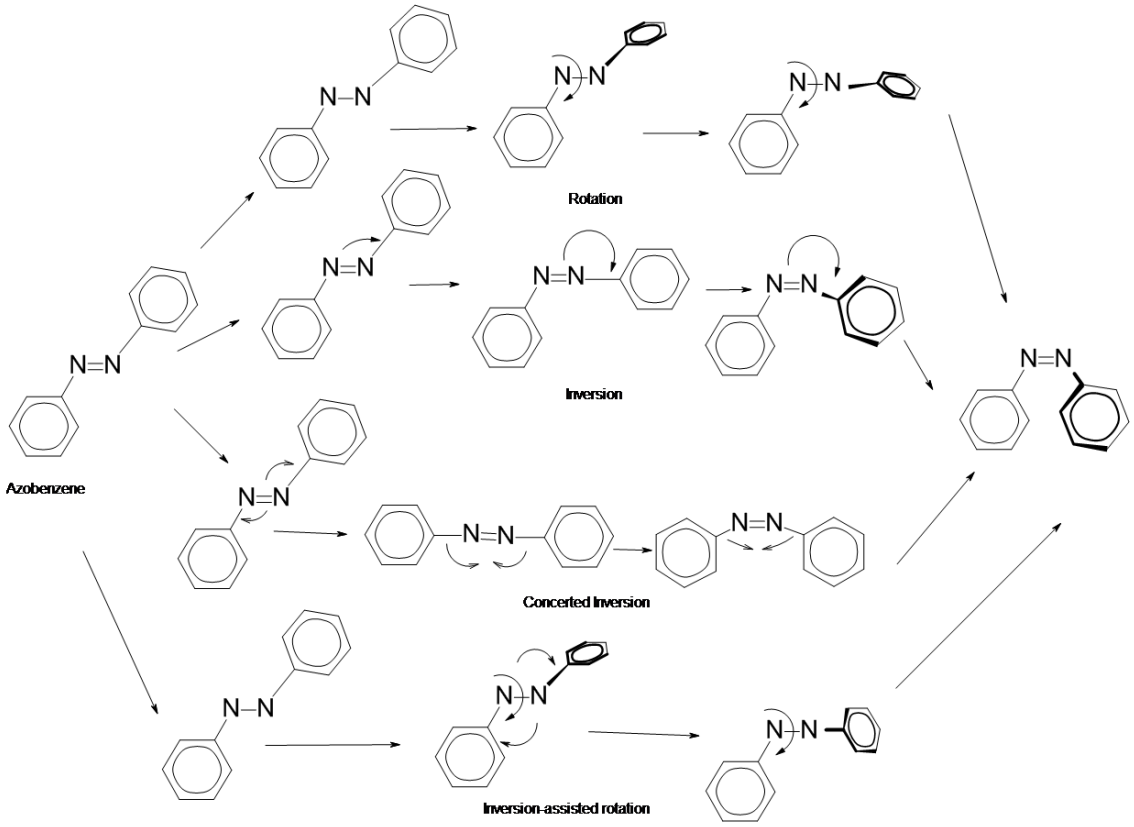

Fig. 1.3 Photoisomerization mechanism of azobenzene when irradiated with UV light, *trans*-form converted to *cis*-form via different steps adopted from [66].

The AB isomerization mechanism has been the subject of interest and controversy since it was isolated. It is important to know the dynamics of the process because rate of photoisomerization and quantum yield depends upon the irradiation wavelength [67–69], substituents on the phenyl rings [57, 70], solvent properties [67, 71, 72], temperature [69, 71, 73], and pressure [74]. Four mechanisms have been proposed as possible pathways for AB photoisomerization [70, 75–77] as shown in Fig. 1.3.

1. Twisting around the central N=N double bond (bond—rotation): The rotational pathway involves rupture of the π bond of N=N to allow free rotation about this bond. Rotation changes the C–N–N–C dihedral angle while the N–N–C angle remains fixed at 120° [77].

2. Inversion mechanism (inversion of both C-N-N angles): In the inversion mechanism, one N=N–C angle increases to 180° while the C–N=N–C dihedral angle remains fixed at 0°, which results in a transition state with one sp hybridized azo-nitrogen atom [78].

3. Concerted inversion: For isomerization to occur by concerted inversion, both N=N–C bond angles increase to 180° generating a linear transition state.

4. Inversion-assisted rotation: In inversion-assisted rotation, large changes in the C–N=N–C dihedral angle and smaller but significant changes in the N=N–C angles occur simultaneously.

All four pathways of the switching mechanism lead to relaxation process and sometime multiple pathways are used to explain experimental observations [79]. For more detailed information, it is referred to the critical review of Bandara *et al.* [66].

1.4.2 Self-assembled monolayers and photoisomerization

Due to well-defined structure, low defect density, and chemical stability, SAMs offer unique opportunities to probe molecular details of interfaces. Introduction of photoactive components into the SAMs is one of the most versatile ways of generating molecular devices. Azobenzene fuctionalized SAMs are extensively studied for their unique photoisomerization behavior.

Large number of azobenzene derivatives readily photoisomerize in solution [80, 81]. The process is extremely rapid, occurring on femto to picosecond time scales, and is characterized by high quantum yields. Selective and efficient light induced transfer and light induced cycling between the states can be performed for a nearly unlimited number of times. However, when AB adsorbs directly on a surface, the photoisomerization efficiency of the switching process is reduced due to quenching by the underlying substrate (adsorbate-surface coupling) [82–89] as well as due to intermolecular interactions with proximate molecules (molecule-molecule coupling) [84, 90–93]. This includes the fast lateral dissipation of the excitation energy due to chromophore-chromophore coupling.

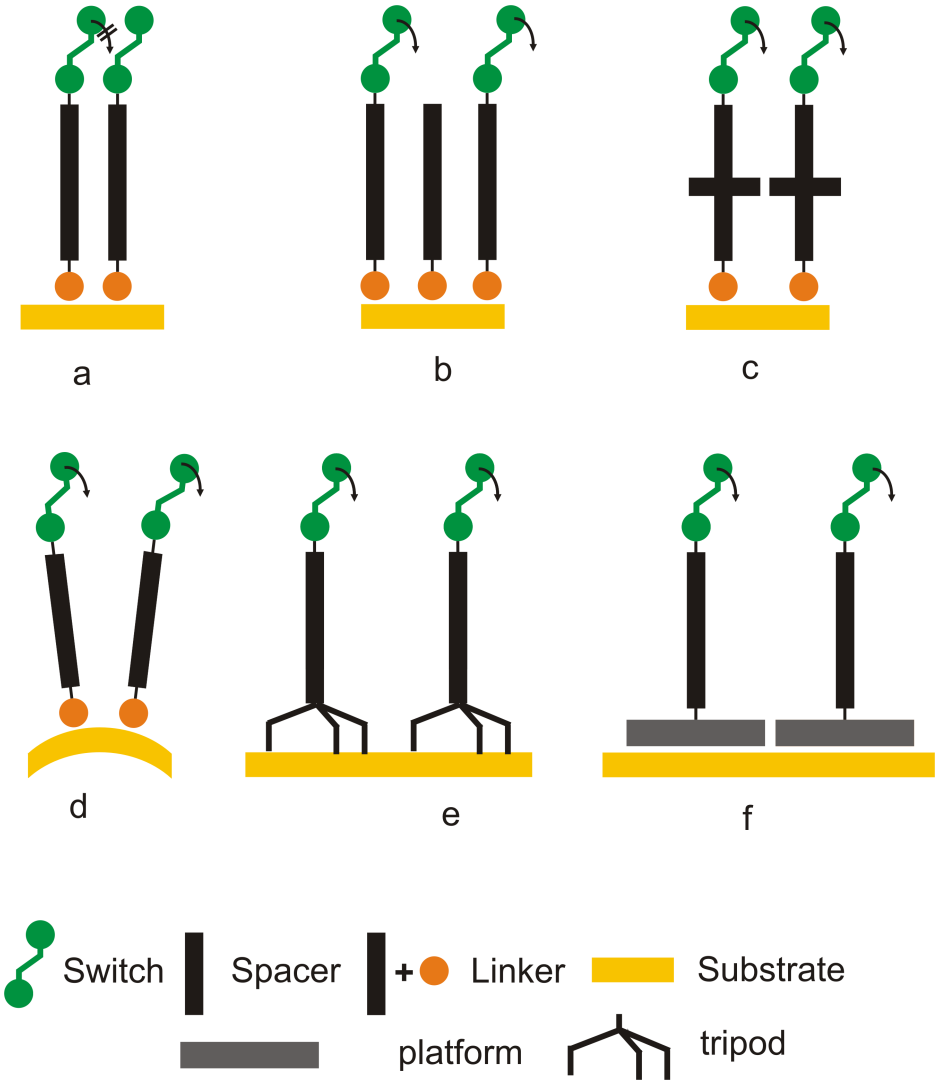

Fig. 1.4 Schematic representation of strategies used to increase photoisomerization efficiency in SAMs. (a) Densely packed layers have no free volume for switching. Free volume increased by (b) adding spacer of appropriate length (c) bulky group in structure (d) using a curved surface substrate (e) tripod linker system with three groups fixed to the surface and (f) platform molecule having a pedestal type molecular group for interaction with the substrate.

Surface quenching is reduced by attaching a non-conductive, saturated tether [84] or by inserting the functional moiety into the SAM matrix thus spatially separating it from the underlying substrate [85, 94, 95]. Molecule-molecule coupling reduces the volume available for photoisomerization. Availability of free volume needed for the planar *trans*-form to isomerize the non-planar *cis*-form is one of the main hurdles for photoisomerization on functionalized surfaces [90, 96, 97]. As a rule of thumb azobenzene group requires 127

Å^3 volume to isomerize from *trans*-form to *cis*-form [98]. Many strategies employed to overcome these problems have been depicted in Fig. 1.4.

The most commonly employed strategy to overcome the problems of limited free volume is incorporation of co-ligands such as short chain alkane thiols [85, 94, 97, 99–105] into the SAM. The approach using mixed monolayers resulting in clearly improved switching properties [100, 101] of the SAMs. However, it was found that in mixed monolayers the distribution and adsorption geometry of the functional groups on the surface is less ordered and in some cases separate phase domain of pure co-ligand and pure molecular switches have been reported [103, 106–108]. In case of mixed monolayers preferential adsorption of one of the co-ligand is also reported [28, 109–111] which results in island formation due to phase segregation in SAMs [110, 112]. In another strategy, steric hindrance is reduced by using curved surface of substrate (gold nanoparticles) [101, 113]. More recently, alternative approaches have been suggested, such as increasing the free volume of molecules in the self-assembled monolayer by integrated bulky spacer groups [114, 115], by using unsymmetrical azobenzene disulphides [106, 111, 116], or by employing large tripod-shaped molecules [97, 117] or platform molecules [118–120]. Tripod linker system includes three groups fixed to the surface and cover the surface area to allow the switching. In the platform approach, azobenzene derivative is attached to triazatriangulene (TATA) or trioxatriangulenium (TOTA) platform [23, 24, 117, 119, 121–123]. These platform units allow the functional groups to mount as free standing unit perpendicular to the surface. Unfortunately, perpendicular chemical functionalization of these molecules is possible by weak coordinative bonds. Stable attachment of vertical functional groups to these adsorbates is therefore more difficult to achieve. Nevertheless, well-ordered and stable monolayers on Au (111) surfaces by the azobenzene-functionalized platforms proved a suitable method to prepare self-assembled monolayers of functional molecules on gold with control of intermolecular distances [119, 120, 123–125]. These molecules strongly adsorb on metals, quartz, and graphite, with the molecular plane parallel to the surfaces, and readily self-organize due to molecular interactions. Adsorption of such units on quartz are still questionable. Immobilization of TATA molecule on quartz surfaces is supposed to be due to physical Van- der-Waals interactions between π electron system and substrate. The approach using platform molecule triazatriangulene (TATA), trioxatriangulenium (TOTA) results in clearly improved switching properties [119, 120, 124, 126, 127].

1.5 Techniques for investigating photoisomerization

Characterization of self-assembled monolayers is challenging, and new efficient analysis techniques are needed to investigate the properties of self-assembled monolayers. So far, several complementary spectroscopic techniques, like X-ray photoelectron spectroscopy (XPS), high resolution XPS (HRXPS), near edge X-ray absorption fine structure spectroscopy (NEXAFS), infrared reflection absorption spectroscopy (IRRAS), plasmon resonance spectroscopy, scanning tunneling microscopy (STM), and sum-frequency generation spectroscopy (SFG) have been applied. However, for photoswitching of molecules or SAMs on very thin substrate layer transmission based techniques such as UV-Vis spectroscopy have been successfully used to characterize such systems as well.

1.5.1 UV-Vis spectroscopy

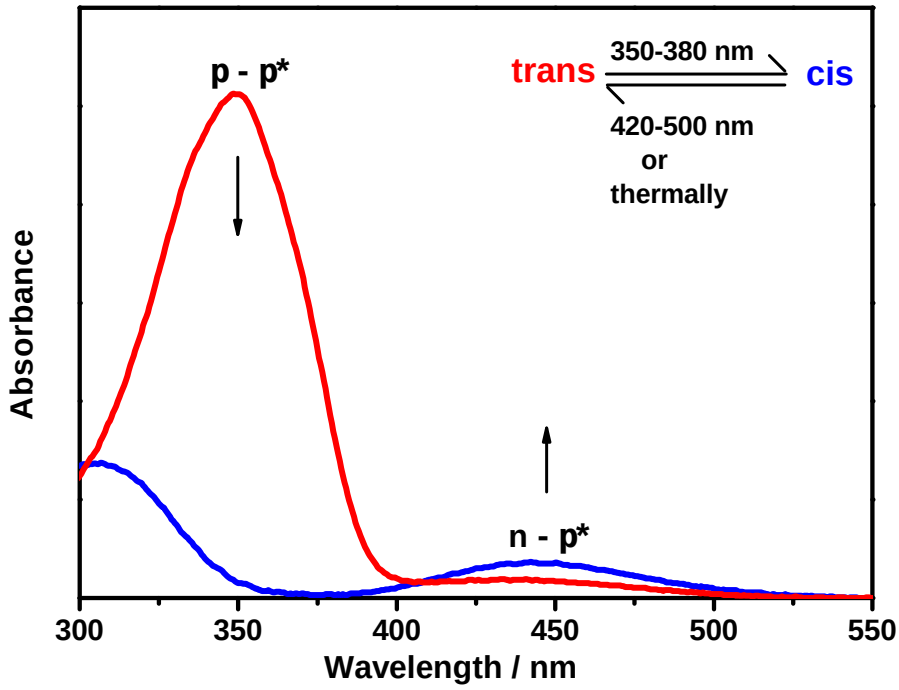

Fig. 1.5 Representative example of an UV spectrum of the azobenzene .Red spectrum: *trans*-isomer; blue spectrum: *cis*-isomer (photostationary state).

Photoisomerization of azobenzene derivatives in solution as well as of functionalized surfaces [91, 115, 126, 128, 129] has been widely studied by UV-Vis spectroscopy. A representative UV spectrum of azobenzene is shown in Fig. 1.5. The ground-state UV-Vis absorption spectrum of azobenzene in solution exhibits a low-intensity $n-\pi^*$ absorption in the visible region around 450 nm, and a much higher intensity $\pi-\pi^*$ absorption in the ultraviolet region around 350 nm [130–132].

Azobenzene has two structural forms, one of these is *trans* form, and other is *cis* form. The *trans* isomer shows two absorption bands corresponding to the $\pi-\pi^*$ transition in UV region and to the n$-\pi^*$ transition in visible region. By the symmetry rules, the n$-\pi^*$ transition is not allowed. For *trans* isomer it appears with weak intensity as a result of non-planar distortion and vibrational coupling [133]. In the *cis* isomer, $\pi-\pi^*$ absorption band significantly decreases in intensity as compared to the *trans*-isomer and simultaneously shifted to shorter wavelengths. Decrease in $\pi-\pi^*$ band is typically related to the packing of *cis* isomers [134] and the lower degree of conjugation [133] due to the non-planar structure of the phenyl group. Meanwhile the n$-\pi^*$ absorption band increases because of the non-planar structure, this electronic transition becomes symmetry-allowed.

Azobenzene undergoes $trans \rightarrow cis$ isomerization by irradiation with wavelengths between $320-380$ nm, while exposure to $400-450$ nm favors the $cis \rightarrow trans$ photo-conversion. During the $trans-cis-trans$ isomerization processes significant changes of properties like the molecular dimensions and dipole moment occur [135, 136]. The elongated *trans*-isomer of azobenzene without any substitution has a zero dipole moment, while the bent *cis* form has a dipole moment of 3 D [137]. An appropriate choice of substitution on azobenzene can change the value of its dipole moment [138].

Molecules are randomly distributed without order in solution while on the surfaces azobenzene molecules are immobilized and are close to each other. UV spectra of azobenzene on SAMs also consist of two absorption bands of $\pi-\pi^*$ and n$-\pi^*$ characters. A blue-shift and broadening of the $\pi-\pi^*$ absorption band is observed in case of SAMs, which is attributed to excitonic coupling of neighboring azobenzene molecules [91, 126, 139, 140]. As it is the case for the solution, while during the $trans-cis$ isomerization in SAMs, a pronounced decrease in the $\pi-\pi^*$ absorption band and increase in the n$-\pi^*$ band is observed [91, 115, 126, 134, 140]. Thus UV-Vis spectroscopy proved useful technique to study the photoisomerization of azobenzene derivatives in solution as well as of functionalized surfaces [91, 115, 126, 128, 129].

1.5.2 Sum Frequency Generation Spectroscopy

Sum frequency generation spectroscopy (SFG) has broadly been used by several researchers to study wide range of systems ranging from material surfaces, electrochemistry, biological interfaces, and environmental interfaces due to its intrinsic usefulness as surface analytical technique. Often SFG has been applied to self assembled monolayers [141] , metal surfaces [142, 143], polymers [144, 145], proteins [146, 147], peptides [148, 149], DNA [150], and lung surfactants [151, 152]. It is a second order non-linear optical technique that is intrinsically surface sensitive for non-centrosymmetric media [153, 154]. In 1986, Ron Shen at Berkeley obtained the first surface vibrational spectrum, using a monolayer of the dye Coumarin on glass [155]. In 1987, Shen and co-workers obtained spectra from methanol on glass and from pentadecanoic acid on glass and water [156]. In the same year, Harris *et al.* published spectra of Langmuir-Blodgett films of cadmium arachidate on silver and germanium and of octadecanethiol (ODT) on gold [157]. Over the following years, various research groups have built SFG spectrometers to study molecules at surfaces, including the gas/liquid, gas/solid, solid/vacuum, solid/liquid, liquid/vapour and solid/solid interfaces [158, 159]. It can be used to probe all types of interfaces as long as they can be accessed by probe light.

SFG provides a vibrational spectrum similar to those collected using Fourier Transform Infrared (FTIR) or Raman spectroscopic techniques, but the spectrum that SFG provides is specifically from the functional groups of molecules directly at the surface or interface. The major advantages of SFG technique include surface specificity, ability to measure the orientation of surface functional groups or molecules, and the capability to probe buried interfaces. It does not require a vacuum, as opposite to many other surface science techniques like X-ray photon spectroscopy (XPS), scanning electron microscopy (SEM), etc. SFG has several advantages over conventional vibrational spectroscopic techniques, like surface selectivity and sub-monolayer sensitivity, can be used in ambient conditions and of requiring small sample volumes. Sum-frequency generation spectroscopy (SFG) can provide detailed information and understanding of the molecular composition [160], interactions [161, 162], orientational and conformational structure of surfaces and interfaces through quantitative measurement and analysis. With SFG, it has been possible to detect and identify vibrations of adsorbed molecules through their vibrational resonances [155, 156, 163, 164]. At the same time, the specific selection rules of SFG have been used to determine the orientation of adsorbates towards the surface [158, 165–168]. The technique is also used to measure changes in molecular orientations under some stimuli [168–170]. It is one of the spectroscopic studies

used to monitor the $trans - cis$ isomerization in monolayers [100, 117, 170, 171]. The theoretical background of SFG will be presented in chapter 2.

Chapter 2

Sum Frequency Generation Spectroscopy

2.1 SFG Principle

Generally SFG can be performed by using nanosecond pulses, femtosecond pulses or picosecond pulses. SFG spectroscopic measurements can be carried out in different modes as illustrated in Fig. 2.1,

1. Scanning SFG (conventional): In case of conventional scanning SFG, the IR wavelength is tuned stepwise over range of interest (which makes this mode slow).

2. Broadband SFG (BBSFG): Here a broad band IR beam is used. BBSFG has application to the molecular level understanding of interfacial processes.

3. Time resolved SFG: The use of ultra-short laser pulses on time-scales of femto to picoseconds makes measurements with ultrafast resolution possible. This can reveal ultrafast transient changes in molecular arrangements and helps to study the dynamics of different processes (energy relaxation, solvation, photoisomerization) at interface [172–174].

4. Polarization dependent SFG: It is used to investigate the orientation of molecules by using different polarization combinations of the three involved beams [175, 176].

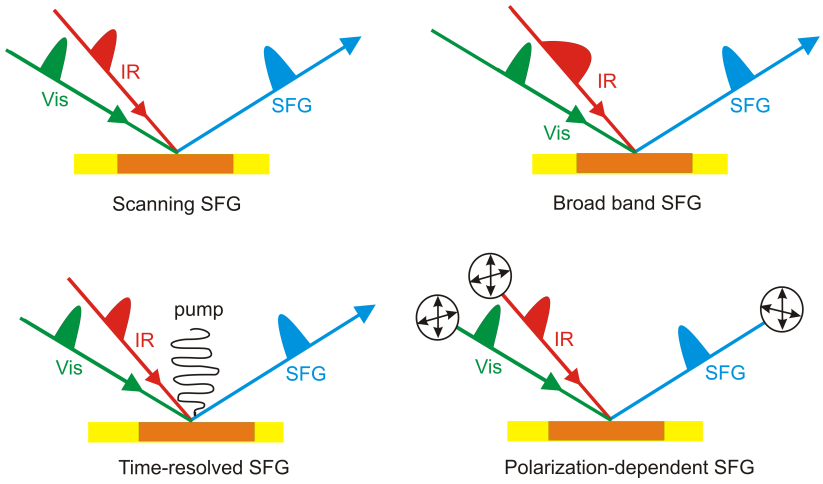

Fig. 2.1 Different modes of SFG measurements. Adopted from [177].

The physics of sum-frequency generation spectroscopy as well as the interpretation of SFG spectra is well developed and explained in many reviews and articles [163, 178]. When an electromagnetic beam (with electric field E) is incident on the dielectric planner surface, it induces a macroscopic electric dipole moment called polarization (P). This polarization acts as a source of radiation. At low light intensities, the induced polarization exhibits a linear dependence on the electric field as given in equation 2.1.

$$P^{(1)} = \varepsilon_o \chi^{(1)} E \tag{2.1}$$

$P^{(1)}$ and E are polarization and electric field, respectively, whereas $\chi^{(1)}$ and ε_0 are the first order (or linear) susceptibility and the vacuum permittivity, respectively. If an external electric field E becomes comparable to the intermolecular field felt by an electron, typically at the order of $10^5 - 10^8$ V/m, non-linear polarization is induced. The non-linearity is mediated by the medium through which the light travels rather than by the light itself. This non-linear optical behavior is not observed when light travels in free space. The induced non-linear polarization becomes

$$P = \varepsilon_o \chi^{(1)} E^1 + \varepsilon_o \chi^{(2)} E^2 + \varepsilon_o \chi^{(3)} E^3 + ... + \varepsilon_o \chi^{(n)} E^n \tag{2.2}$$

and

$$P = P^{(1)} + P^{(2)} + P^{(3)} + ... + P^{(n)} \tag{2.3}$$

Where $\chi^{(1)}$, $\chi^{(2)}$, $\chi^{(3)}$ are first, second, and third order non-linear susceptibilities. By using two laser beams with different wavelength for example one within the IR and other within the Vis spectral range, the non-linearity of material induces field components oscillating with several different frequency components.

Let us consider the second-order polarization in a material with optical fields oscillating at two frequencies, ω_{IR} and ω_{Vis};

$$P^{(2)} = \varepsilon_o \chi^{(2)} E_{\mathrm{IR}} \; E_{\mathrm{Vis}} \tag{2.4}$$

where E_{IR} and E_{Vis} are applied electric fields. Note that $\chi^{(2)}$ is the tensor of the second-order non-linear susceptibility and appropriate tensor elements need to be considered to calculate the overall components of polarization vector (see below). For the sake of clarity, let us consider the electromagnetic field in its most simple form,

$$E_i = E_i \cos(\omega_i t) \tag{2.5}$$

then the second order polarization becomes

$$P_i^{(2)} = \varepsilon_o \chi^{(2)} [E_i \cos(\omega_i t)]^2 \tag{2.6}$$

Considering the two laser beams (IR and visible), $P^{(2)}$ becomes

$$P^{(2)} = \varepsilon_o \chi^{(2)} [E_{\mathrm{IR}} \cos(\omega_{\mathrm{IR}} t) + E_{\mathrm{Vis}} \cos(\omega_{\mathrm{Vis}} t)]^2 \tag{2.7}$$

By using trigonometric relations $\cos^2\alpha = \frac{1}{2}(1+\cos(2\alpha))$ and $\cos\alpha\cos\beta = \frac{1}{2}(\cos(\alpha-\beta)+\cos(\alpha+\beta))$ the solution of quadratic equation yields four contributions in term of frequency;

$$\begin{aligned} P^{(2)} = \frac{1}{2}\,\varepsilon_0\,\chi^{(2)} \Big(& (E_{\mathrm{Vis}}^2 + E_{\mathrm{IR}}^2) && \text{OR/DC} \\ & + \left(E_{\mathrm{Vis}}^2 \cos(2\omega_{\mathrm{Vis}} t) + E_{\mathrm{IR}}^2 \cos(2\omega_{\mathrm{IR}} t)\right) && \text{SHG} \\ & + \left(2E_{\mathrm{Vis}} E_{\mathrm{IR}} \cos((\omega_{\mathrm{Vis}} - \omega_{\mathrm{IR}})t)\right) && \text{DFG} \\ & + \left(2E_{\mathrm{Vis}} E_{IR} \cos((\omega_{\mathrm{Vis}} + \omega_{\mathrm{IR}})t)\right) \Big) && \text{SFG} \end{aligned} \tag{2.8}$$

Simple trigonometry shows that non-linear polarization does not only oscillate at ω_{IR} and ω_{Vis} but also at other new frequencies. This non-linear polarization acts as a source of radiation

at those new frequencies. Among these four oscillating dipoles the constant term is called optical rectification (OR) and describes a time independent component of quasi -static electric field. The term $2\omega_{IR}$ and $2\omega_{Vis}$ is called second harmonic generation (SHG) or frequency doubling, it is the generation of light with a doubled frequency (half the wavelength). Here two photons are destroyed creating a single photon at two times the frequency. The term (ω_{IR}-ω_{Vis}) is called difference frequency generation (DFG) where generated light has a frequency that is the difference of two frequencies. The fourth term (ω_{IR}+ω_{Vis}) is called sum frequency generation (SFG), and is generation of light with a frequency that is the sum of two other frequencies.

From symmetry consideration it follows that the non-linear second order polarization is only non-zero when there is a break of inversion symmetry. Consequently, SFG can occur in anisotropic crystals, but also at an interface where the inversion of symmetry is broken. Whereas bulk media below or above the interface is isotropic and therefore, is not SFG active.

The generation of SFG photon is illustrated in Fig. 2.2. Next to energy conservation,

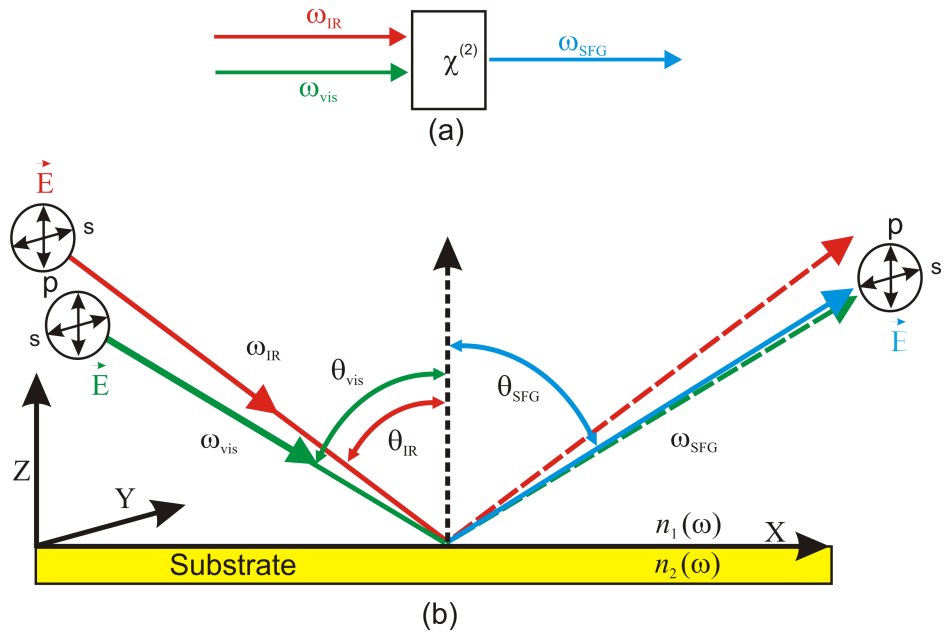

Fig. 2.2 Sum-frequency generation. (a) The frequency of output beam is the sum of frequencies of two incident (IR, Vis) beams. (b) Schematic setup for the generation of a sum frequency signal at a surface with co-propagating IR and Vis beam. ω_{IR}, ω_{Vis} and ω_{SFG} are frequencies of IR, Vis and SFG beams. θ_{IR} is the angle of incidence of IR beam, θ_{Vis} of visible beam and θ_{SFG} of sum frequency beam. p-polarized radiation has an electric field component that is in parallel orientation and the s-polarized radiation is in vertical orientation with respect to the plane of incidence, respectively.

$$\omega_{SFG} = \omega_{IR} + \omega_{vis} \tag{2.9}$$

phase matching and momentum conservation needs to be considered. The general phase matching condition is

$$\vec{k}_{SFG} = \vec{k}_{Vis} + \vec{k}_{IR} \tag{2.10}$$

Here $\vec{k}$ are the wave vectors of the different radiation components.

For SFG of interfaces (see Fig. 2.2) the phase matching condition can be written as

$$n_{SFG}\omega_{SFG}\sin\theta_{SFG} = n_{Vis}\omega_{Vis}\sin\theta_{Vis} + n_{IR}\omega_{IR}\sin\theta_{IR} \tag{2.11}$$

Phase matching occurs when a constant phase relationship is maintained between the generated and propagating waves. From equation 2.11 it become clear that SFG intensity is observed in a given direction. Therefore, it is very easy to detect low SFG intensities by spatial filtering. The direction of the emitted photon is simply given by equation

$$\theta_{SFG} = \sin^{-1}(n_{IR}\omega_{IR}\sin\theta_{IR} + n_{Vis}\omega_{Vis}\sin\theta_{Vis})/n_{SFG}\omega_{SFG} \tag{2.12}$$

The energy diagram in Fig. 2.3 makes clear that the SFG process can be understood as IR

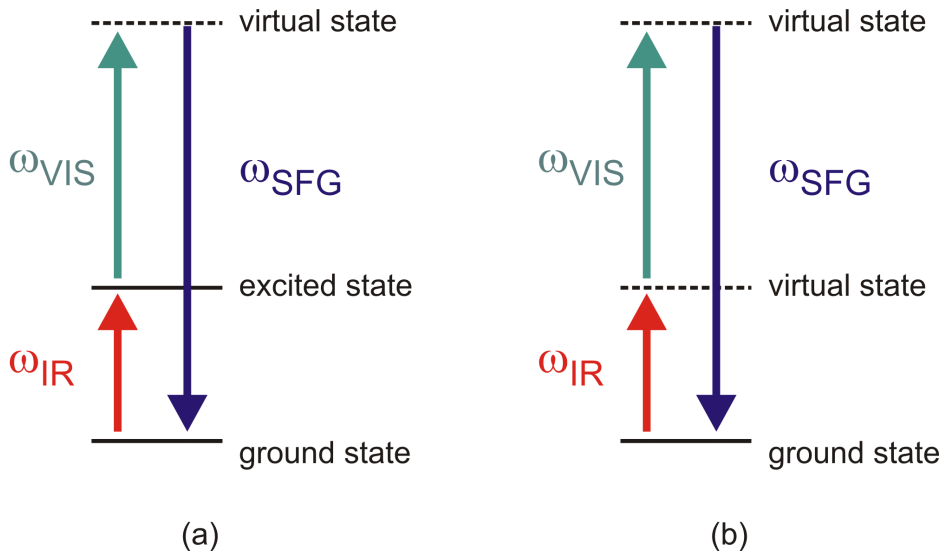

Fig. 2.3 SFG process: (a) Energy level scheme illustrating the possible vibrational resonance in SFG. (b) Energy level scheme illustrating a non-resonant SFG process:-

excitation followed by an anti-stokes Raman transition. Whereas, the excited state does not necessarily coincide with an eigen state of medium, resonance enhanced SFG is observed when the IR photon is resonant with a vibrational transition. To this effect, it is possible to measure surface IR spectra, by tuning the IR frequency. This is called sum frequency spectroscopy, SFG [179].

A complete description of SFG from the surface must consider all possible components of second-order nonlinear optical susceptibility $\chi^{(2)}$

$$P^{(2)}_{\mathrm{SFG}} = \sum_{i}^{x,y,z} P^{(2)}_{i,\mathrm{SFG}} = \varepsilon_0 \sum_{i}^{x,y,z} \sum_{j}^{x,y,z} \sum_{k}^{x,y,z} \chi^{(2)}_{ijk} E_{j,\mathrm{vis}} E_{k,\mathrm{IR}} \tag{2.13}$$

The polarization induced in the i direction by the E fields in j and k direction in terms of the magnitudes of electric field at the interface is given in term of s and p polarization:

$$P^{(2)}_{i,\mathrm{SFG}} = \varepsilon_0 \chi^{(2)}_{ijk} \hat{j} K_j E_{p/s,\mathrm{Vis}} \hat{k} K_k E_{p/s,\mathrm{IR}} \tag{2.14}$$

Where $P^{(2)}_{i,\mathrm{SFG}}$ is polarization induced in i direction, K is Fresnel factor that converts the incident field to the surface field, $\hat{j}$ and $\hat{k}$ are unit vectors. The non-linear polarization at the interface generates an SFG beam in a specific angle, which is determined by phase matching equation 2.11. The non-linear induced polarization at the interface generates a surface bound electric field. To relate the induced polarisation to the emitted surface bound electric field and to take into account phase matching, non-linear Fresnel factors, or L factors are employed. The electric field components of the SFG field can be given by

$$E_{i,\mathrm{SFG}} = L_i P_{i,\mathrm{SFG}} \tag{2.15}$$

L_i takes into account additional non-linear Fresnel factors, further details are given in [180].

Second order-nonlinear susceptibility

The second-order nonlinear optical susceptibility$\chi^{(2)}$ describes the nonlinear response of the medium to the fields. It is a third rank tensor containing 27 elements, describing possible combinations of the three Cartesian components of the polarization and of the two interacting electric fields. The non-linear susceptibility tensor $\chi^{(2)}_{ijk}$:

1. describes the interaction of the incident light with the medium or the molecule to the visible and IR electric field components. It changes with IR wavenumber and carries spectroscopic information that enables us to learn microscopic details about the surface.

2. It also provides information about the surface structural symmetry.

3. Its spatial variation over the surface directly reflects the spatial variation of the surface structure.

4. Its time variation indicates how the surface structure changes with time.

Different tensor elements can be probed by selecting different polarization contributions of the incident and SFG light.

For molecular systems the Cartesian axis system (x,y,z) is often replaced by molecular bound coordinate system (α,β,γ) and non-linear susceptibilty is given as

$$\chi^{(2)}_{ijk} = \frac{N}{\varepsilon_0}\sum_{\alpha\beta\gamma}\left\langle R(\psi)R(\theta)R(\varphi)\beta^{(2)}_{\alpha\beta\gamma}\right\rangle \tag{2.16}$$

N is the number of molecules per unit volume, $\beta_{\alpha\beta\gamma}$ is molecular hyperpolarizibility, $\chi^{(2)}_{ijk}$ is macroscopic average of molecular hyperpolarizibility. $R(\psi)R(\theta)R(\phi)$ is the product of three rotation matrices using all three Euler angles to convert from the molecular to surface bound co-ordinate systems. Near resonance, $\beta_{\alpha\beta\gamma}$ can be expressed as

$$\beta_{\alpha\beta\gamma} = \frac{1}{2\hbar} \frac{M_{\alpha\beta} A_{\gamma}}{(\omega_{\nu} - \omega_{IR} - i\Gamma)} \tag{2.17}$$

$M_{\alpha\beta}$ and A_{γ} are the Raman and IR transition moments respectively. When substituting $\beta_{\alpha\beta\gamma}$ into equation 2.16 it yields

$$\chi^{(2)}_{ijk} = \frac{N}{\varepsilon_0} \sum_{\alpha\beta\gamma} \left\langle R(\psi) R(\theta) R(\varphi) \frac{1}{2\hbar} \frac{M_{\alpha\beta} A_{\gamma}}{(\omega_{\nu} - \omega_{IR} - i\Gamma)} \right\rangle \tag{2.18}$$

For SFG

1. $\chi^{(2)}_{ijk} \neq 0$, $\chi^{(2)}_{ijk}$ must change the sign if the direction of axis is reversed.

2. The IR and Raman transition moments must be non-zero. Hence, the observed vibrational transition must be both IR and Raman active.

Being a third rank tensor, $\chi^{(2)}_{ijk}$ has 27 components and is direction dependent. In a centrosymmetric environment $\chi^{(2)}_{ijk}$ is identical for opposite directions. Hence, SFG is forbidden in centrosymmetric media. As the inversion of symmetry is broken at interfaces SFG is surface selective. From 27 tensor components only a limited number of vector combinations of $\chi^{(2)}_{ijk}$ can satisfy SFG selection rules. For a surface with C(∞) symmetry $z \neq -z$ while $x \equiv -x$ and $y \equiv -y$, out of 27 components only 7 components are non zero and only 4 components are different from each other. These elements are

$$\chi^{(2)}_{xxz} \equiv \chi^{(2)}_{yyz} \ , \ \chi^{(2)}_{xzx} \equiv \chi^{(2)}_{yzy} \ , \ \chi^{(2)}_{zxx} \equiv \chi^{(2)}_{zyy} \ , \ \chi^{(2)}_{zzz}$$

The SFG signal intensity I is related to the effective second-order nonlinear susceptibility $\chi^{(2)}_{\text{eff}}$ of the sample surface and the intensities of the two laser input beams by the following equation

$$I_{\text{SFG}} \propto P^{(2)}_{\omega_{\text{SFG}}} \tag{2.19}$$

and

$$I \propto E^{(2)} \tag{2.20}$$

For given polarization combinations, the measured SFG intensity I_{SFG} is proportional to the intensity of incoming light intensities.

$$I_{\mathrm{SFG}} \propto P^{(2)}_{\omega_{\mathrm{SFG}}} \propto \left|\chi^{(2)}_{\mathrm{eff}}\right|^2 I_{\mathrm{IR}} I_{\mathrm{Vis}} \tag{2.21}$$

Non-resonant and resonant susceptibility

The non-linear susceptibility is sum of resonant $\chi^{(2)}_{\mathrm{R}}$ and non-resonant terms $\chi^{(2)}_{\mathrm{NR}}$. The non-resonant term is associated with the substrate and adsorbate while the resonant term is associated with the vibration modes of the adsorbate.

$$\chi^{(2)}_{\mathrm{eff}} = \left|\chi^{(2)}_{\mathrm{NR}} + \chi^{(2)}_{\mathrm{R}}\right|^2 \tag{2.22}$$

The non-resonant susceptibility arises from non- resonant SFG process as shown in Fig. 2.3. Its intensity is more or less invariant as the IR beam is scanned. However, for easily polarizable surfaces, such as metals or semi-conductors, the non-resonant susceptibility can be quite large. In contrast, for most liquid systems the non-resonant contribution is either small or zero [181]. In all cases, the non-resonant SFG signal is only weakly dependent on the wavelength. The resonant SFG signal provides molecularly specific information about the identity, bonding, and orientation of molecules in the interfacial region. As the resonant term $\chi^{(2)}_{\mathrm{R}}$ is associated with the vibrational transition and becomes very large when the frequency of the IR field is resonant with a vibrational transition. An important consequence of the resonance is that the transition frequencies between two energy levels of a system can be directly obtained from the frequency dependence of $\chi^{(2)}_{\mathrm{eff}}$. In practice, one measures the intensity of the SFG signal while tuning ω_{IR}. Assuming the presence of both non-resonant

and resonant contributions, the total measured SFG intensity becomes:

$$I_{\mathrm{SFG}} \propto \left|\chi^{(2)}_{\mathrm{NR}} + \chi^{(2)}_{\mathrm{R}}\right|^2 I_{\mathrm{IR}} I_{\mathrm{Vis}} \tag{2.23}$$

As already mentioned, $\chi^{(2)}_{\mathrm{NR}}$ is to be more or less constant, hence, providing a spectral background signal only. While

$$\chi^{(2)}_{\mathrm{R}} = \frac{A_\omega}{\omega_\nu - \omega_{\mathrm{IR}} - i\Gamma} \tag{2.24}$$

A_ω is the amplitude of the observed vibration mode, Γ is damping constant that determines the linewidth, and ω_ν is the vibrational frequency. In order to account for the superposition of the resonant and non-resonance signal contribution, the phases of two susceptibilities needs to be taken in account

$$\chi_{\mathbf{R}}{}^{(2)} = \left|\chi^{(2)}_{\mathrm{R}}\right| \mathbf{e}^{\mathbf{i}\delta}, \qquad \chi^{(2)}_{\mathrm{NR}} = \left|\chi^{(2)}_{\mathrm{NR}}\right| \mathbf{e}^{i\varepsilon} \tag{2.25}$$

Here δ is the phase change relative to the incident beam of the resonant susceptibility, ε is the non-resonant phase of the substrate and is fixed. The phase of non-resonant susceptibility depends upon the properties of metal and nature of possible surface plasmon resonances.

$$\chi^{(2)} = \left|\chi^{(2)}_{\mathbf{R}}\right| \mathbf{e}^{\mathbf{i}\delta} + \left|\chi^{(2)}_{\mathbf{NR}}\right| \mathbf{e}^{i\varepsilon} \tag{2.26}$$

equation 2.23 gives

$$I_{\mathrm{SFG}} \propto \left|\left|\chi^{(2)}_{\mathbf{R},ijk}\right| \mathbf{e}^{\mathbf{i}\delta} + \left|\chi^{(2)}_{\mathbf{NR},ijk}\right| \mathbf{e}^{i\varepsilon}\right|^2 I_{\mathrm{IR}}\, I_{\mathrm{Vis}} \tag{2.27}$$

Depending on the relative phase of resonant and non-resonant contributions, the superposition can yield constructive or destructive interference. Due to this effect, line shapes may occur in many forms for example, vibrations and resonances may appear as positive or negative SFG signal contributions. More detail is given in section 3.4.2 in chapter 3.

Polarization

Polarization is a fundamental property of light. Different polarization contributions used for SFG experiment are denoted by specifying the polarizations in the order of SFG, Visible and IR. Contributing tensor elements to specific polarization combinations are given in Table 2.1.

Table 2.1 All possible polarization combinations and respective tensor elements that contributes to the signal. Combinations are labeled according to polarization in order SFG, Vis and IR beams.

Polarization	**Tensor elements combination**	**metal surface**	**dielectric surface**
ssp	χ_{yyz}	✓	✓
sps	χ_{yzy}	✗	✓
pss	χ_{zyy}	✗	✓
ppp	χ_{zzz}, χ_{zxx},χ_{xzx},χ_{xxz}	✓	✓

The four independent tensor elements

$$(\chi^{(2)}_{xxz} \equiv \chi^{(2)}_{yyz})\ ,\ (\chi^{(2)}_{xzx} \equiv \chi^{(2)}_{yzy})\ ,\ (\chi^{(2)}_{zxx} \equiv \chi^{(2)}_{zyy})\ ,\ \chi^{(2)}_{zzz}$$

contribute to the SFG signal under the four different polarization conditions *ssp*, *sps*, *pss*, and *ppp*. For dielectric surfaces (e.g silica) both s and p polarization of the incident beams produce surface electric fields and all four polarization contribution can yield SFG signal. This is different for metallic surfaces with high reflectance (i.e., the surface electrons directly follow the polarization induced by the incoming laser beams, and hence induce charge that cancel out the overall polarization). Hence only resonant susceptibilities with z component (i.e., p-polarized IR beam) yield SFG signal.

Modes of motion have parallel or perpendicular contributions, which vibrational modes contribute to SFG signal of a particular polarization combination depends upon the polarization of the IR field and the direction of the IR and Raman transition moments. The ssp polarization combination accesses vibrational modes with dipole transition moments that have components perpendicular to the surface plane. The sps and pss polarization combinations access modes that have transition moments with components parallel to the surface plane. The intensity under ppp polarization conditions contains contributions from all of the tensor element. Thus vibrational modes with components perpendicular and parallel to the surface plane will present in ppp-polarized SFG spectra. In conclusion, different possible

SFG measurement modes yields signal according to

$$I_{\mathrm{ssp}} \propto \left|\chi^{(2)}_{(\mathrm{eff}),yyz}\right|^2 I_{\mathrm{IR}}\, I_{\mathrm{Vis}} \tag{2.28}$$

$$I_{\mathrm{ppp}} \propto \left|\chi^{(2)}_{(\mathrm{eff}),zzz} + \chi^{(2)}_{(\mathrm{eff}),zxx} + \chi^{(2)}_{(\mathrm{eff}),xzx} + \chi^{(2)}_{(\mathrm{eff}),xxz}\right|^2 I_{\mathrm{IR}}\, I_{\mathrm{Vis}} \tag{2.29}$$

$$I_{\mathrm{sps}} \propto \left|\chi^{(2)}_{(\mathrm{eff}),\mathrm{yzy}}\right|^2 I_{\mathrm{IR}}\, I_{\mathrm{Vis}} \tag{2.30}$$

$$I_{\mathrm{pss}} \propto \left|\chi^{(2)}_{(\mathrm{eff}),\mathrm{zyy}}\right|^2 I_{\mathrm{IR}}\, I_{\mathrm{Vis}} \tag{2.31}$$

2.2 Application of SFG to CH vibrational spectroscopy

SFG helps to identify the molecular species and chemical groups. It also provides information of the interfacial structure such as molecular orientation. This type of information can be obtained in regions of the spectrum that are particularly dense, such as the range spanned by the stretching modes of CH- containing moieties. CH vibrational modes often have high IR and Raman transition probabilities. Due to this reason many SFG studies concentrated on CH stretching range at wavenumbers of $2800-3200\ \mathrm{cm}^{-1}$. Consequently, organic monolayers are good candidates for analyzing CH vibrational spectra [182], and to determine the hydrocarbon chain structure [183]. The CH stretching range is largely devoid of contributions from other chemical moieties, which somewhat simplifies the assignment of band structures in this region of the vibrational spectrum. However, an accurate assignment is complicated by the fact that there is a multitude of CH stretching modes. The primary contributing chemical moieties of an organic monolayer are the methyl (CH_3), methylene (CH_2), and methane (CH) groups of sp^3 hybridized carbon. Both the methyl and methylene groups exhibit symmetric and antisymmetric stretching modes that have non-vanishing IR and Raman cross sections. Symmetric and antisymmetric stretching vibration modes of CH_3 and CH_2 of aliphatic chain are termed r^+ and r^- for the methyl group and d^+ and d^- for the methylene group, respectively. The two symmetric stretching modes of CH_3 are split by Fermi resonances with the overtone of the bending mode and with the overtone of the

deformation mode in SFG spectra [178]. The vibrational modes of the CH_2 group of an alkyl chain, which are IR and Raman active, are shown in Fig. 2.4.

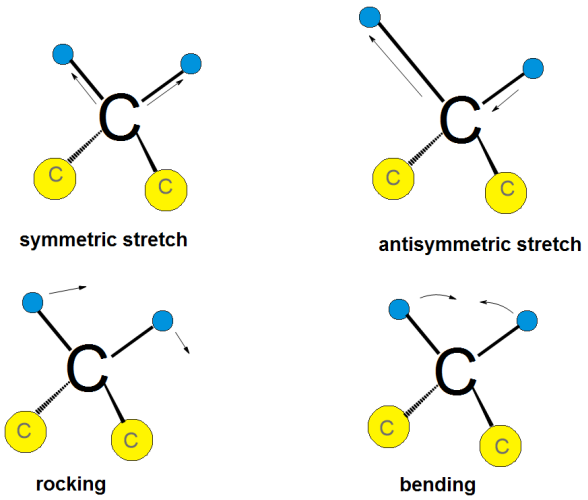

Fig. 2.4 The atoms in a CH_2 group, commonly found in organic compounds, can vibrate in six different ways: symmetric and antiymmetric stretching, scissoring, rocking, wagging and twisting. The four vibrational modes of the CH_2 group of an alkyl chain yielding SFG intensity are shown here.

Orientational Analysis and Peak assignment of CH vibrational units

The symmetry properties of the investigated molecule or functional group is of immense importance when performing vibrational spectroscopy as it dictates the selection rules describing whether a particular vibration is active or not in IR and / or Raman spectroscopy. Symmetry selection rules show that some molecular vibrational modes are SFG active. The measured values of non-linear susceptibility tensor are related to the orientationally averaged hyperpolarizibility tensor (β) with the result that molecular orientation can be obtained. As already discussed, the macroscopic susceptibility for Cartesian axis system (x,y,z) $\chi^{(2)}_{xyz}$ is related to molecular hyperpolarizibility tensor $\beta_{\alpha\beta\gamma}$ by equation.

$$\chi^{(2)}_{xyz} = \frac{N}{\varepsilon_0} \sum_{\alpha\beta\gamma} \langle R(\psi)R(\theta)R(\varphi)\beta^{(2)}_{\alpha\beta\gamma} \rangle \tag{2.32}$$

It is useful to determine from the symmetry properties of the functional group, which hyperpolarizability (β) elements carry the vibration of interest that contribute to SFG spectrum.

Methyl groups are among the best studied functional groups. Here the SFG spectrum of the methyl group at the end of an aliphatic chain will be described, but it also applies to other functional groups having the same symmetry properties. The methyl group has approximately C_{3v} symmetry assuming that it can rotate freely around the C-C bond to the adjacent methylene group. In the molecular coordinate system the c axis coincides with the symmetry (C_{3v}) axis of the methyl group and the plane formed by a and b axis is perpendicular to the c axis with the a axis along the projection of one of the CH bonds in the ab plane. The C_{3v} group has eleven non-vanishing hyperpolarizibility tensor(β) elements [184]. Hirose *et al.* [180] and Wang *et al.* [176] derived the relation of molecular orientation angle (tilt angle) and susceptibility factor for the antisymmetric and symmetric vibrations by applying equation 2.32 and integrating over the Euler angles. By comparing the experimental ratio between the intensities of the symmetric and antisymmetric methyl CH stretches (r^+/r^-) of the ppp spectra with a theoretical predictions, Wang and Hirose were able to approximately determine the tilt angle of the terminal methyl groups of a monolayers. Equations given in [180] reveal that methyl SFG intensities are extremely sensitive to the methyl axis tilt angle (θ). The tilt angle is angle of probed moiety with respect to the surface normal. It has been particularly useful to characterize the conformational order of methyl terminated alkanethiols on different metals. The alkanethiol molecules in the SAMs are oriented with an average tilt angle of $\sim 10^\circ$ to $\sim 30^\circ$, depending on the metal substrate [185]. Change in the tail group can change this angle. The methyl tilt angle θ and the SFG intensities are plotted for symmetric and antiymmetric stretching mode in Fig. 2.5 which was adopted from [180, 186]. For small θ, ssp intensity of the symmetric stretch vibration is larger than antisymmetric stretch. In Fig. 2.6 the SFG intensities are plotted as a function of angle θ for different polarization combinations for the symmetric and antisymmetric stretching vibration of methyl group of an aliphatic chain. The figure clarifies the fact that methyl SFG intensities are extremely sensitive to methyl axis tilt angle for different polarization combinations. The intensity of symmetric mode of methyl group is higher in ssp than ppp polarization combination whereas for antisymmetric mode the ppp intensity is higher than ssp polarization combination. This is due to the fact that the intensities of vibrational modes depend upon the orientation of the dipole moment with respect to surface normal. The symmetric and antisymmetric stretching modes of the methyl group are orthogonal, as the C_{3v} axis of the CH_3 group tilts from 0° to 90° along the surface normal. Consequently, the direction of the transition dipole moment of symmetric stretch is parallel to the symmetry axis of methyl group that's why intensity of

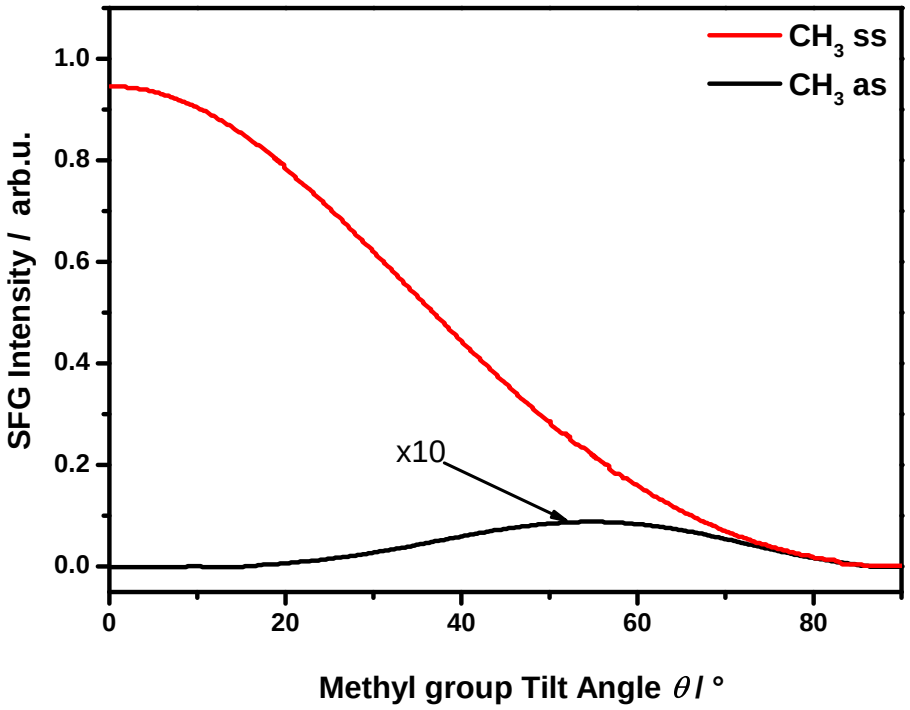

Fig. 2.5 Intensities of the antisymmetric (CH_3-as) and symmetric (CH_3-ss) methyl stretches as a function of the tilt angel θ, for the ssp polarization combination. Adopted from [180, 186]

symmetric stretch vibration of the methyl group in ssp polarization combination is higher than for ppp.

These intensity trends also help for the assignment of vibrations in SFG spectra. As an example, the SFG spectrum of Dipalmitoylphosphatidylcholine (DPPC), is shown in Fig. 2.7. The peak at 2970 cm^{-1} in SFG spectrum of Dipalmitoylphosphatidylcholine has been assigned as antisymmetric peak because it has larger intensity in ppp spectrum as compare to the ssp polarization combination. While the peak at 2883 cm^{-1} can be assigned as symmetric stretch of the methyl group of long alkyl chain due to high intensity in the ssp combination. The peak at 2950 cm^{-1} in the ssp polarization combination can be assigned as Fermi resonance of methyl group [158, 187].

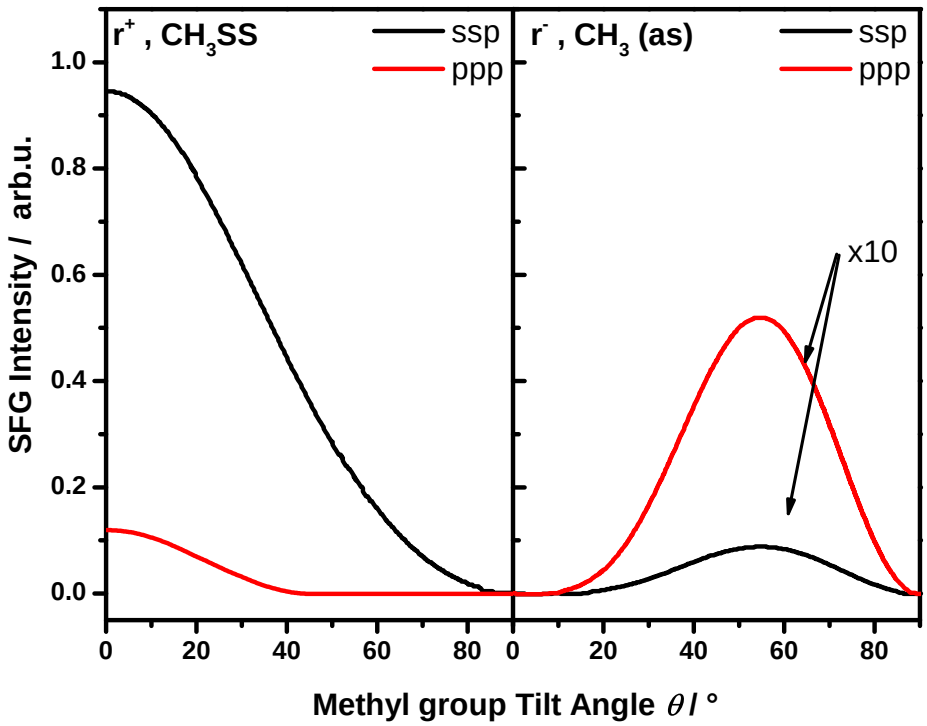

Fig. 2.6 Intensities of the antisymmetric (CH_3-as) and symmetric (CH_3-ss) methyl stretches as a function of the tilt angle θ, for the two polarization combinations. Adopted from [180, 186]

Structural changes studied by SFG

As discussed above, SFG intensities of symmetric and antisymmetric vibrations are extremely sensitive to tilt angle (θ). This orientational dependence of sum frequency generation spectroscopy (SFG) can be used to investigate the structural changes resulting from photoisomerization as well. A sensitive vibrational marker is required to study the orientation and structural changes. In this section, the SFG intensities of methyl as SFG marker group of the photochromic molecule upon *trans*- to -*cis* photoisomerization will be discussed. Here, the methyl group is attached to outer phenyl unit of azobenzene i.e., Methyl azobenzene (MeAB). Schematic illustration of reversible change in tilt angle of azobenzene of alkanethiol monolayer upon irradiation is shown in Fig. 2.8 (a). Photoisomerization changes the projection of the methyl group attached to azobenzene. If change in orientation of methyl group increases its tilt angle, the direction of dipole moment of methyl symmetric stretch has no longer a strong perpendicular component with respect to the surface and therefore, the SFG

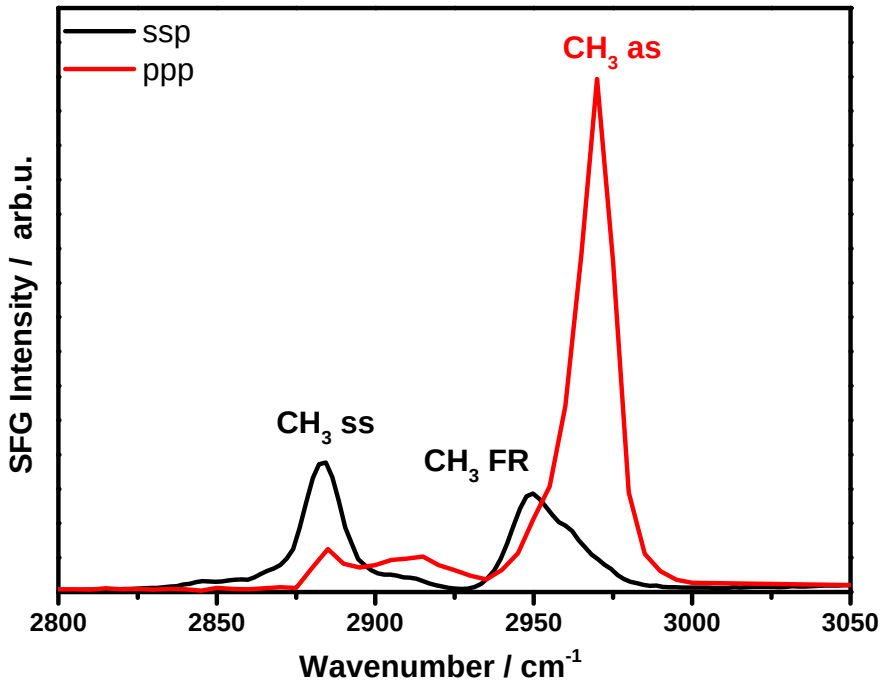

Fig. 2.7 SFG spectrum of DPPC/water interface at two different polarization combination.

intensity of symmetric mode is expected to decrease. In contrast the SFG intensity for the antisymmetric stretch should become higher. In principle, this change in signal intensity of the symmetric and antisymmetric stretch vibration can be used to monitor photoisomerization process as discussed in section 1.4. Recently, SFG has been successfully employed to study the behaviors of some *cis-trans* photoswitchable surfaces [100, 117, 170, 171, 188].

Even-Odd effect studied by SFG

Orientational dependence of SFG can also be employed to investigate the even-odd effect. Depending on the even or odd number of methylene units of the alkyl chains, the marker terminal methyl groups have different orientation. This is an example of the well-known even-odd effects [189, 190]. For a dense monolayer of $CH_3(CH_2)_n$S-Au (n = odd) the terminal CH_3-CH_2 bond is more or less perpendicular to the substrate plane. While for the monolayer with n = even, the methyl group is tilted away from the surface normal [191]. Consequently, the intensities of the r^+ and r^+_{FR} modes are higher than the intensity of the r^- mode in the odd

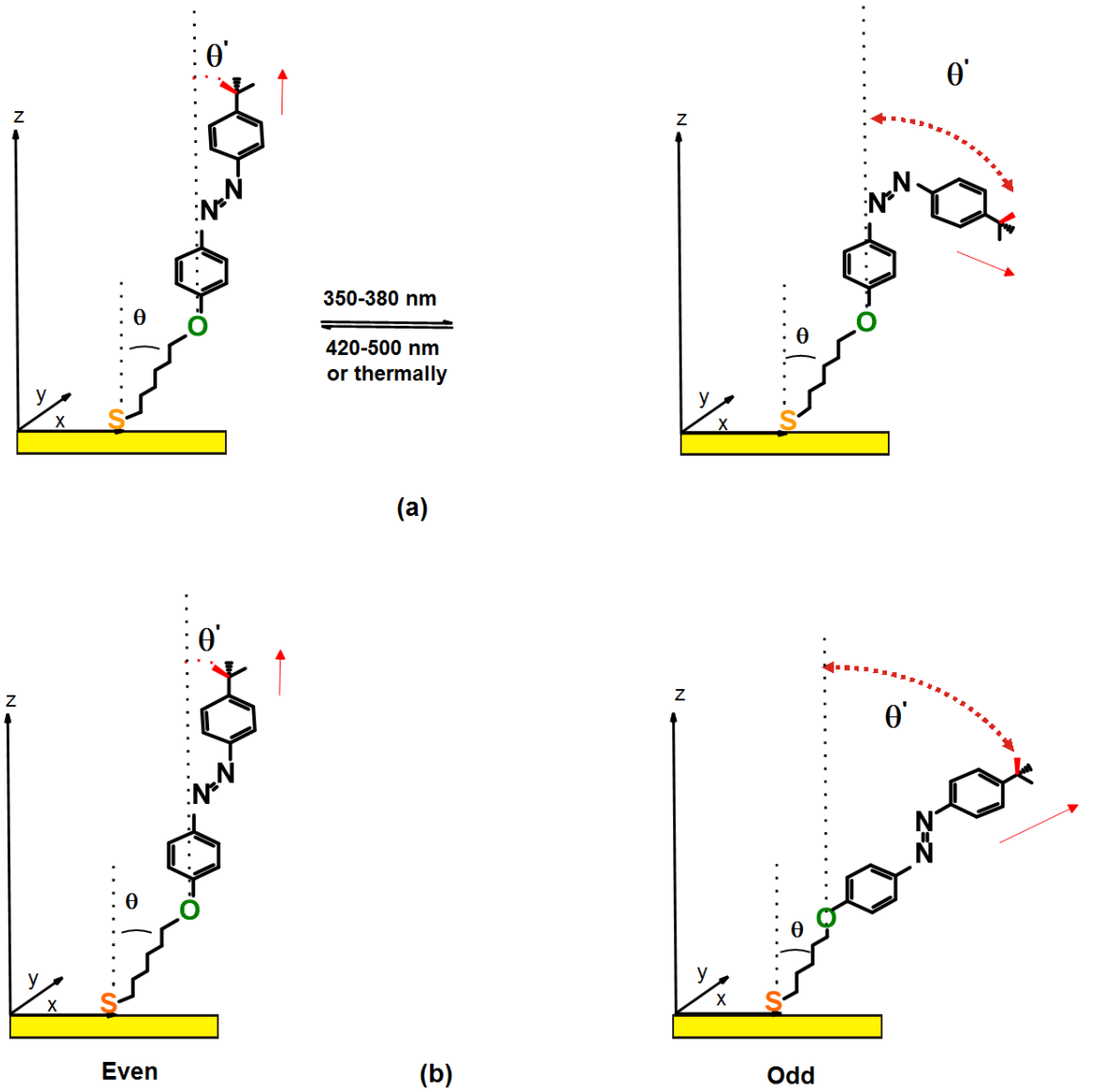

Fig. 2.8 Schematic illustration of the expected change of tilt angle of the azobenzene upon photoisomerization ultimately changing the projection of SFG marker methyl group of alkane thiol monolayer. (a) Change in θ from $trans \rightarrow cis$ should lead to change in the intensities of the symmetric (CH_3- ss) and antisymmetric (CH_3- as) methyl stretches (b) orientation of the SFG marker group is different for an even and an odd number of C atoms in alkanethiol spacer.

case, and lower in even case. Fig. 2.8 (b) illustrates the different orientations of methyl SFG marker group for even and odd number of alkyl spacer chain. This means that orientation and intensity of interfacial dipoles can be tuned by changing the chemical composition and

the number of methylenes (odd or even) of the alkyl chains of the alkanethiol adsorbates [192, 193]. Thus, the SFG spectroscopy is highly effective technique of the even-odd effect.

Chapter 3

Experiment and Techniques

Three different systems of azobenzene derivatives (i.e, azobenzene alkylthiol, azobenzene triazatriangulene, azobenzene cholesterol) on three different substrates (i.e, gold, quartz, water) have been studied. Firstly, this chapter in section 3.1 describes the synthesis and SAM preparation of azobenzene derivatives. Secondly, section 3.4 describes the experimental techniques (SFG and UV-Vis) used to investigate the structure and switching properties of monolayers. Finally, the procedure for simulating and fitting of recorded spectra will be explained in some detail.

3.1 Azobenzene on Gold Substrate

Synthesis

All of the reagents used for synthesis were purchased and used as received. Solvents of technical grade were purified by distillation under reduced pressure. Solvents of spectroscopic grade (denoted: spec. grade) were acquired from Merck (Uvasol, 99.9%). Methyl substituted azobenzenes with decanoxy or undecanoxy thiol were synthesized via a procedure adopted from Lesely *et al.* and Brett *et al.* [194, 195].

3.1.1 Synthesis of 4-(11-Mercapto-undecanoxy)-4'-methylazobenzene (MeAB-OC11-Thiol)

Morphology and photoisomerization of the azobenzene derivatives 4-(11-Mercapto-undecanoxy)-4'-methylazobenzene (MeAB-OC11-Thiol) and 4-(10-Mercapto-decanoxy)-4-methylazobenzene (MeAB-OC10-Thiol) have been studied on self-assembled monolayers deposited on gold substrates. The molecule necessary for monolayer preparation has been prepared in a four-steps synthesis process [194, 195]. The synthetic route to the methyl substituted azobenzene alkylthiol is outlined in Fig. 3.1.

1. Base-catalyzed azo-coupling of *p*-toluidine with phenol in reaction with nitrite gives 4-Hydroxy-4'-methylazobenzene (MeAB-OH) with a reasonable yield (60%).

2. MeAB-OH was used as a reagent in a Williamson ether synthesis reaction with 11-Bromo-1-undecene, yielding 4-undec-(10-enyloxy)-4'-methylazobenzene (MeAB-C11-en) (55%).

3. The third step was a radical addition of thioacetic acid to double bond, giving 4-(11-Thioacetoxyundecanoxy)-4'-methylazobenzene (MeAB-C11-S-Acetyl) with a yield of 65%.

4. The final product 4-(11-Mercapto-undecanoxy)-4'-methylazobenzene was obtained via hydrolysis of MeAB-C11-S-Acetyl in acidic conditions (78%).

3.1.2 Synthesis of 4-(10-Mercapto-decanoxy)-4'-methylazobenzene (MeAB-OC10-Thiol

To reduce the length of alkyl chain (from C11 to C10) to study the effects of even or odd numbered alkyl chains the another azobenzene derivative MeAB-OC10S was synthesized. In principle, the same method as used for MeAB-OC11S was employed, the four-step synthesis procedure is described in [194].

1. Base-catalyzed azo-coupling of *p*-toluidine with phenol in reaction with nitrite gives MeAB-ol with a reasonable yield (60%).

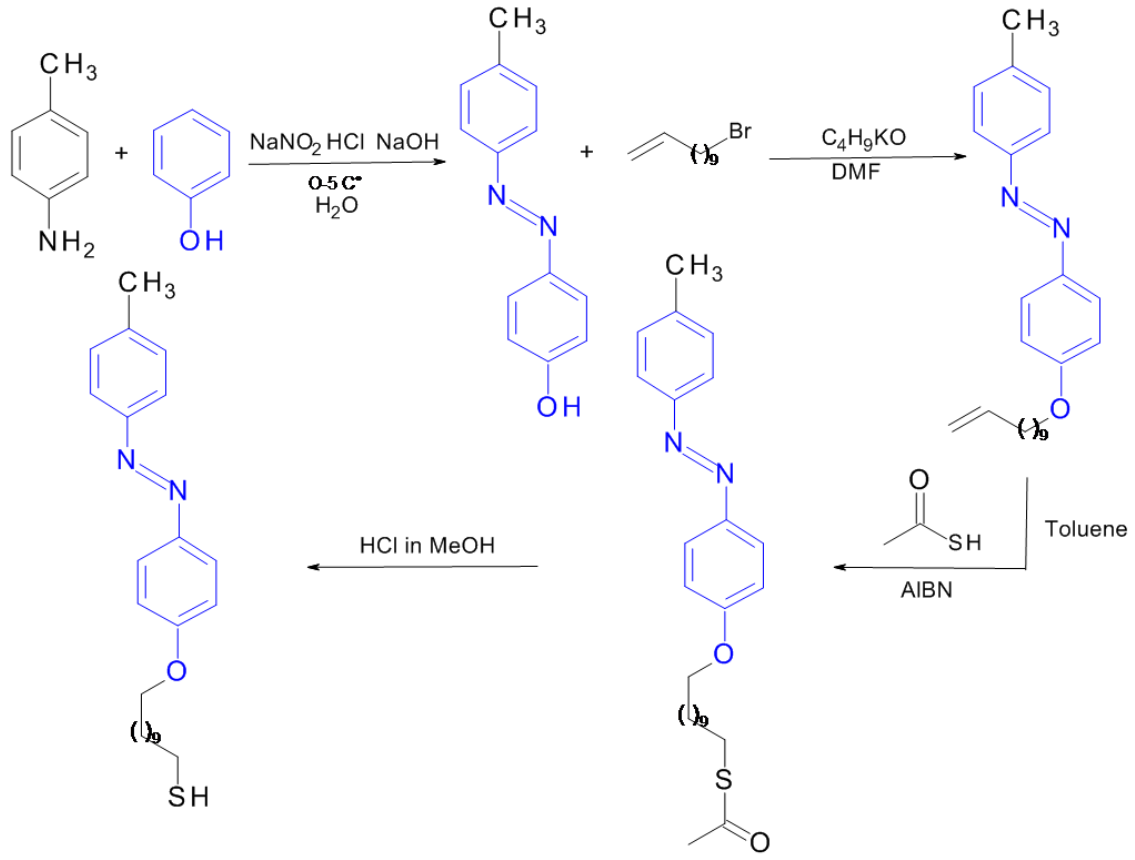

Fig. 3.1 Reaction scheme for the synthesis of MeAB-OC11S. Methyl substituted azobenzene attached to an alkyl chain with 11 carbons and a thiol functional group.

2. MeAB-ol was then used in a Williamson-ether-synthesis reaction with 10-Bromo-1-decene yielding MeAB-C10-en (50%).

3. A radical addition of thioacetic acid to the double bond, yielding 4-(11-Thioacetoxy-decanoxy)-4'-methylazobenzene MeAB-C10-S-acetyl with a yield of (60%).

4. The final product 4-(11-Mercapto-decanoxy)-4'-methylazobenzene was obtained via hydrolysis of MeAB-C10-S-acetyl in acidic conditions (70%).

Sample preparation

Self-assembled monolayers of alkylthiols on gold can easily be prepared without any special equipment or environmental conditions. In this study SAM preparation has been accom-

plished via a procedure reported in the literature [42, 196, 197]. For SFG measurements, SAMs were prepared on 100 nm thick Au (111) plated glass. Such slides of 1.5 mm thick glass substrate, measuring 25×6 mm dimension were purchased from EMF company. Before SAM preparation the gold slides were cleaned in freshly prepared Piranha solution (H_2SO_4 :H_2O_2, mixing ratio being 3 : 1) for 30 s. The preparation of azobenzene functionalized SAMs was done by simply immersing those Piranha cleaned gold-coated glass plates in the respective 1 mM thiol solution for $12 - 18$ h. The SAM-coated plates were washed with ethanol and then with distilled water. Finally, the slides were dried in a nitrogen/ argon gas flow as necessary. An alternative treatment of the sample by tempering (flame annealing) the slides in butane gas flame was also tried by bringing the metal with a soft flame to a hot enough temperature long enough to cause annealing. SFG spectra of both type of SAMs depicted that the formed monolayers were not so much different in structure.

Mixed monolayers were prepared by immersing the gold slides in a mixture of two thiols with appropriate composition. Mixed monolayers (mSAMs) were prepared from 0 % to 100 % MeAB thiol with different co-ligands, including non-deuterated like decanethiol(C10), and deuterated compounds like perdeuterated 1-dodecane-d_{25}-thiol, and perdeuterated 1-hexadecane-d_{33}-thiol. All molecular systems are illustrated in Fig. 3.2. The following pure and mixed monolayers were prepared for SFG studies:

1. Pure MeAB-OC11S/Au
2. Pure MeAB-OC10S/Au
3. Pure AB-OC11S/Au
4. Pure C10-S/Au
5. Mixed monolayer containing 0-100 % MeAB-OC11S + C10-S/Au
6. Mixed monolayer containing 0-100 % MeAB-OC11S + dC12 or dC16-S/Au

For UV-Vis analysis 10 nm thick gold layers on glass slide manufactured by Phasis have been used for SAMs preparation. In contrast to the 100 nm EMF substrates, these samples allowed for measurements in transmission configuration.

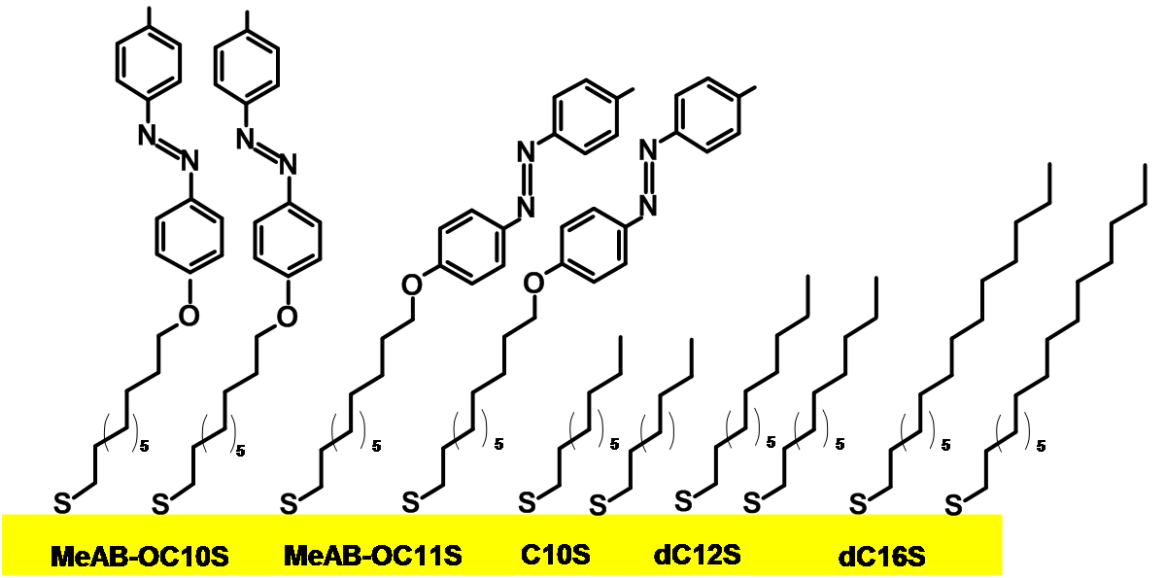

Fig. 3.2 Compilation of azobenzene derivatives deposited on gold substrates. Pure monolayers contain just one respective thiol, whereas mixed monolayers were prepared from combination of two different thiols (i.e, azobenzenethiol and alkylthiol).

3.2 Azobenzene derivatives on quartz

3.2.1 TATA based aromatic olefines adlayer

The second class of systems studied in this thesis were triazatriangulene (TATA) based azobenzene derivatives on quartz substrates. The structure as well as photoswitching behavior of the TATA adlayers on quartz has been studied by means of SFG. The investigated systems differed in the side alkyl chains attached to the TATA platform (either octyl or 1-hydroxypropane) or in azobenzene substitution (CH_3 or CN) as SFG marker group.

Synthesis

The synthesis of TATA-based azobenzene derivatives has been accomplished in the group of Prof. Rainer Herges at the Institute of Organic Chemistry, Kiel University. The synthesis procedures can be found in the literature [23, 24]. The following derivatives have been used, and their structure is outlined in Fig. 3.3.

1. 12c-Ethynyl-4, 8, 12-tri-n-octyl-4, 8, 12 -triazatriangulene (8-TATA).

2. (E)-12c-[4-(4-Methylphenyldiazenyl)phenyl]ethynyl -4,8,12-tri-n-octyl-4, 8, 12 triazatriangulene (Me-Azo-8-TATA). The corresponding molecular structure is given in Fig. 3.3, where structure (B) is attached to functional group I.

3. (E)-12c-[4-(4-cyanophenyldiazenyl)phenyl]ethynyl-4, 8, 12- tri-n-octyl-4, 8, 12-triazatriangulene. (CN-Azo-8-TATA). The corresponding molecular structure is given in Fig. 3.3, where structure (B) is attached to functional group II.

4. (E)-12c-[4-(4-Cyanophenyldiazenyl)phenyl]ethynyl-4, 8, 12- tri-n-propanol-4, 8, 12-triazatriangulene (CN-Azo-8-TATA(propanol)). The corresponding molecular structure is given in Fig. 3.3, where structure (C) is attached to functional group II.

Sample Preparation

Azobenzene-based TATA platform SAMs on quartz substrates were prepared in a group of Prof. Olaf Magnussen at the Institute for Experimental and Applied Physics, Kiel University and have been used as supplied for SFG measurements. A blank quartz sample was used as reference. The blank quartz substrate was cleaned by dipping the sample in Piranha solution (H_2SO_4 :H_2O_2, mixing ratio being 3 : 1) for $2-3$ hr and subsequent annealing for 1 min in a blueish flame of butane gas.

3.2.2 Silanol based Azobenzene adlayers

As an alternative to the TATA platform approach, adlayers formed from azobenzene attached to the quartz by covalent bond via silanol bridges have been studied via SFG as well.

Synthesis

The synthesis and functionalization of silanol-based azobenzene derivatives has been accomplished in the group of Prof. Friedrich Temps at the Institute of Physical Chemistry, Kiel

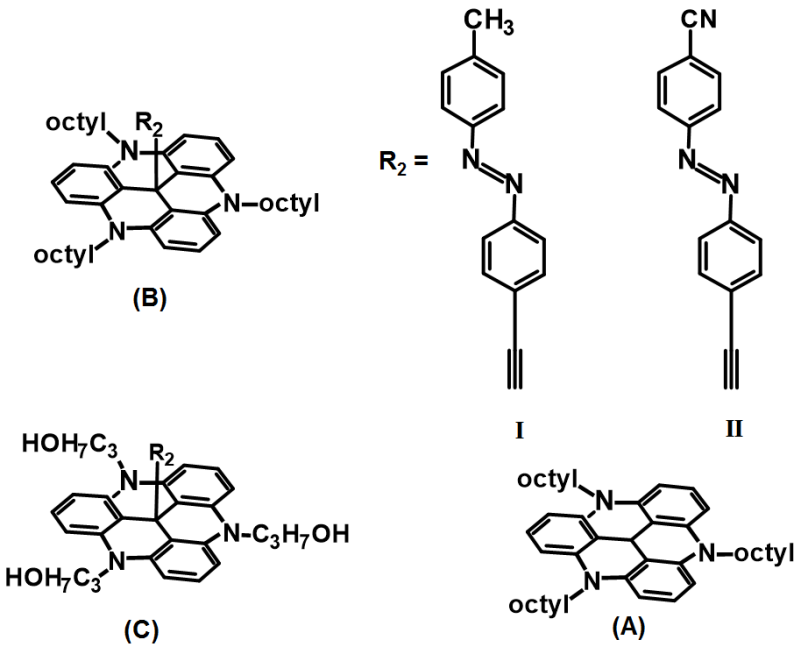

Fig. 3.3 Molecular structure of the TATA molecules and attachment of functional group to the TATA platform for preparation of self-assembled adlayers on quartz. (A) Structure of bare TATA platform. (B) TATA platform with three n-octyl side chains and attached to either one of the functional group R_2 (C) TATA platform with three 1-hydroxypropyl side chains and attached to the functional group R_2= II

University. Synthesis details of azobenzene derivatives are reported in the Bachelor thesis of Rebecca Stellmacher.

Sample Preparation

Silanol functionalized planar quartz surfaces were functionalized with azobenzene or methyl substituted azobenzene via klick chemistry. The structure of such a layer is shown in Fig. 3.4.

3.3 Azobenzene based lipid monolayers on water

A stock solution of 5% azobenzene-cholesterol and 95% Dipalmitoylphosphatidylcholine (Azo-chol/DPPC) was received from Bridget Murphy, Institute for Experimental and Applied

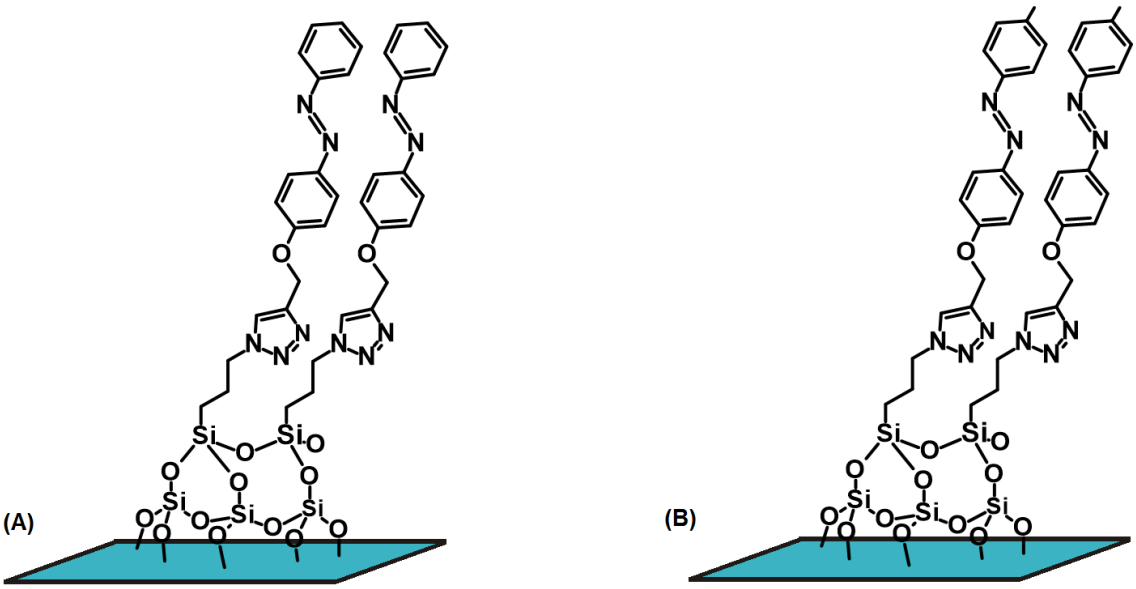

Fig. 3.4 Silanol based azobenzene derivatives attached covalently to quartz surfaces via silanol bridges. (A) Azobenzene (B) Methyl substituted Azobenzene

Physics, Kiel University. The structure of the molecular system of azo-chol/ DPPC is illustrated in Fig. 3.5. A spreading solution was prepared from the 1 nmol / μL stock solution dissolved in a mixture of methanol and chloroform (5:1).

3.3.1 Sample Preparation

A solution of 5% Azobenzene-cholestrol / DPPC in chloroform was spread on an air-water interface in a Langmuir trough or alternatively, in a 5.2 cm diameter Teflon dish for the SFG experiments. In the Langmuir trough from Riegler & Kirstein GmbH, two barriers were employed to provide a symmetric film compression. The surface pressure and the mean molecular area were continuously monitored during film compression by the Wilhelmy plate method. The measured surface pressure was accurate to ≤ 0.5 mN m^{-1}. The trough was filled with pure water (18 MΩ cm from the Ultra Purelab Ultra unit) as the subphase. The water surface could vary between 190 and 27 cm^2 by means of two movable barriers. The bottom surface of the Langmuir trough was heated by an integrated Peltier element. The temperature during measurements was slightly below the room temperature (i.e, 21.0 ± 0.4°C) to keep evaporation effects small. In order to check if freshly prepared subphase was clean, a surface-pressure-area-isotherm was always measured before spreading the monolayer. Only if

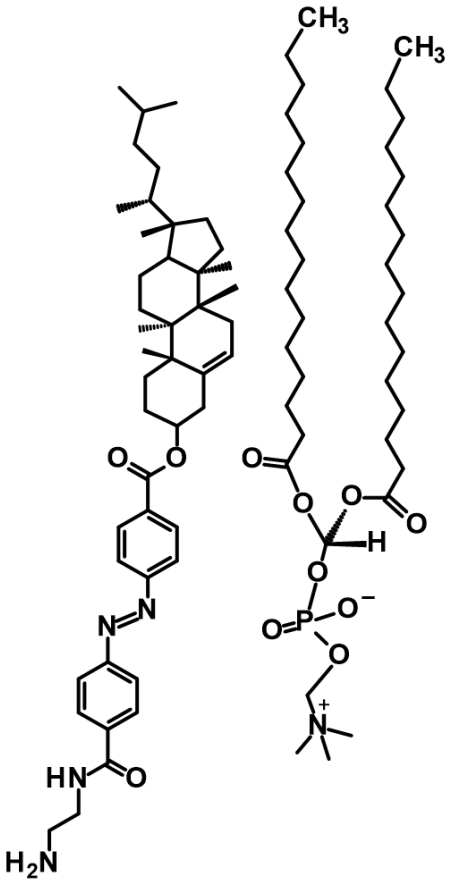

Fig. 3.5 Molecular structure of DPPC and Azobenzene-cholesterol.

there was no significant increase (less than $\Delta\Pi = 0.8\,\mathrm{mN\,m^{-1}}$) observed upon compression, the experiment was conducted. Otherwise the Langmuir trough was cleaned with special cleaning agent Tickopur R 33 (Dr. H. Stamm GmbH). When performing the SFG study, the monolayer was first compressed by the two barriers to reach a given surface pressure. The barriers were then halted, and an SFG spectrum was recorded.

3.4 Experimental Techniques

3.4.1 Sum-frequency generation spectrometer

A commercial EKSPLA SFG spectrometer based on a picosecond pump laser (PL2241A), a harmonic unit (PL2241A) and an optical parametric generator/amplifier/ difference frequency

generator (OPG/OPA/DFG PG 401) was used during the research. The fundamental 1064 nm beam with the pulse duration ≤ 35 ps at a repetition rate of 10 Hz has been generated by a Nd:YAG laser system. The beam diameter was about 8 mm and the pulse energy was between 30 and 40 mJ / pulse. The harmonic unit converted the fundamental radiation into the second and third harmonics of 532 nm and 355 nm wavelength by using potassium dihydrogen phosphate crystals. The pulse of the second harmonic with energies of about 600 μJ was used in SFG process. The fundamental and third harmonic beam pumped the OPG, equipped with a lithium triborate (BBO) crystal. The OPG/DFG unit generated the tunable IR-laser pulse with the aid of the fundamental and the third harmonic beam. According to the equation ($2\ \omega_{\text{pump}} = \omega_{\text{Signal}} + \omega_{\text{Idler}}$) a signal beam (420 - 680 nm) and an idler beam (740-2300 nm) is generated. The idler beam was used to generate IR radiation within the range of $2300 - 10000$ nm and 200 μJ pulse energies resulting from DFG process in a silver-galliumsulphide crystal. Other optics included: filter, mirrors, lenses, and glan prisms for shaping the beam profile and adjusting the probe energy, and for polarization control. A motorized sample stage with 6 axis (three translational and three rotational) enabled sample mapping. The layout of SFG spectrometer is given in Fig. 3.6. With spatial and temporal overlap of the 532 nm

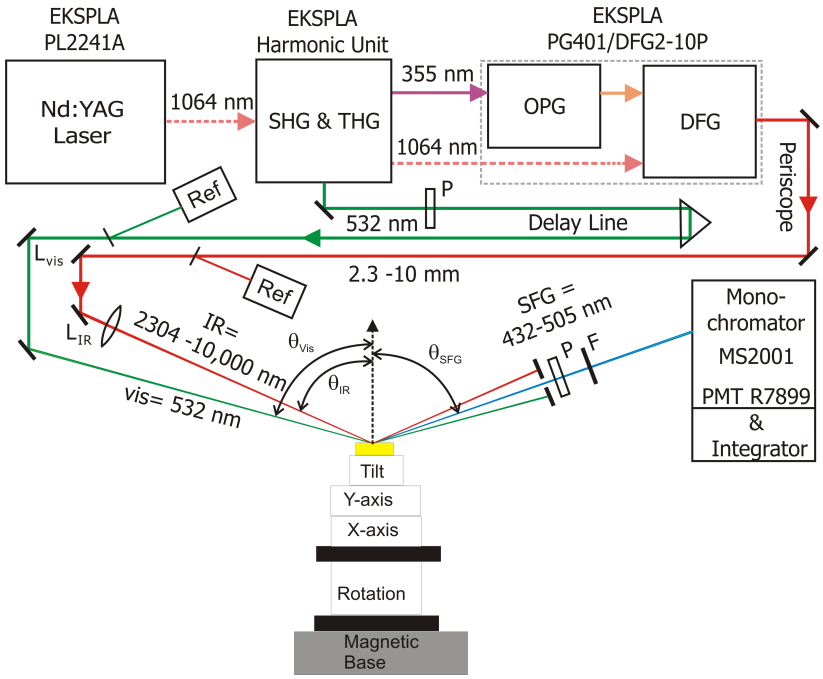

Fig. 3.6 Layout of SFG spectrometer used in our Lab [186, 198].

Vis and tunable IR incident beams at angles $\theta_{\text{Vis}} = 59^\circ$ and $\theta_{\text{IR}} = 53^\circ$ SFG beam at angle $\theta_{\text{SFG}} = 58^\circ$ was generated. For SFG signal detection, a monochromator MS2001 along with

a gated photomultiplier (R7899, Hamamatsu) was used. The control system on the PC was a *LabView* based user interface.

Gold surfaces are quite sensitive to high-intensity incoming light beams. To avoid damage of the substrate, an unfocused 532 nm beam of 160 μJ was used to avoid damage of gold surface. Typically the SFG signal intensity was averaged over 100 laser pulses for each data point. All spectra were measured in ssp polarization.

To ensure good and repeatable performance of the spectrometer, spectra of octadecyltrichlorosilane (OTS) on glass were recorded on daily basis.

In photoisomerization experiments, laser diodes at wavelengths of 365 nm and 455 nm (from Nichia corporation) were used for illumination of the SAMs. The output intensities of the 365 nm and 455 nm diodes measured by a power meter were 18 mWcm $^{-2}$, and 7 mW cm^{-2}, respectively, at the sample surface. For some experiments, an additional 532 nm diode with output intensity of 14 mW cm $^{-2}$ has been used.

3.4.2 SFG Spectra Simulations

As discussed in previous chapters, the interference between the resonant and non-resonant responses as well as between the different contributing vibrational modes can play a large role in the appearance of SFG spectra. Such interfering effects can be well understood by fitting the observed SFG spectra. However, fitting of SFG spectra is difficult, and great care must be exercised when making peak assignments [199, 200]. According to SFG principle (details given in chapter 2), the SFG intensity measured with a certain polarization combinations and an experimental configuration is a square function of effective second-order susceptibility [176].

$$I_{\mathrm{SFG}} \propto \left|\chi^{(2)}_{\mathrm{eff}}\right|^2 I_{\mathrm{IR}}\, I_{\mathrm{Vis}} \tag{3.1}$$

With

$$\chi^{(2)}_{\mathrm{eff}} = \left|\chi^{(2)}_{\mathrm{NR}}\right| \mathbf{e}^{i\varepsilon} + \left|\chi^{(2)}_{\mathrm{R}}\right| \mathbf{e}^{\mathbf{i}\delta} \tag{3.2}$$

Here the term ε refers to non-resonant phase, which is approximately invariant with IR frequency and depends upon intrinsic properties of the substrate. In contrast, δ is the resonant phase, which depends upon IR frequency. Being proportional to square modulus of $\chi^{(2)}_{\text{eff}}$, the resonant and non-resonant SFG signals do not simply add but rather interfere with each other. Therefore, the resonant peaks in the SFG spectra may appear unsymmetrical. The emitted SFG light intensity from the interface is:

$$I_{\text{SFG}} \propto \left|\chi^{(2)}_{\text{NR}}\right|^2 + \left|\chi^{(2)}_{\text{R}}\right|^2 + 2\left|\chi^{(2)}_{\text{NR}}\right|\left|\chi^{(2)}_{\text{R}}\right|\cos(\varepsilon - \delta) \tag{3.3}$$

Whereas the magnitudes of the first two terms are positive, the cross-term might have a positive or a negative value. A positive cross-term results from constructive interference giving rise to a positive peak. On the other hand, a negative cross term results from a destructive interference giving rise to a dip in the spectrum [201]. This inversion of peaks arises from the interference between resonant molecular vibrations and the non-resonant background from the substrate as shown in equation 3.3. In SFG experiments, only the phase difference $(\varepsilon - \delta)$ is measured directly. Non-resonant terms in the equation take a nearly constant values since ω_{Vis} is fixed. The resonant contributions $\chi^{(2)}_{\text{R}}$ arise from the molecular vibrations and essentially describe the frequency dependence of the SFG signal with respect to ω_{IR}. Since $\chi^{(2)}_{\text{R}}$ depends on the infrared frequency and vibrational frequencies as follows.

$$\chi^{(2)}_{\text{R}} = \sum_i \frac{A_i}{\omega_{\text{vi}} - \omega_{\text{IR}} - i\Gamma_i} \tag{3.4}$$

A_i is the amplitude oscillator strength, Γ_i is the Lorentzian line width of vibrational resonance (damping constant) and ω_{vi} is the vibrational frequency. Spectra in this thesis were fitted according to the standard SFG equation 3.4 by home-written software based on the number of vibrational modes and their corresponding peak positions using the program gnuplot. In a spectral fit, the resonances from vibration modes can be described by four parameters:

1. Position (resonance frequency ω_{vi})
2. Amplitude oscillator strength A_i
3. Line width Γ_i
4. Phase difference $\phi = (\varepsilon - \delta)$

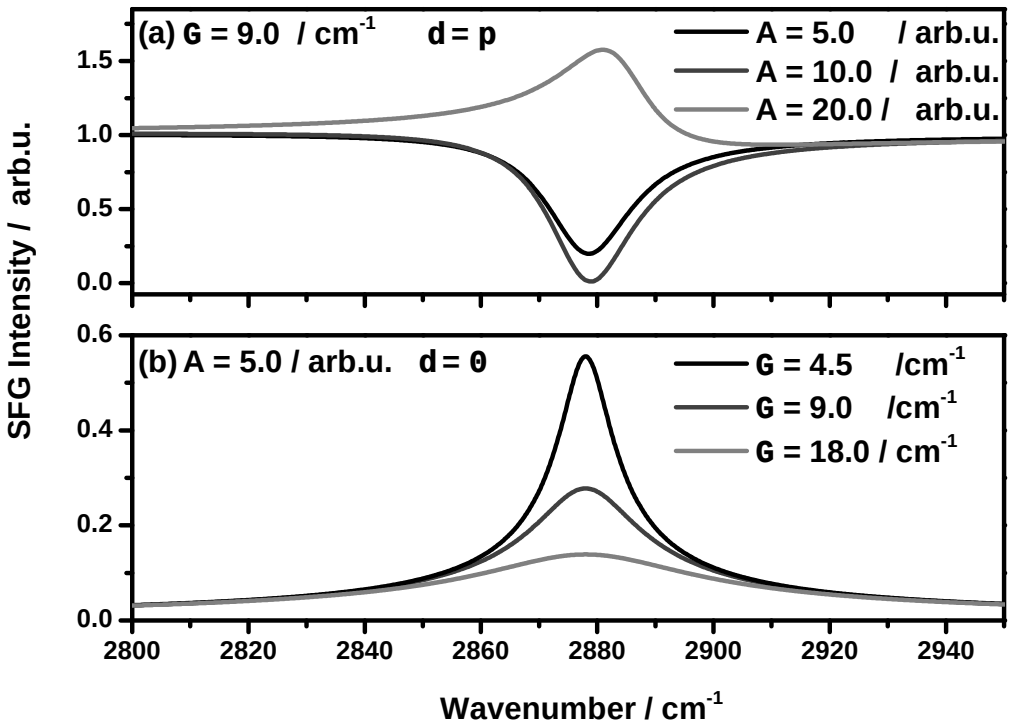

Fig. 3.7 Illustration of SFG signal behavior for different contribution of the parameters A_i, Γ_i, and δ in fitting spectra.

In an harmonic model, δ only takes values from 0 to π in other words, considering positive or negative signal contributions.

In order to simulate the spectra, several physical assumptions had to be considered:

- First, the assignment of individual vibrations is done by using data from literature of SFG spectra, IR vibrational spectra, Raman spectra, and normal coordinate analysis.

- Secondly, it can be assumed that the damping constant is same for vibrational modes arising from identical molecular groups.

- Thirdly, the resonance frequencies vary slightly around the known values from the literature (about 3 cm^{-1} i.e., the laser spectral resolution). Due to constructive/ destructive interference between resonant and non-resonant signals positive or negative SFG peaks appear in SFG spectra.

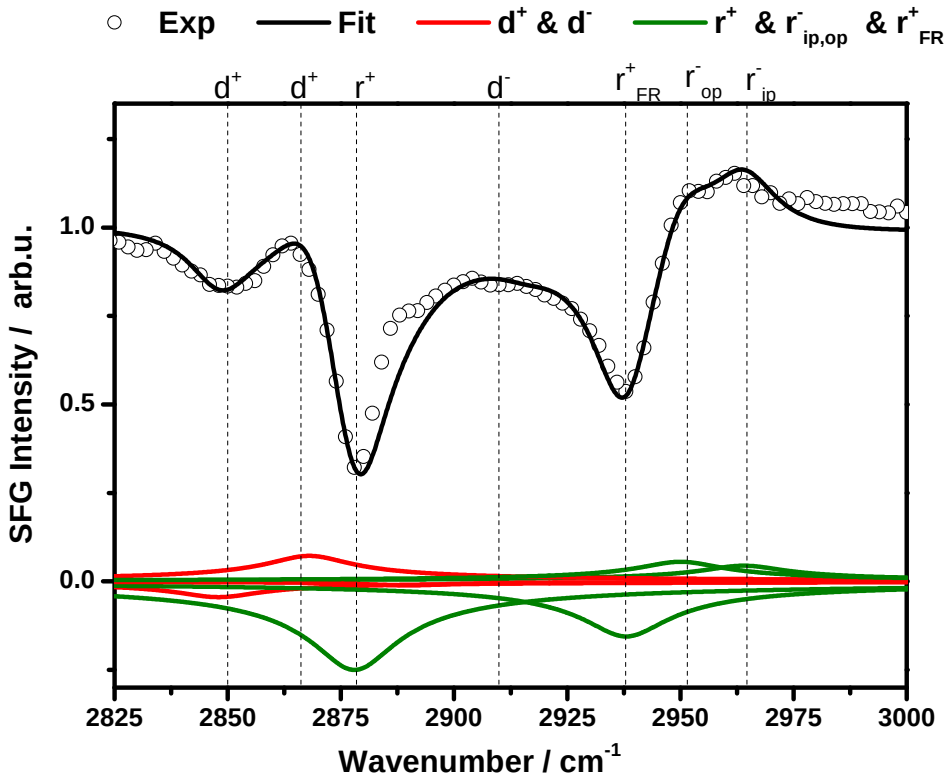

Fig. 3.8 Simulation of CH stretching region of an SFG spectrum of decanethiol on gold in ssp polarization. Example data and fitted curves are represented by open circles and curves, respectively. The assignment is in agreement with literature [32] and is further discussed in the (see chapter 2 and 4). r_{ip}^{-} is antisymmetric vibration in plane, where as r_{op}^{-} is antisymmetric vibration out of plane.

As discussed above A_i, ω_{vi}, Γ_i, and δ are adjustable parameters for simulation of SFG spectra. SFG signal behavior for the contribution of the parameters A_i, Γ_i is illustrated in Fig. 3.7 a and b. Here in Fig. 3.7 (a) SFG intensity is plotted as a function of IR wave-number for a peak 2880 cm^{-1} with $\delta = \pi$ and $\Gamma_i = 9$ at the different values of the A_i. Larger the A_i value more steeper the peak is but up to a certain limit. After this limit peak is inverted and become positive i.e., for $A_i = 20.0$ / arb.u. the negative peak at $\Gamma_i = 9$ cm^{-1} changed to a positive peak (gray line). In Fig. 3.7 (b) the simulated SFG signal is plotted as a function of IR wave-number at constant value of $A_i = 5$ for different values of Γ_i . The peak with $\delta = 0$ at the 2880 cm^{-1} is fitted in the figure. With larger Γ_i value steepness of the peak decreases.

In contrast to above discussion, the two parameters A_i, Γ_i are interfering with the two adjacent peaks. Table 3.1 illustrates the correlation of A_i and Γ_i for two adjacent peaks at wavenumber of 2880 cm^{-1} and 2868 cm^{-1}. If Γ_i of one of adjacent peaks (2868 /cm^{-1}) varies, the A_i of

both peaks changes. As a result adjustment of such parameters is very critical for simulation. A great care is required for simulating such peaks.

Table 3.1 Correlation between amplitude A_i and linewidth Γ_i for adjacent peaks.

Γ_i (2868) /cm^{-1}	Γ_i (2878) /cm^{-1}	A_i **(2868) arb.u.**	A_i **(2878) arb.u.**
4.5	9	0.4	4.0
9	9	1.3	4.5
18	9	2.3	4.7

For SFG spectral fitting in this thesis, A_i and ω_{vi} of equation 3.4 were used as potential/ adjustable parameter, whereas Γ_i and δ were kept constant when they characterize the same molecular vibration for samples of different surface concentrations. For each fit the initial A_i, ω_v, Γ_i were estimated and then the software was allowed to optimize all of these fit parameters. As an example, fit of SFG spectrum of decanethiol on gold is represented in Fig. 3.8. The spectrum is fitted by using seven resonance frequencies: For CH_3, the symmetric stretching mode (r^+), its corresponding Fermi resonance (r^+_{FR}), the out-plane antisymmetric stretch (r^-_{op}) and the in-plane antisymmetric stretch (r^-_{ip}). For the methylene group, the symmetric and antisymmetric stretches d^+, d^- vibrations are used [32, 160, 202]. The bottom peaks in Figure 3.8 show the fitted Lorentzians for these observed peaks. The red colored lines present the peaks for methylene group and green colored lines present peaks for methyl group vibrations. Set of parameters giving the best fit of the SFG spectra of decanethiol on gold is given in Table 4 in Appendix.

3.4.3 UV-Vis spectroscopy in present study

UV-Vis absorption spectroscopy was performed with a commercial double-beam and single-monochromator UV benchtop spectrometer (UV-2401 PC Shimadzu Corporation). The spectra of 1 mM solutions of the compounds were measured in a spectral range of 220 – 1100 nm using a quartz cuvette with the same solvent in the reference path.

UV spectra of SAMs were recorded with the same setup in transmission, using a hand-made holder. To obtain the spectra of the azobenzene SAMs, the spectra of bare gold substrates were measured as a reference. Gold exhibit strong absorbance band in the visible region (500 - 600 nm). The *trans-cis* and *cis - trans* photoisomerization in the samples was induced by irradiating the sample from the front side in the spectrometer with LEDs. The

photoisomerization experiments were carried out at room temperature. UV-Vis absorption spectra of the solutions and SAMs were measured before and after the irradiation experiments. In some experiments, the photoisomerization and the thermal relaxation of the samples under study were followed by time-resolved UV-Vis spectroscopy. The experimental process was followed by monitoring the temporal evolution of the peak absorbance corresponding to the π-π^* transition. The reverse $cis-trans$ isomerization was also observed by irradiation with 450 nm . The photo-switching could be repeated several times and the behavior was fully reproducible indicating that under the experimental conditions no significant degradation of sample took place.

Chapter 4

Azobenzene derivative on gold substrate

Pure and mixed monolayers of different thiols and azobenzene functionalized thiols on gold substrate have been probed by SFG. All the spectra in this chapter have been normalized with respect to I_{Vis} and I_{IR} intensities to account for variations and drift in the IR and visible laser pulse energies. Moreover, the averaged spectra were normalized to non-resonant substrate signal. The uniformity of the film was determined by measuring spectra at different spots. Similarity of spectra at different spots indicates the uniformity of prepared sample. All spectra are measured in *ssp* polarization. The SFG intensity is plotted as function of IR wavenumber, then corresponding spectrum is fitted by equation based on Lorentzian line shape equation 2.24 as described in chapter 2. Molecular systems studied are shown in Fig. 3.2 in chapter 3.

4.1 Reference spectra

For background signal and peak assignment of SFG spectra of a clean gold substrate, azobenzenethiol, and decanethiol have been recorded and analyzed.

4.1.1 Gold substrate

SFG signal from a clean gold (Au (111)) substrate was taken before any sample measurement. A typical non-resonant SFG signal from gold substrate is shown in Fig. 4.1.

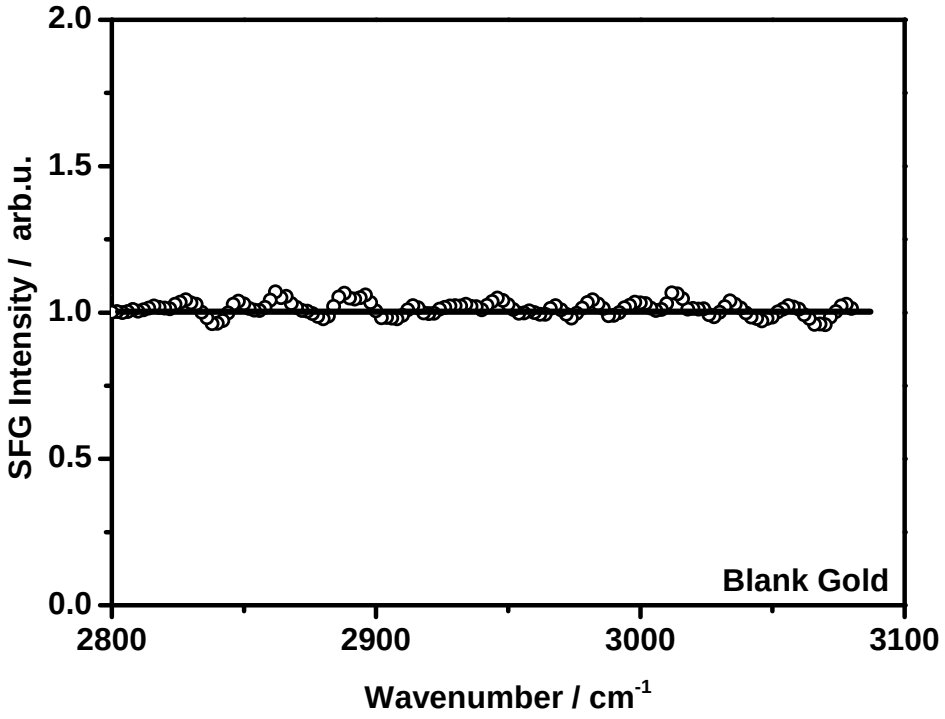

Fig. 4.1 Typical background-corrected, normalized SFG spectrum of a cleaned blank gold substrate.

The SFG signal from Au (111) is expected to show non-resonant background signal across the spectral range of interest [203]. No smoothing has been applied on the SFG spectrum of gold shown in Fig. 4.1. The spectrum looks noisy due to strong non-resonance background signals from the gold substrate.

4.1.2 Thiol and Azobenzenethiol

For the assignment of vibrational peaks from thiol co-ligands and AB moieties SFG spectra of decanethiol (C10S) (Fig. 4.2) and azobenzenethiol (AB-OC11S) (Fig. 4.3) have been

recorded for reference. Peak assignments for the spectrum were adopted from the literature [32, 160, 168, 202, 204–208]. The SFG spectrum of decanethiol shown in Fig. 4.2 has characteristic resonance features from CH_2 and CH_3 vibrations in a range of 2800 - 2970 cm^{-1}. Among these resonances, four peaks are assigned to methyl stretching modes: the symmetric stretching mode (r^+) at 2878 cm^{-1}, its corresponding Fermi resonance (r^+_{FR}) at 2938 cm^{-1}, the out-plane antisymmetric stretch (r^-_{op}) at 2950 cm^{-1}, and in-plane antisymmetric stretch (r^-_{ip}) at 2964 cm^{-1} [32, 160, 202]. Peaks at 2809 cm^{-1}, 2848 cm^{-1}, and 2868 cm^{-1} are assigned to the symmetric stretching modes of methylene groups and referred as (d^+) [32, 160]. The methylene d^+ peak at 2868 cm^{-1} appears as a positive peak, whereas 2848 cm^{-1} appears as negative which may be due to the different orientation of CH_2 groups. In the molecular structure, different types of methylene groups are present in the alkyl chain which may have different orientations [32, 209]. A peak at 2900 cm^{-1} assigned to antisymmetric stretching of CH_2 group (d^-), is fitted with very low amplitude in the spectrum and appears with negative phase, whereas CH_3, r^- yields positive peak, again indicating the different overall orientation of both groups in the monolayer. The assignment of the peaks is tabulated in Table 4.1. Overall CH_3 peaks are more dominant than CH_2 peaks in the spectrum indicating the fact that there is well-ordered monolayer of alkylthiol. In *trans* configuration CH_2 groups are centrosymmetric and thus SFG inactive (i.e., the SFG intensities canceled).

The SFG spectrum of AB-OC11S recorded in *ssp* polarization on gold is shown in Fig. 4.3. In contrast to the decanethiol spectrum, the spectrum has features of stretching vibration from the azobenzene unit at wavenumber above 3000 cm^{-1}. Three peaks at 2849, 2857 and 2868 cm^{-1} are assigned to methylene stretches (d^+) [32, 160], whereas the peaks at 2922 cm^{-1} is commonly assigned to the Fermi resonances d^+_{FR} [210, 211]. A peak at 2900 cm^{-1} as d^- is also fitted with small amplitude. Three peaks in CH vibrations range of $3052 - 3079$ cm^{-1} are assigned to the CH vibrations of phenyl group [168, 202, 205, 208]. Out of these three peaks, two peaks at 3053 cm^{-1}, 3071 cm^{-1} appear with negative phase, whereas peak at 3079 cm^{-1} has a positive phase with respect to the non-resonant gold background. The SFG spectrum of AB-OC11S is distinctly different from typical SFG spectrum of an alkylthiol. First of all because of the missing terminal methyl group but also the molecular surrounding of the methylene groups of AB-OC11S is different from that of decanethiol. In AB-OC11S there are at least three types of methylene groups. Among these: one is the CH_2 unit attached to sulphur (also present in alkylthiol) and another is attached to the oxygen of ethoxy group. The remaining CH_2 groups have other methylene group in their vicinity but it can be expected that the CH_2 groups on β-position to the oxygen / sulphur groups are also

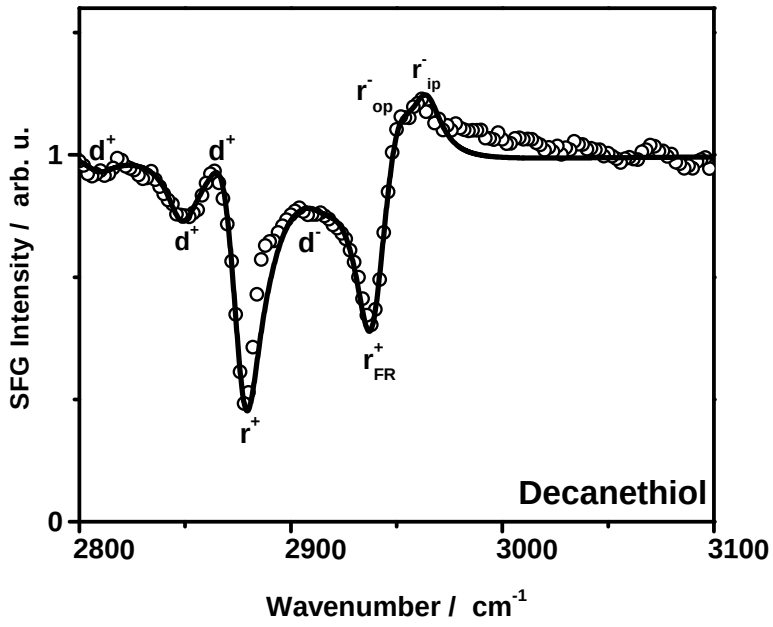

Fig. 4.2 SFG spectrum of decanethiol on Au (111) measured in *ssp* polarization.

spectroscopically different. The main difference, however, is the presence of CH resonances of phenyl group and absence of methyl stretch mode in spectra of azobenzene thiols.

Methyl substituted AB (MeAB-OC11S)

The MeAB-OC11S molecule has a CH_3 substituted azobenzene and CH_2 groups of the alkyl chain of the spacer in its structure. The SFG spectrum of MeAB-OC11S in Fig. 4.4 is markedly different from the spectrum of AB-OC11S and decanethiol. The MeAB-OC11S spectrum on gold has five negative peaks at $2875, 2922, 2993, 3024$, and $3057\ \mathrm{cm}^{-1}$, respectively, and three positive peaks at 2857, 2957, and $3071\ \mathrm{cm}^{-1}$, respectively. According to Hommel *et al.* [205] and Achtyl *et al.* [206] the symmetric stretching mode (r^+) of methyl group attached to a phenyl ring appears in the region $2915 - 2920\,\mathrm{cm}^{-1}$. Consequently, the strong negative peak in the SFG spectrum of MeAB-OC11S at $2922\,\mathrm{cm}^{-1}$ in Fig. 4.4 can be assigned to the symmetric stretch vibration of the CH_3 group [205, 206]. A weak negative peak also appears at this wavenumber, in case of AB-OC11S indicating the small contributions from CH_2 of C11 carbon alkyl chain as well. However, in case of MeAB-OC11S the peak is at least two times more intense than that for AB-OC11S, although both

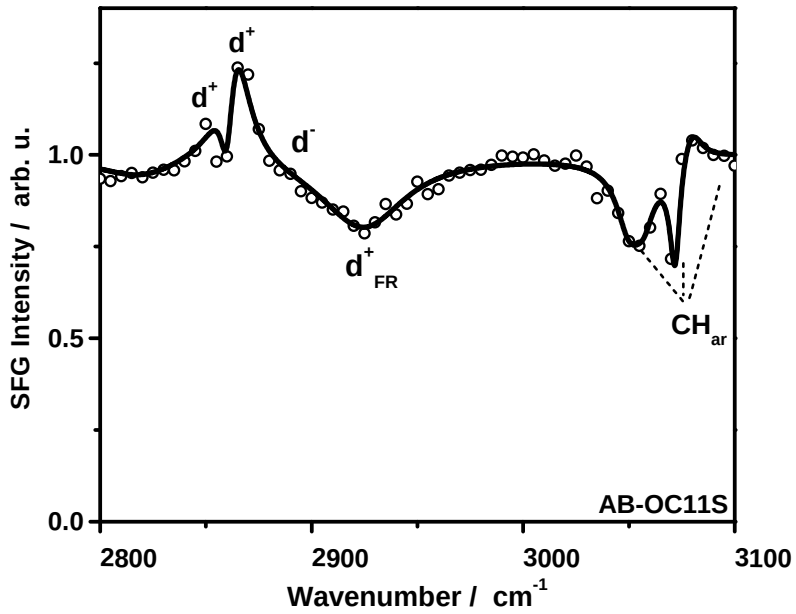

Fig. 4.3 SFG spectrum of AB-OC11S on Au (111) to show resonance signals for vibrational modes of CH_2 & $CH_{aromatic}$ in the CH vibrational region.

have same length of alkyl chain. So, the major contribution can clearly be attributed to CH_3. The negative peak at $2875\,cm^{-1}$ is assigned to the Fermi resonance of the stretching and bending mode or overtone of CH_3 stretching vibration or may be some combination band [205, 212]. Small contribution of d^- appears at $2901\,cm^{-1}$. The peaks at $2957\,cm^{-1}$ and $2993\,cm^{-1}$ correspond to out of plane and in plane antisymmetric stretch vibration of the methyl group [32, 205]. Three peaks in a range of $3025-3079\,cm^{-1}$ are assigned to the CH of phenyl group as in the spectrum of AB-OC11S [168, 202, 205, 208]. Similar to AB-OC11S spectrum, two out of three peaks at the $3025,\ 3053\,cm^{-1}$ are negative and one positive peak at $3071\,cm^{-1}$ (see Fig. 4.4). The spectral position of the CH stretches of the phenyl group of MeAB-OC11S is somewhat different from that of AB-OC11S because substitution on the phenyl ring may shift the vibration frequencies and the reduced symmetry may change the intensity pattern. All the spectra are shown in comparison in Fig. 4.5. Note that the spectra have been shifted by arbitrary offset to facilitate an easy comparison. Assignment of peaks is given in Table 4.2 while corresponding fitting parameter including the phase of peaks is given in Tables in the Appendix.

Table 4.1 Summary of peaks assignment of reference and probed SAMs in CH range.

Vibrational mode	**MeAB-OC11S** $\tilde{\nu}$ /cm^{-1}	**AB-OC11S** $\tilde{\nu}$ /cm^{-1}	**Decanethiol** $\tilde{\nu}$ /cm^{-1}
CH_3 (r^+)	2922	-	2878
CH_3 (r^-_{op})	2957	-	2950
CH_3 (r^-_{ip})	2993	-	2964
CH_3 (r^+_{FR})/comb/overtone	2875	-	2938
CH_2 (d^+)	2845	2857, 2868	2809, 2848, 2868
CH_2 (d^+_{FR})	-	2922	-
CH_2 (d^-)	2901	2900	2900
CH (aromatic)	3024, 3053, 3071	3053, 3071, 3079	-

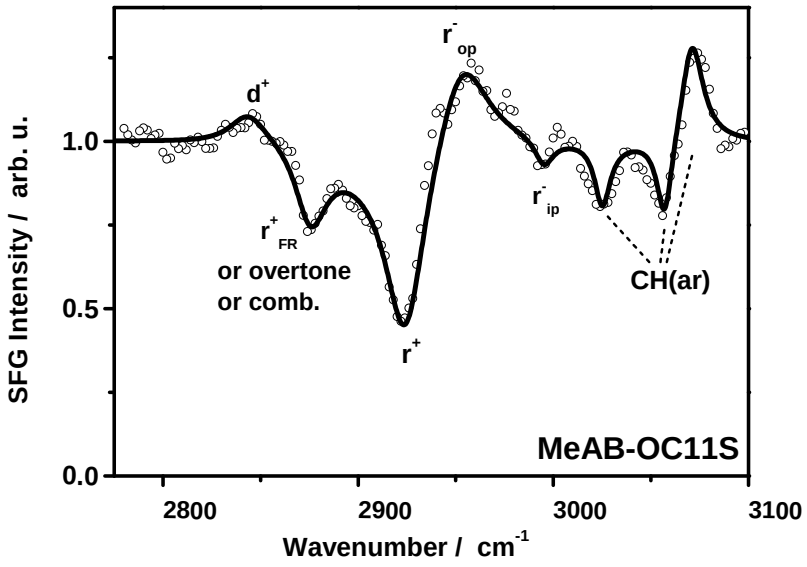

Fig. 4.4 SFG spectrum of MeAB-OC11S on Au (111) to show resonance signals for vibrational modes of CH_2, CH_3, CH(aromatic) in CH vibrational region.

Morphology of mixed monolayer

Photoswitching in SAMs is affected by steric constraints between neighboring chromophore molecule. In order to reduce the steric hindrance and provide free volume between chromophore molecules, mixed monolayers with alkylthiol co-ligand of different chain lengths, non-deuterated and deuterated ones were prepared.

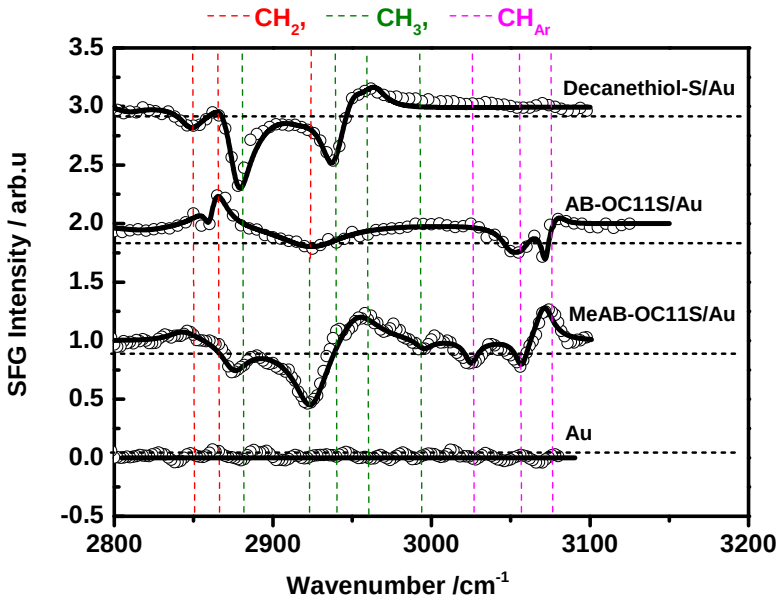

Fig. 4.5 Comparison of SFG spectrum of pure thiol monolayers on gold for Au, AB-OC11S, MeAB-OC11S, and Decanethiol. The normalized spectra have been shifted for clarity by units of -1, +1, +2 as indicated in the plot.

MeAB-OC11S/ Decanethiol monolayer

The spectrum of a MeAB-OC11S diluted with decanethiol is shown in Fig. 4.6. It has a number of peaks in CH vibration region that are characteristic of CH_2 and CH_3 group of MeAB-OC11S and of decanethiol. Actually, in the 50 : 50 mixed monolayer (MeAB-OC11S:C10S) the assignment of the peaks turned out to be very challenging as the resonance peaks of the CH_3 and CH_2 stemming for the vibration of decanethiol and MeAB-OC11S are overlapping. Keeping in mind that there should be contribution from both thiols in the CH vibration region, it was first tried to fit the spectrum as the superposition of two independent pure MeAB-OC11S and decanethiol spectra. Such superposition fit is represented by the green line in Fig. 4.7. As it is clearly visible in Fig. 4.7, that the fit does not describe the experimental data of the mixed monolayer. Consequently, in order to improve the fit, the peak positions were allowed to slightly shift and the resulting fit is given as a black curve in Fig. 4.7. The peaks are best fitted by slightly shift in wavenumber. The contributions of decanethiol and MeAB-OC11S in a 50 : 50 mixed monolayer have been labeled in more detail in Fig. 4.6.

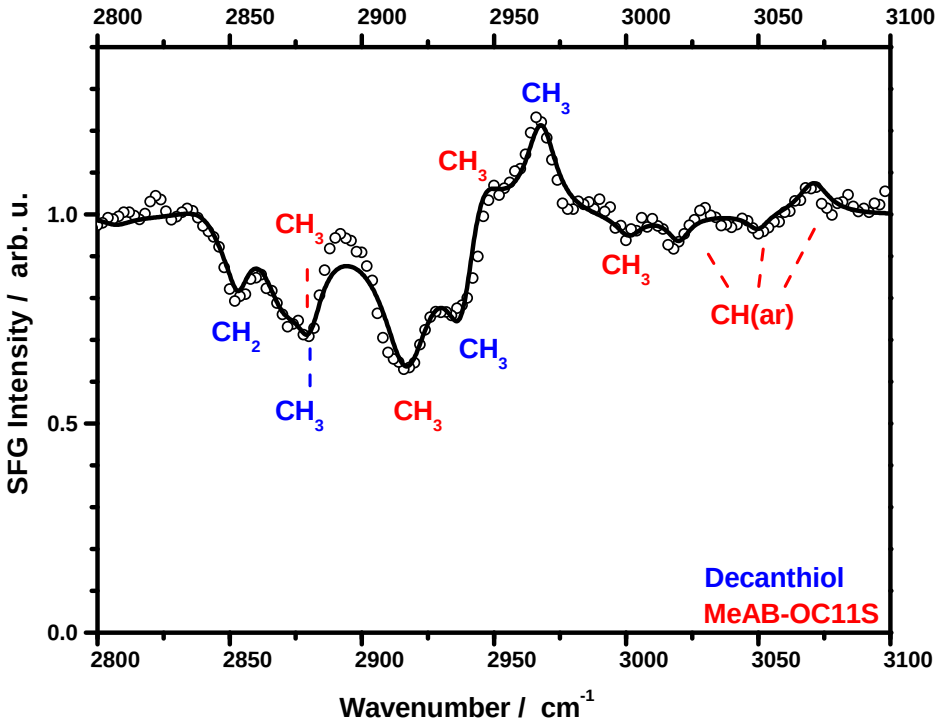

Fig. 4.6 SFG spectrum of mixed monolayer MeAB-OC11S:C10S in 50 : 50 mixing ratio. Peaks assignment is done by consulting reference spectrum of decanethiol and MeAB-OC11S.

The peak of the mixed monolayer at 2852 cm^{-1} is assigned to CH_2 symmetric stretch of decanethiol as it is present in reference spectrum of decanethiol at 2849 cm^{-1}. A negative peak at 2880 cm^{-1} is expected to yield from the contribution of CH_3 of both thiols as both have negative peaks at 2875, and 2878 cm^{-1}, respectively. Next, the negative peak at 2915 cm^{-1} is assigned to CH_3 contribution of MeAB-OC11S and at 2937 cm^{-1} is assigned to decanethiol. As already mentioned above, these two peaks are clearly visible in spectrum in contrast to superposition spectrum. Since the pure MeAB-OC11S has a positive peak at 2957 cm^{-1} due to antisymmetric stretch of its CH_3 group so the positive peak of the mSAM at 2941 cm^{-1} is considered as CH_3 contribution of MeAB-OC11S and the 2969 cm^{-1} has to be assigned as a contribution to the methyl group of decanethiol. Three peaks above 3000 cm^{-1} are from the aromatic CH of MeAB-OC11S. Contribution of CH_2 and CH_3 is summarized in Table 4.2.

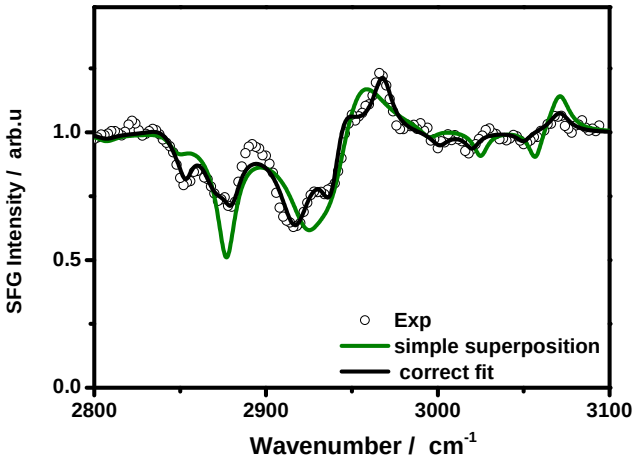

Fig. 4.7 SFG spectrum of mSAM for MeAB-OC11S and C10S in a 50 : 50 mixing ratio. Green spectra is fitted by superposition of the fit of pure MeAB and C10. Superposition fit (green) is different from the fit of experimental spectra (black circle) which is fitted by slight shift of peaks (black line).

Table 4.2 Summary of contribution CH_3 and CH_2 of MeAB-OC11S and decanethiol in mSAM of equimolar solution.

Vibrational mode	**MeAB-OC11S $\tilde{\nu}$/ cm $^{-1}$**	**Decanethiol $\tilde{\nu}$cm $^{-1}$**
CH_3	2880	2880
-	2915	2937
-	2941	2969
-	2999	-
CH_2	-	2852
CH(aromatic)	3020, 3055, 3071	-

In the case of mixed monolayers, it has been reported that phase separation may occur [213]. Phase separated domain of pure thiol and MeAB would not provide the free volume and hence spoil the aims of this study. If separated domains would be present, however, then it would be expected that the SFG spectrum of the mixed monolayer should be approximately given by superposition spectrum. This is obviously not the case. Hence the slight shift in the spectra of mSAM can be taken as indicator of the presence of mixed domains. Moreover, the peak shift indicates that the surrounding around the molecules in the mixed monolayer is different from the pure SAMs.

Morphology of MeAB-OC11S/ perdeuterated co-ligand monolayer

For better separation of vibrational features of MeAB-OC11S from that of the thiol co-ligand, the perdeuterated co-ligands, i.e., dodecanethiol (dC12S) and hexadecanethiol (dC16S) were used. Perdeuterated dodecanethiol (dC12S) or hexadecanethiol (dC16S) have vibration peaks of CD_2 and CD_3 stretching in the spectral range between 2000 and 2250 cm^{-1} [214]. The SFG spectrum of pure perdeuterated dodecanethiol (dC12S) is given in Fig. 4.8, whereas the peak assignment is outlined in Table 4.3.

Table 4.3 Peak assignment of perdeuterated dodecanethiol in CD range.

Vibrational mode	$\tilde{\nu}$ **/cm** $^{-1}$
CD_3 (r^+)	2079
CD_2 (d^+)	2100
CD_3 (r^+_{FR})	2130
CD_2 (d^+_{FR})	2158
CD_3 (r^-)	2220

The SFG spectrum of pure perdeuterated hexadecanethiol is very similar to dC12S and is given in Fig. 1in the Appendix.

Fig. 4.9 illustrates SFG spectrum of a mSAM for MeAB-OC11S : dC12S in a 50 : 50 mixing ratio. The spectrum shows CH resonances originating from MeAB moiety and CD resonances from perdeuterated co-ligand. The CH vibrational features of CH_3 and CH_2 of MeAB-OC11S moiety appear in the $2800-3100$ cm^{-1} spectral region, whereas the CD_3 and CD_2 of dC12S appear in 2000 - 2250 cm^{-1} region. As it was the case for the MeAB-OC11S/ Decanethiol monolayer, a shift in line position is also observed for mixed monolayer. The peaks at 2845 cm^{-1} and at 2903 cm^{-1} are assigned to d^+ and d^- of CH_2 group. Whereas peak at 2920 is assigned to r^+ of the CH_3 group. The SFG spectrum of monolayer with different compositions is given in Fig. 2 in the Appendix, and the corresponding fitting parameters are listed in Table 5 for the CH range and Table 8 for the CD range in Appendix.

The SFG spectrum of similar system of mixed monolayer having long chain co-ligand hexadecanethiol is shown in Fig. 3 and Table 9 in Appendix. The spectrum clearly shows the vibrational features of MeAB-OC11S and dC16 as well.

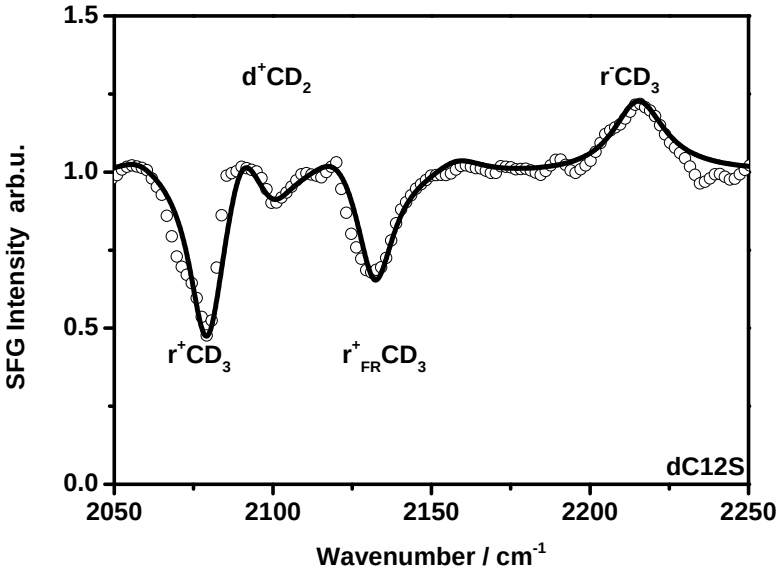

Fig. 4.8 SFG spectrum of a dC12S monolayer on Au (111).

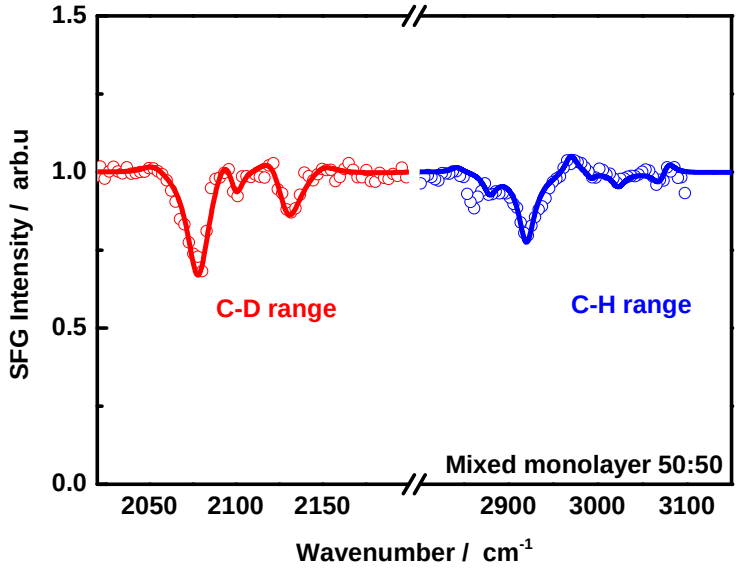

Fig. 4.9 SFG spectrum of 50 : 50 mixed monolayer containing MeAB-OC11S:dC12S.

4.2 Surface composition and structure

The SFG signal is sensitive to orientation and surface coverage (surface concentration of vibrating molecule on the surface). To investigate the composition and structural order of mixed thiol monolayers, the intensities of the methyl and methylene symmetric and antisymmetric stretch peaks in the SFG spectra are examined for the samples prepared from 1 mM thiol and at several successive lower concentrations of the immersion solution of thiol. Fig. 4.10 reveals a distinct change of the intensity of methyl symmetric stretch with decreasing MeAB-OC11S in the immersion solution. Here, it is important to mention that the ratio of the thiol in immersion solution used for surface functionalization does not necessarily reflect their exact ratio at the surface [215, 216]. Intensities of other peaks also vary with the concentration of the respective thiol in the immersion solution. As it is clear in Fig. 4.10 in CH range and Fig. 4.11 in CH as well as in CD range, peak intensities for CH vibrational modes (also revealed from amplitude of the peaks) decrease from 100% to 50% MeAB-OC11S in immersion solution, on other hand peak intensities of thiol increase. A similar trend is observed for all percentages from 100-0% of dC12S in C-D range in agreement to previous studies [100, 160]. Similar behavior is observed for MeAB-OC11S:dC16S in Fig. 3 in Appendex. Bain *et al.* [160] studied the SFG spectra of mixed monolayers of octadecanethiol and perdeuterated octadecanethiol on gold and silver. They found a linear relationship between the intensity of SFG peaks and composition of mixed monolayer. Valley *et al.* [100] also observed the same relationship between the amplitude of the resonant stretch signal of azobenzene moiety and percent composition of mixed monolayer. In contrast X-ray spectroscopy by Moldt *et al.* [101] revealed that the total number of thiolates in the SAM increases slightly by diluting azobenzene with alkylthiol.

The fits of the spectra of mixed monolayers indicate that peak intensities of the respective thiols are correlated with the concentration of immersion solution. Tables for all fitting parameters of vibrational resonances for several successive lower concentrations of the immersion solution of thiol are given in Tables in Apendix. In Fig. 4.12 relative intensities deduced from the spectral fitting parameter A (amplitude) is plotted as function of composition of immersion solution. This figure indicates that peak intensities for the co-ligand (dC12S) consistently decreases with decrease in its concentration in immersion solution, revealing the expected linear correlation of dC12S intensities with concentration of immersion solution. This behaviour represents the ideal mixing of alkylthiol, whereas different trend is observed for MeAB-OC11S spectra. Here, the decrease in signal intensity is not linear. The decrease starts earlier with dilution of MeAB moiety. This is clearly observable from the peak intensity

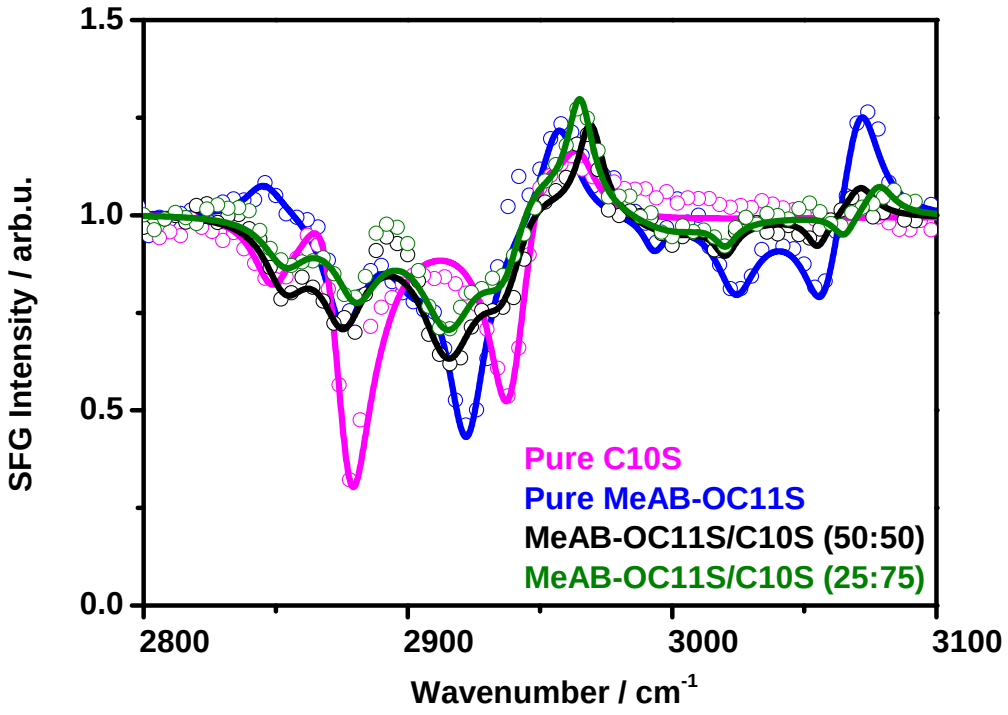

Fig. 4.10 SFG spectra of pure and mixed thiol monolayers of dC12 and MeAB-OC11S on gold.

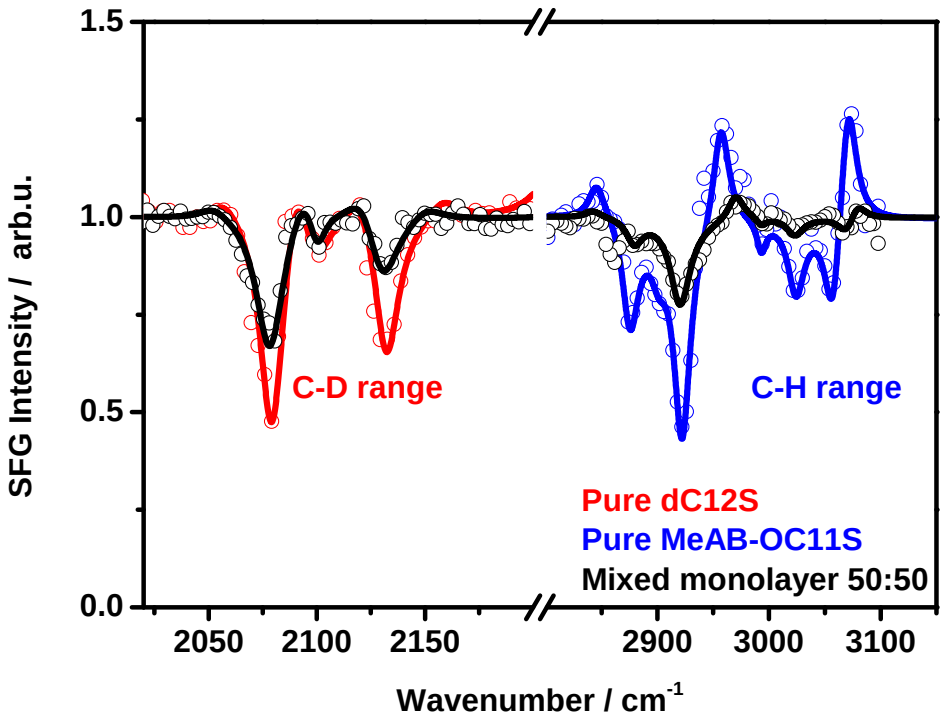

Fig. 4.11 SFG spectra of pure and mixed thiol monolayers of dC12 and MeAB-OC11S on gold.

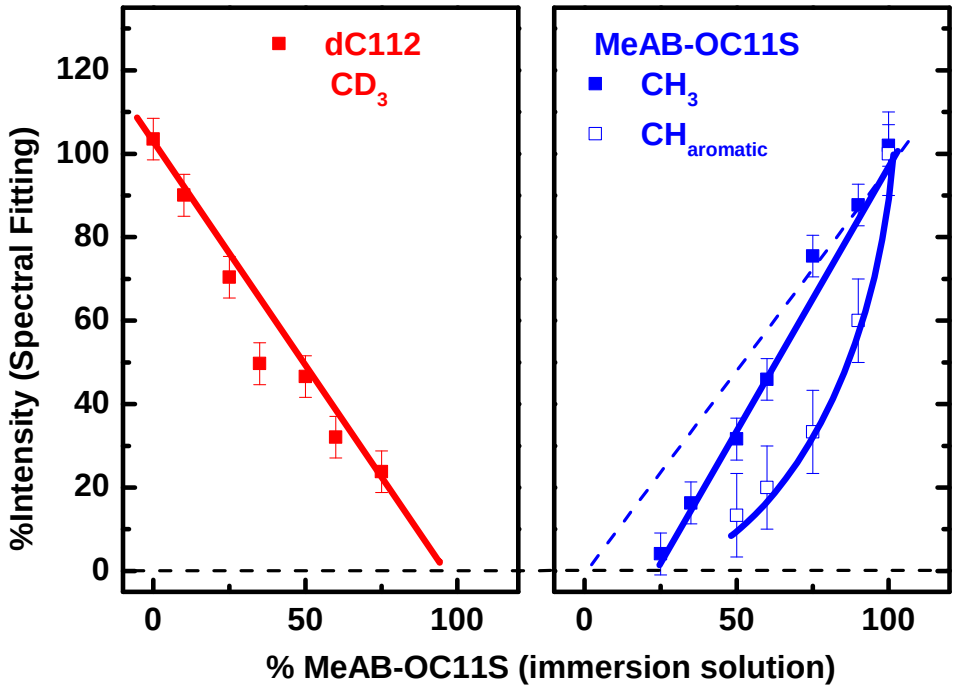

Fig. 4.12 Amplitude of CH_3, CH (aromatic) of MeAB and CD_3 of perdeuterated dodecanethiol in *ssp* polarized spectra as function of MeAB immersion solution used to form SAM. Loss of aromatic CH signals of MeAB on dilution is prominent as compared to CD_3 of perdeuterated dodecanethiol.

of CH $_3(r^+)$ and CH (aromatic) in Fig. 4.12. The curve with blue filled squares in the Figure reveals the loss of projection of MeAB group with respect to the surface. Whereas the curve with blue open squares may indicate the loss of chromophore-chromophore interaction of neighbor in the MeAB units. As it is described in Fig. 4.13, at higher MeAB-OC11S surface concentration there might be π-π stacking, whereas at intermediate surface concentration there is no π-π stacking but still an ordered structure with upright direction of AB moieties. Hence, the relative orientation of phenyl rings is lost leading to a significant loss of aromatic CH signals. Thirdly, at lower concentration, the MeAB units lost their upright orientation. Consequently, the loss of MeAB signal may be attributed to the fact that orientation of MeAB moiety changes from upright-standing position to a flat-lying position. This is in agreement with the fact reported by Moldt *et al.* [101]. They concluded from their data that orientation of the chromophores with respect to the surface normal changes from a tilted to an upright position with increasing azobenzene density. Their optical spectroscopic studies for planar

gold substrate and curved gold nanoparticle system revealed a pronounced excitonic shift with the chromophore density.

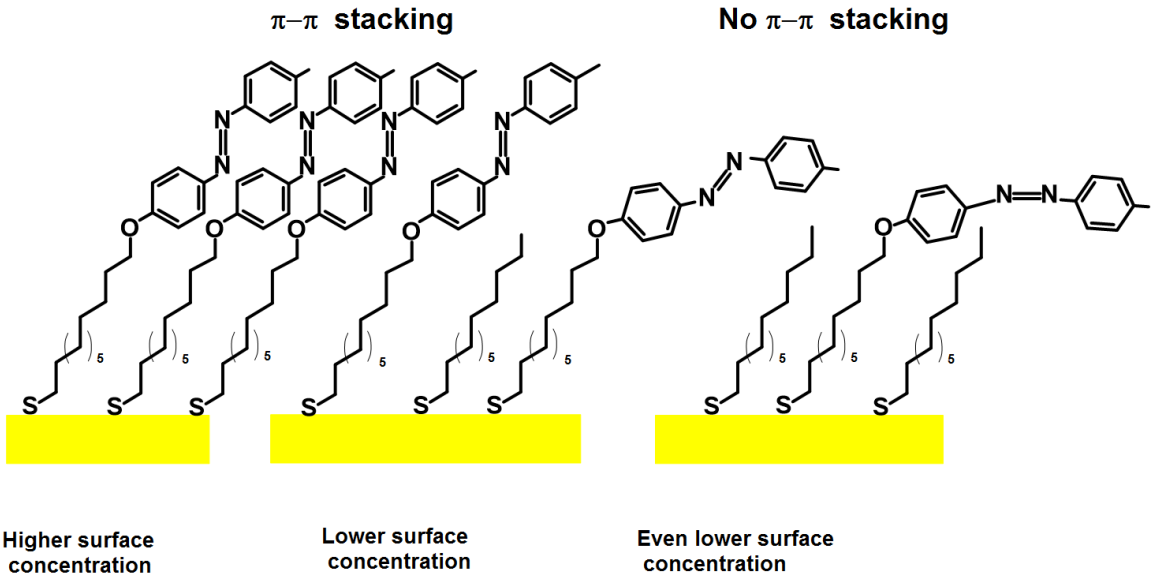

Fig. 4.13 Schematic drawings of the orientation of MeAB-OC11S for its different surface concentration.

The methylene CH_2 stretch is sensitive to conformation order of the alkyl chains in monolayer. CH_2 signal is only present when alkyl chain exhibit gauche defects in the chain. The number of gauche defects in the alkyl chain also affect the intensity of the methyl peaks, as a large number of gauche defects causes random methyl group orientation. Comparison of SFG spectrum of pure and mixed monolayer reveals that there is only one d^+ peak that can be clearly assigned to CH_2 groups at 2845 cm^{-1} in the pure monolayer, whereas in mixed monolayers there are two peaks; one in the range of $2845-2853$ cm^{-1} and the other in the range of $2860-2870$ as shown in Table 4.1 and Tables given in the Appendix. The data indicate that for diluted monolayers the number of shoulders for CH_2 stretching increases in the spectra. This reveals the fact that the larger number of molecules in pure monolayer are in *trans* conformation as compared to mixed monolayers. The amplitude ratio between CH_3 and CH_2 modes is an other parameter to infer the degree of conformational order for adsorbed alkyl chains. This methodology has widely been used by many groups to qualitatively assess the degree of conformational order of MeAB-OC11S at interface [165, 175, 178, 217–219]. As shown in Fig. 4.14 this ratio of amplitudes of corresponding CH_3 and CH_2 modes of MeAB-OC11S (taken from the fitting parameters given in Tables in Appendix) increases with dilution of thiol in mixed monolayer. The increase in this ratio is an indication of

conformational order of chains in monolayer [165, 219]. The r^+/r^- and r^+/d^+ ratios of the experiments are shown in Fig.4.14. In contrast to expectations these seem to be an increase of both ratios upon dilution. Note that the uncertainty in the fitting was quite large, in particular below 50% azobenzene content the relative error in the ratio was large. As the methyl group tilts away from the surface normal, the intensity of the r^- mode should increase, whereas the r^+ mode should decrease. In fact the intensities for the CH_3 symmetric stretches (r^+) are higher than for the CH_3 antisymmetric stretches (r^-) in the spectra of pure and mixed monolayer, however the ratio of the intensities for the symmetric and antisymmetric CH_3 stretches (r^+/r^-) calculated from the fitting parameter increases with dilution of MeAB-OC11S (see Fig. 4.14). However, within error limits this trend is not really robust. It may concluded that the spectra is not efficient to uncover the overall effect and/or that there is in fact not much in the structural orientation of the terminal CH_3 group down to surface dilution of about 50 %.

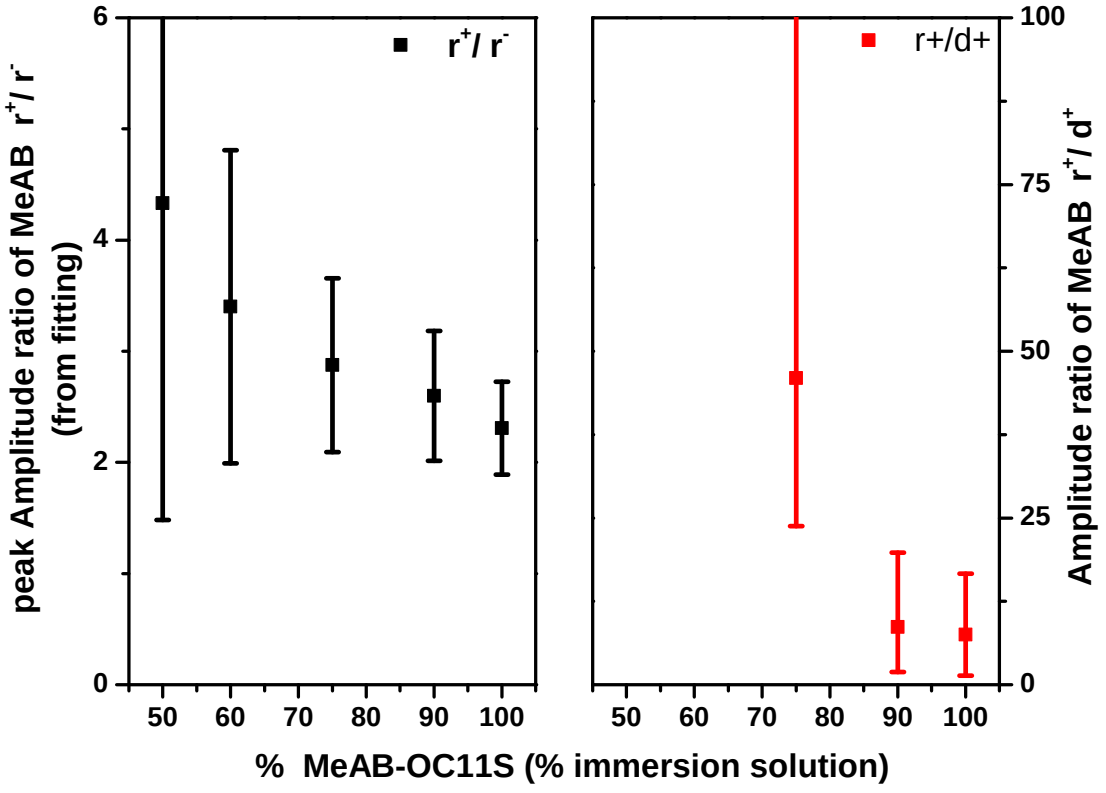

Fig. 4.14 Ratio of the amplitudes (left) for the symmetric and antisymmetric CH_3 stretches(r^+/r^-) (right) for the CH_3 symmetric stretch and CH_2 symmetric stretch (r^+/d^+).

4.3 Photoswitching

4.3.1 Photoswitching probed by SFG Spectroscopy

Having determined the structural properties of the MeAB functionalized SAMs on gold, these systems were finally subjected to photoswitching experiments. In such systems the azobenzene carries a methyl group at the para position of the phenyl ring which acts as a marker group for the position of AB moieties. To investigate the *cis–trans* isomerization of the azobenzene unit by SFG, the intensity change of r^+ stretching vibration occurring upon photo-irradiation was monitored. Photoswitching experiment was performed as follow:

1. SFG spectra measurement: The SFG spectrum of the sample was measured in the spectral region of CH stretch vibration. Terminal methyl and methylene of alkylthiol and azobenzene fuctionalized thiols are the primary source of signal in this region.

2. Switching experiment: The time dependence of the SFG intensities was recorded at resonance and reference wavenumber in repeated cycles with the sample irradiated with LED of 365 nm(on) or not irradiated (off).

3. After a waiting period or by following back-switching illumination with a 455 nm LED on, the SFG spectrum has been measured again to check if the sample has been damaged during the measurement or not.

Typically, light exposure with the 365 nm at photon dose of 4×10^{16} (number of photons, np) for $1-3$ minutes lead to an increase of the amplitude of the CH_3 (r^+). However, the overall change of the signal was small compared to the uncertainties in the spectral intensities. In fact the determination of exact changes of the signal intensities from the normalized spectra was very sensitive to the baseline correction. A normalized SFG spectra before and after illumination is also shown in Fig. 4.15. Nevertheless, in most cases the peak intensity of the negative r^+ peak decreased and peak intensities of positive r^- peak increased.

A better signal contrast could be obtained by repeated on-off cycle experiment. Such a time dependent behavior of MeAB-OC11S:C10S monolayers in $50:50$ is shown in Fig. 4.16, where the CH_3 signal intensity has been monitored at 2915 cm^{-1} wavenumber.

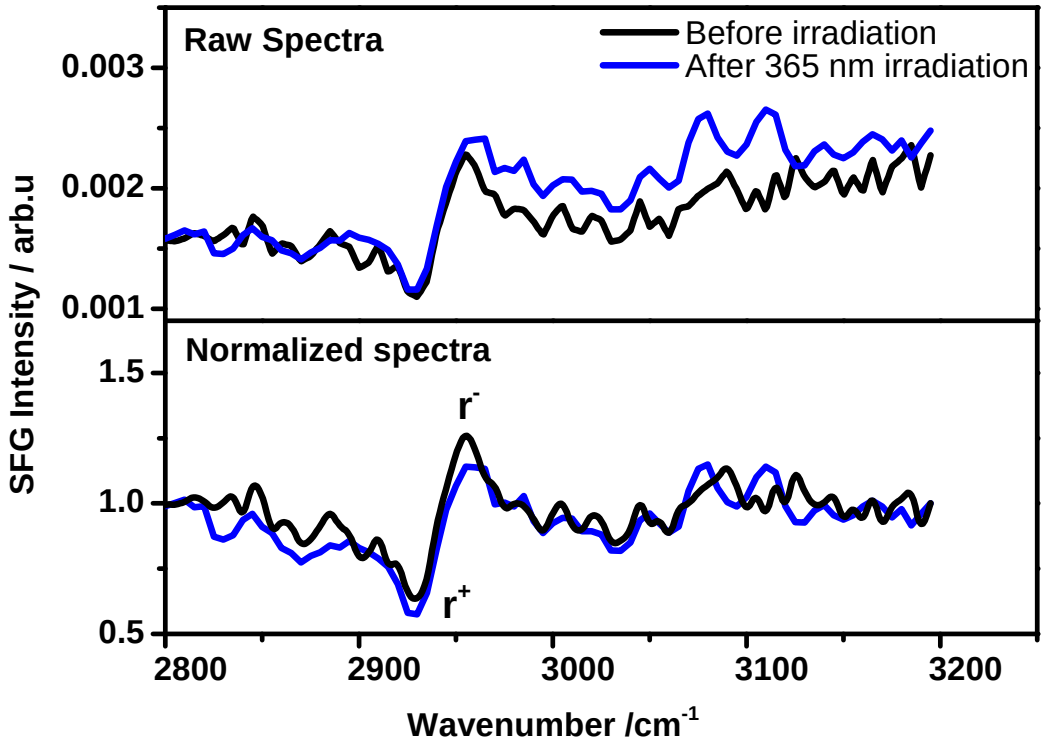

Fig. 4.15 Raw and normalized SFG spectrum before and after illumination.

The Figure depicts the photoisomerization experiment of an azobenzene functionalized sample and a unfunctionalized reference (gold) sample. Moreover, the signal behavior at wavenumber of 2600 cm^{-1} (where there is no CH_3 vibrational mode) is also shown in Fig. 4.16. No change for pure gold sample has been observed at 2600 cm^{-1} as well as at 2915 cm^{-1}. In contrast, a pronounced change in signal intensity of the functionalzed surfaces upon UV exposure has been observed. The changes in average signal for different samples are summarized in Table 4.4.

During these measurements, there is a change in signal intensity on non-resonant reference wavenumbers (where there is no CH_3 vibrational mode) with UV-illumination. So, the signal change cannot be totally attributed to the change in orientation of the marker group alone but has also contributions from the gold substrate. Probably, the background variations arise from changes in the strong non-resonant inter-band contribution from bulk gold upon sample heating and for structure damages in the monolayer. The pulse energy is mainly received

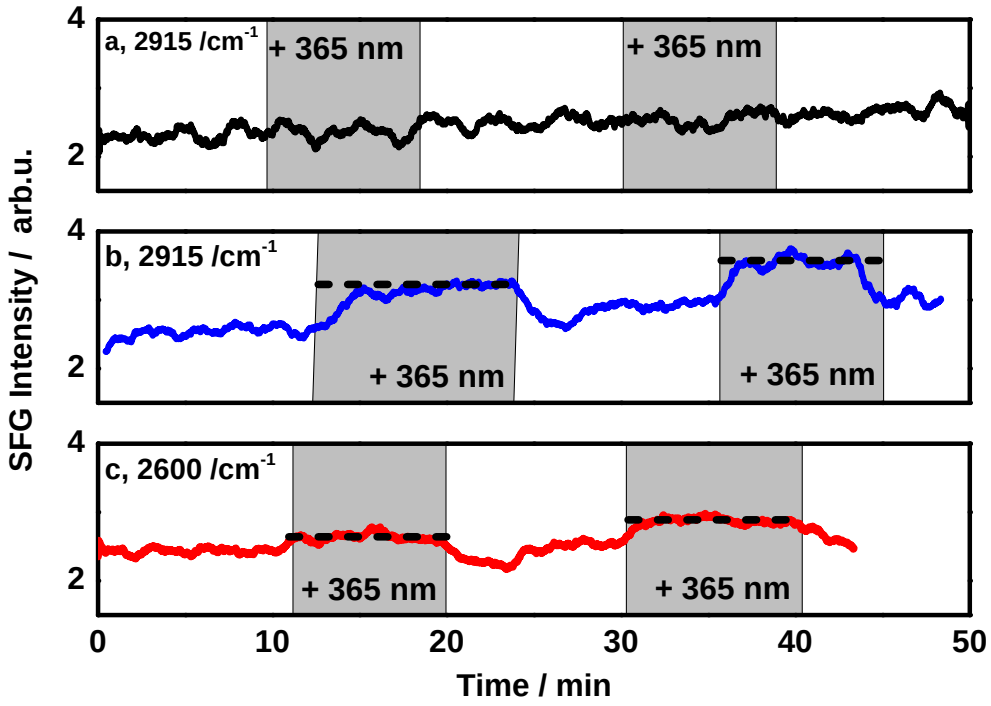

Fig. 4.16 Change in signal intensity upon illumination with 365 nm for a (a) pure gold and (b) mSAM with MeAB:C10 (50 : 50) at 2915 cm^{-1} (c) SFG signal of functionalized mSAM at 2600 cm^{-1} (non-resonant gold background), used for background correction of the observed signal change at 2915 cm^{-1}.

Table 4.4 Average signal change of resonance vibration (2915 cm^{-1}) for SAMs upon 365 nm illumination.

Monolayer	**Average signal change %**
Blank Gold	2.0 ±2.1
Pure MeAB-OC11S	7.5±3.1
Pure MeAB-OC10S	11.5±3.1
Short chain co-ligand C10 or dC12	7.7±3.1
Long chain co-ligand	3.3±0.4

by the electrons of gold. The excess energy of the hot electrons accounts for the dominant part of heat transfer from the gold surface to the monolayer. It has been reported, this strong non-resonant contribution cause amplification of SFG signals [220]. These effects are pronounced in functionalized surfaces as compared to pure gold surfaces. The heat transfer from the Au substrate into the SAM may cause thermal orientational disorder in the chain of organic coating and its structural state has an influence on the intensity of the non-resonant

background as well [221]. Keeping these factors in mind, the change in signal intensity measured on resonance needs to be corrected for changes in the non-resonant background. The change in signal intensity of the r^+ resonance vibration due to isomerization is evaluated

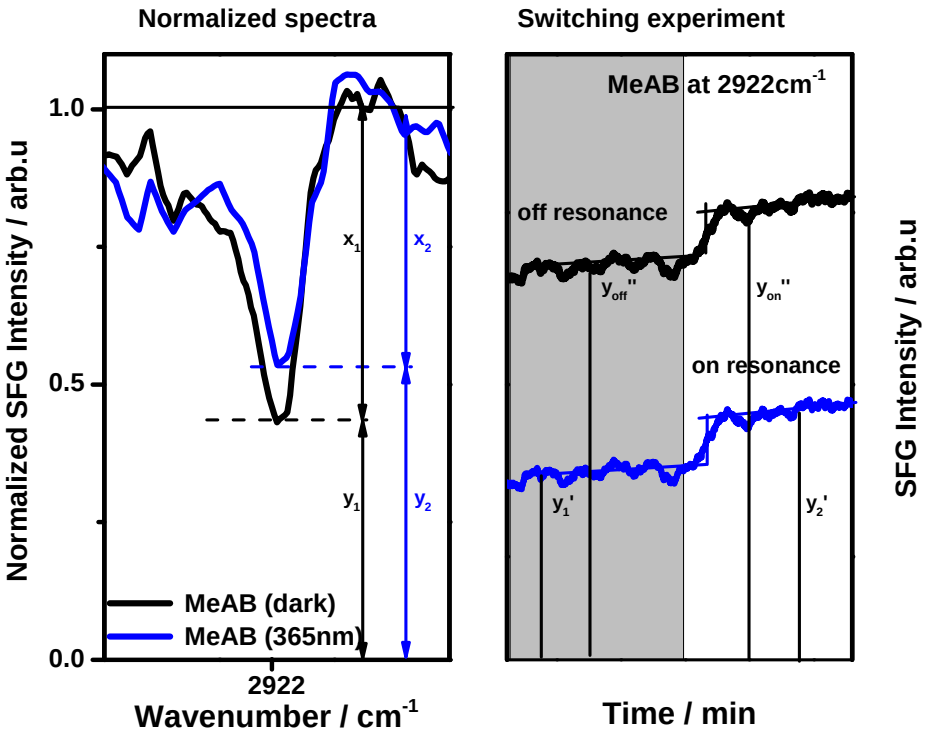

Fig. 4.17 Calculation of switching efficiency of functionalized surfaces taking into account background corrections.

by background correction which is explained in following steps as well as in Fig. 4.17.

Step 1

% signal change needs to be corrected by the measured off-resonance signal at reference wavenumber (i.e., 2600 cm^{-1}).

$$\frac{\%\text{ref change}}{100} = \frac{y''_{on} - y''_{off}}{y''_{off}} = \frac{y''_{on}}{y''_{off}} - 1 \tag{4.1}$$

on rearrangement, equation 4.1 becomes

$$\frac{\mathrm{y''_{on}}}{\mathrm{y''_{off}}} = \left(1 + \frac{\%\text{ref change}}{100}\right) = \mathrm{F} \tag{4.2}$$

Step 2

Light induced baseline offset is corrected by assuming that %reference change is wavelength independent. Hence an approximate correction can be applied by considering a correction factor F, assuming F is wavelength independent, and that the baseline offset behaves linear w.r.t total signal intensity. This mean all measured *y* values with the LED switched on can be corrected by

$$\mathrm{y''}_{on} = \mathrm{F.y''}_{off} \tag{4.3}$$

Step 3

Signal change obtained from switching experiment is

$$\frac{(\%\text{signal change})'}{100} = \frac{y'_2 - y'_1}{y'_1} = \frac{y'_2}{y'_1} - 1 \tag{4.4}$$

$$\frac{y'_2}{y'_1} = \frac{(\%\text{signal change})'}{100} + 1 \tag{4.5}$$

Step 4

From normalized spectrum, measured in the switching experiment, one would obtain

$$\frac{\%\text{signal change}}{100} = \frac{x_1 - x_2}{x_1} = \frac{(1-y_1)-(1-y_2)}{(1-y_1)} = \frac{y_2 - y_1}{1-y_1} \quad \Big| . \frac{1-y_1}{y_1} \tag{4.6}$$

$$\frac{1-y_1}{y_1}\frac{\%\text{signal change}}{100} = \frac{y_2 - y_1}{y_1} = \frac{y_2}{y_1} - 1 \tag{4.7}$$

The ratio $\frac{y_2}{y_1}$ from the spectra measurements should be equal to the corrected ratio $\left(\frac{y_2'}{y_1'}\right)_{\text{corr}}$ from the fixed frequency experiments. From equation 4.3

$$\left(\frac{y_2'}{y_1'}\right)_{corr} = \frac{y_2'}{y_1'.\text{F}} \tag{4.8}$$

$$\frac{1-y_1}{y_1}\frac{\%\text{signal change}}{100} = \frac{y_2'}{y_1{}'.\text{F}} - 1 \tag{4.9}$$

substituting the $\frac{y_2'}{y_1'}$ from equation 4.7 and F from equation 4.2

$$\frac{1-y_1}{y_1}\frac{\%\text{signal change}}{100} = \left(1 + \frac{(\%\text{signal change})'}{100}\right)\left(1 + \frac{\%\text{ref change}}{100}\right)^{-1} - 1 \quad \Big| . \frac{y_1}{1-y_1} \tag{4.10}$$

$$\frac{\%\text{signal change}}{100} = \frac{y_1}{1-y_1}\left[\left(1 + \frac{(\%\text{signal change})'}{100}\right).\left(1 + \frac{\%\text{ref change}}{100}\right)^{-1} - 1\right] \tag{4.11}$$

Calculated values are given in Table 4.5

Table 4.5 Calculated background corrected % signal change.

% Composition	**signal change %**
Pure MeABC10	4.7±1.2
Pure MeABC11	2.8±1.0
MeAB-OC11S + dC12	
90	8.9±4.6
75	2.9±1.0
60	4.5±2.4
50	6.1±1.0
35	7.4±7.4
MeAB-OC11S + dC16	
90	-0.2±1.9
75	0.1±1.9
60	0.4±0.9
50	0.0±2.4
35	11.0±4.5
MeAB-OC11S + C10	
50	7.4±16

Results given in Table 4.5 reveal that already the pure monolayer of MeAB-OC11S and MeAB-OC10S switches which was unexpected. This may be due to the fact that the monolayer is not densely packed. Some chains may be tilted toward the surface such that space is available for photoisomerization. Alternatively, monolayer molecules adsorbed on defects of gold surface may have been responsible for switching effect [222, 223]. In such locations, the molecules are more weakly bonded to the substrate or are loosely packed. For such substrates morphology may affect the molecular structure of monolayer, however, quantitative study relating SFG spectra and average defect density in SAMs are not available. The free volume of the azobenzene moiety to change its conformation is increased by dilution with simple thiol molecules. It was expected that dilution of the monolayer increases the switching efficiency of the mixed monolayers. The switching contrast of the substituted azobenzene monolayer has been calculated by procedure mentioned above and shown in Fig. 4.18. Overall, the SAMs show low switching efficiency contrasts, which can be attributed either to disordered structure of the monolayers or due to non-resonant signal contribution or to the fact that the switching process simply does not induce an overall change of structural orientation of SFG marker. Unfortunately, during the switching experiments it turned out that it was difficult to reproduce the switching behavior of a given mSAM composition. Often, sample damage occurred during the measurements, so that overall laser beam intensity

(particularly of the up conversion pulse) had to be reduced. This resulted in very low signal intensities, which made the experiments very challenging.

Simillarly Valley *et al.* [100] observed a decrease of 10 % SFG signal intensity upon illumination of azobenzene on polycrystalline gold using a cyano group as the SFG marker. In their case, 100 % azobenzene SAMs did not exhibit photoisomerization due to tight packing, but reversible switching was observed for the mixed SAMs with 34% and 50% of alkane thiol spacers. They also discussed that preferential orientation of $cis-isomer$ lead to 5% (per molecule per photon) quantum yield of photoisomerization in the monolayer on the surface being approximately one-half of that in solution i.e.,11%. The pure azobenzene SAMs did not isomerize in their case but isomerize in our case. Wagner *et al.* [117] also studied the reversible, photoinduced $trans/cis$ isomerization of an azobenzene-functionalized SAM using tripodal linker system on a gold surface with a cyano marker group and observed signal change upon UV irradiation and found 4×10^{-18} cm^2 effective cross sections for the reaction.

Another important information revealed in Fig. 4.18 is that switching contrast for mSAMS with long-chain co-ligand i.e, dC16 was low as compared to short chain co-ligand (i.e., dC12 or C10). The reason may be strong steric hindrance. This important finding will be discussed in section 4.4.

4.3.2 Photoswitching probed by UV-Vis Spectroscopy

To check if monolayers switch, photoswitching experiments were also performed by UV-Vis spectroscopy. UV-Vis experiments were performed as follows:

1. UV-Vis spectrum of the MeAB solution in ethanol, SAMs and pure gold sample were measured.

2. The spectrum of SAMs subsequently irradiated with 365 nm LED and then with 455 nm were measured.

3. The time dependent absorbance of the absorption band at 350 nm was measured in repeat cycles with the sample irradiated with LED of 365 nm for known time. Afterwards, irradiated with 455 nm to follow the back-switching.

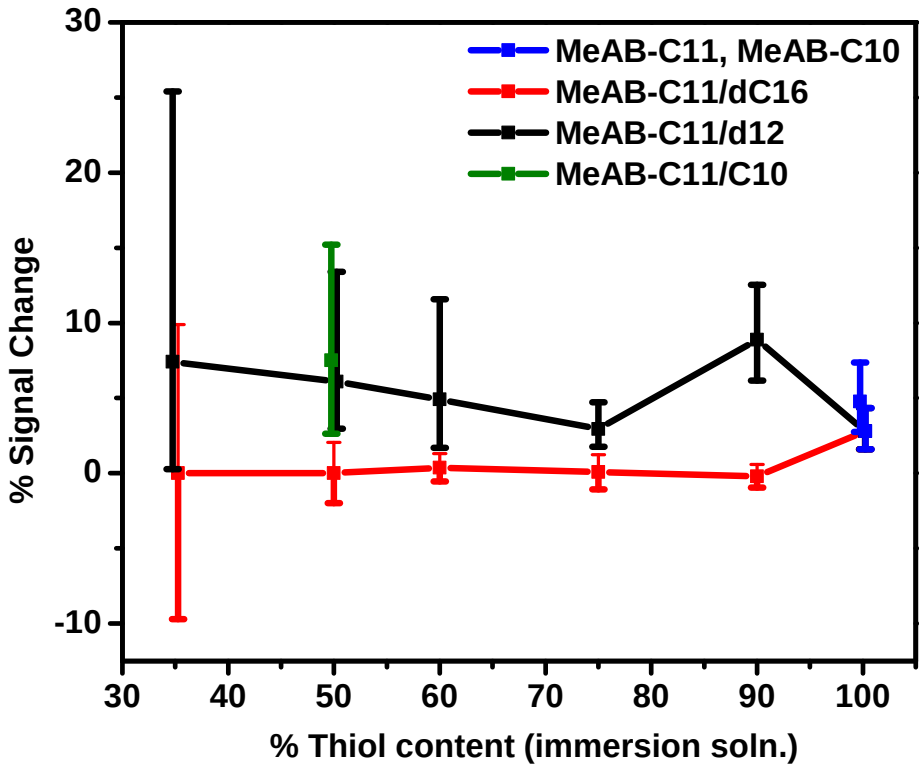

Fig. 4.18 Switching contrast of pure (blue) and mixed monolayer with short (green, black) and long alkyl chain (red) alkylthiol as co-ligand.

Fig. 4.19 shows UV-Vis spectra of MeAB-OC11 thiol solution in ethanol and its corresponding SAM on 10 nm polycrystalline gold. The absorption spectrum in solution showed two typical peaks at 350 nm and 450 nm that are due to π-π^* and n-π^* transitions. Upon irradiation with UV light (365 nm) the *trans* isomer switches to the *cis* isomer with photoefficiency of more than 95% in the photostationary state. The irradiation induces photoisomerization and leads to a decrease in intensity of π-π^* and slight increase in n-π^*. This can be monitored in the UV-Vis spectra by a decreasing absorbance of the $\pi - \pi^*$ band at 350 nm and an increasing absorbance of the $n - \pi^*$ band at 450 nm. The molar absorption coefficient for 0.036 M solution of MeAB calculated from Fig. 4.19 is 2.2×10^4 L mol^{-1} cm^{-1} at 350 nm for *trans* isomer. Fig. 4.19 shows the comparison of MeAB SAM difference spectra on gold with that in solution. Gold substrate has strong background in UV-Vis region, nevertheless, the change in $\pi - \pi^*$ band at 350 nm illumination can be identified. From the difference of

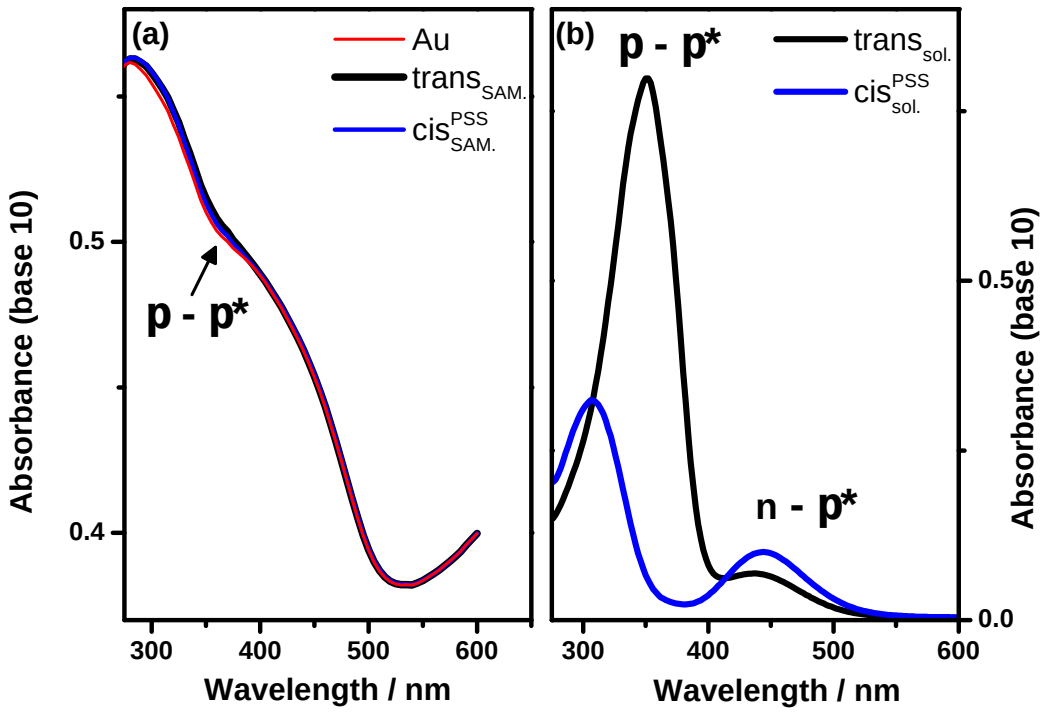

Fig. 4.19 (a) UV absorption spectra of MeAB thiol SAM on gold in comparison with gold substrate. (b) Absorption spectra of 1 mM thiol solution in a 1 cm cuvette.

the spectra of pure gold and the functionalized gold the surface coverage can be estimated. Surface coverage for SAM is calculated from Fig. 4.19 and is given as follows:

A = 4.4×10^{-3} and $\varepsilon = 2.2 \times 10^{4}$ L mol^{-1} cm^{-1} assumed to be the same as in solution

$$A = \varepsilon c$$

c is surface concentration in mol/cm^2 with $c = 1.99 \times 10^{-10}$ mol/cm^2.

This corresponds to $cN_A = 1.2 \times 10^{14}$ molecules / cm^2 or surface area of 83 Å^2 per molecule. Typically a densely packed monolayer has a surface area of 25 Å^2 per molecule [224–226]. In Fig. 4.20 change in intensity of the $\pi - \pi^*$ band at 350 nm and n-π^* at 450 nm upon illumination for SAMs as well as for solution is shown. For the monolayer the change of $\pi - \pi^*$ absorption band for SAM is 2×10^{-3}, indicating that the switching efficiency for such SAM is 50% . After the illumination with 455 nm , the absorbance yields limited value ,hence the switching is 100% reversible.

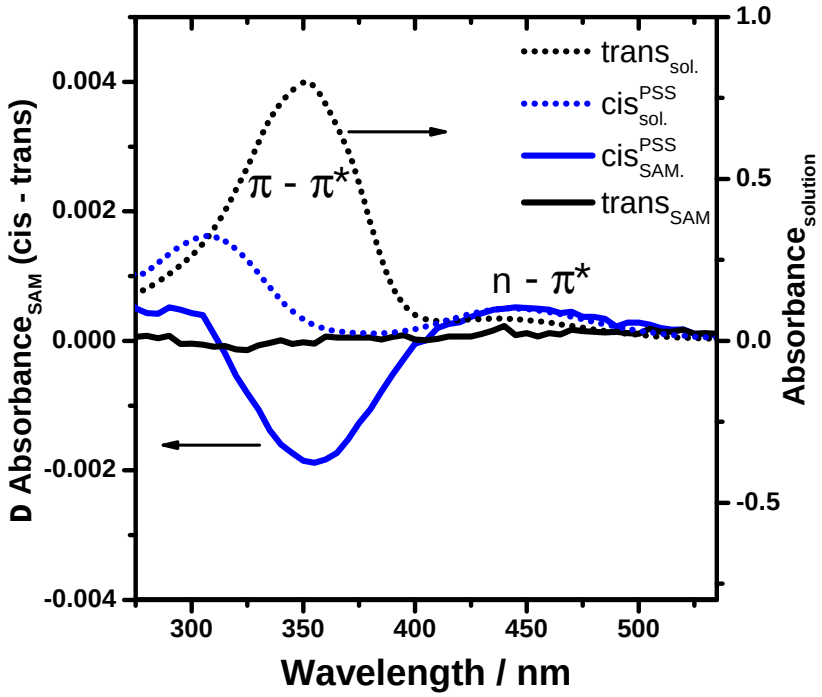

Fig. 4.20 comparison of switching properties of MeAB SAM with corresponding solution.

Time dependent measurements for the photoisomerization were performed by monitoring the absorption band at a fixed wavelength of 350 nm for monolayers on gold as shown in Fig. 4.21. In such experiment, first the sample was irradiated by 365 nm UV light and then followed by 455 nm blue light until a photo-stationary state was reached. During the light illumination there were instantaneous jumps of the signal. These jumps were caused by stray effects and have been removed in the presented data. In the experiments absorbance changed from 0 to 8×10^{-4}. This change was highly reversible and reproducible.

UV back isomerization dynamics

UV-Vis transmission spectra of pure MeAB-C10 monolayers on 10 nm thin polycrystalline gold revealed good switching properties with highly stable *cis* layers, even more stable than in solution. But three times constants $\tau_1 = 5$ min, $\tau_2 = 50$ min, and $\tau_3 = 17$ h have been observed, as shown in Fig. 4.22. These time constants are calculated from time dependent measurements of solution and SAMs by using a tri-exponential fit equation.

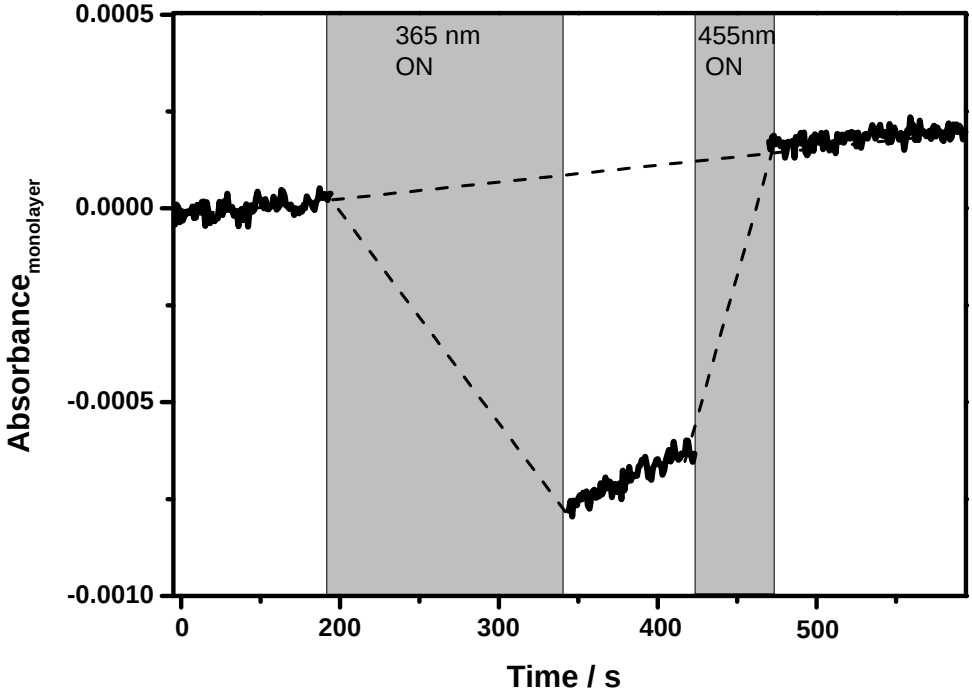

Fig. 4.21 Photoisomerization measurement of the absorption change at 350 MeAB-OC10S SAM upon UV and blue light irradiation.

For the SAM systems initially the back isomerization is fast with a short time constant. Unexpectedly, the process is retarded as described by the second time constant ($\tau_2 = 50$ min). This may be indicating different domains that switch with different probabilities. Whereas for solution single time constant $\tau_1 = 33$ min (see Fig. 4.22) have been observed. The *cis-trans* isomerization at different illumination wavelengths as a function of time is shown in Fig. 4.23. The time constant for the process is calculated from the fit of Δ absorbance verses time for each wavelength. The photo efficiency of switching process describes the constant k at different wavelengths and then calculated by taking account the power P of the respective LEDs.

$$\Delta A = \Delta A_0 \exp(-\frac{t}{\tau}) \tag{4.12}$$

$$\frac{1}{\tau} = kP \tag{4.13}$$

$$= \Delta A_0 \exp(-kPt) \tag{4.14}$$

The calculated parameters are tabulated in Table 4.6.

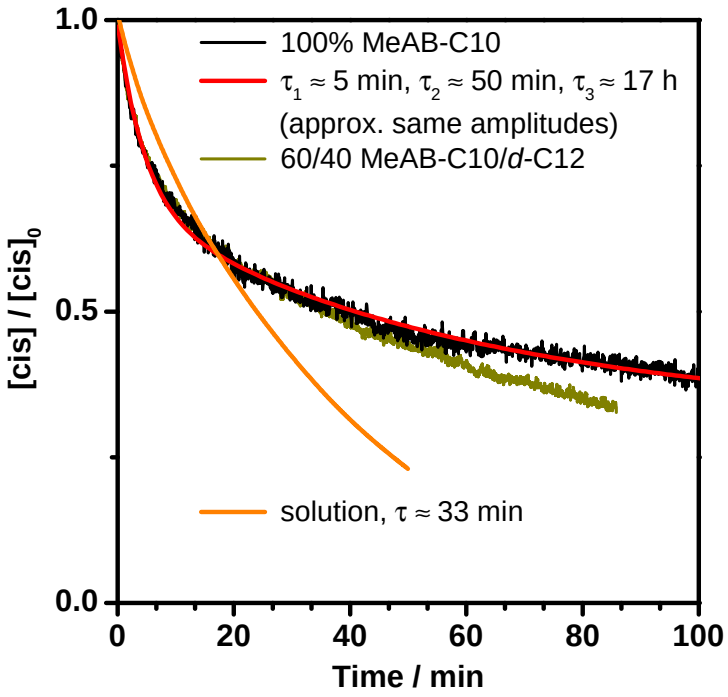

Fig. 4.22 Thermal back isomerization of *cis* to *trans*. Data are fitted by a tri exponential equation to determine the time constants for the process.

Table 4.6 Time constants for photoisomerization monolayer on gold when illuminated with three diodes of different wavelengths.

LED λ/ nm	365	455	530
P /(mW /cm^2)	25	9.3	2.7
τ /s	3	15.6	259
k / s mW/cm^2	75	145	700

Note that during SFG measurements 532 nm up-conversion pulse may induce backisomerization.

4.4 Photoisomerization for co-ligand of different chain length

The switching property of azothiolates with long alkylthiolate co-ligands dC16 as well with short alkylthiolate co-ligands C10, dC12 is also compared. As the used photoswitches have a

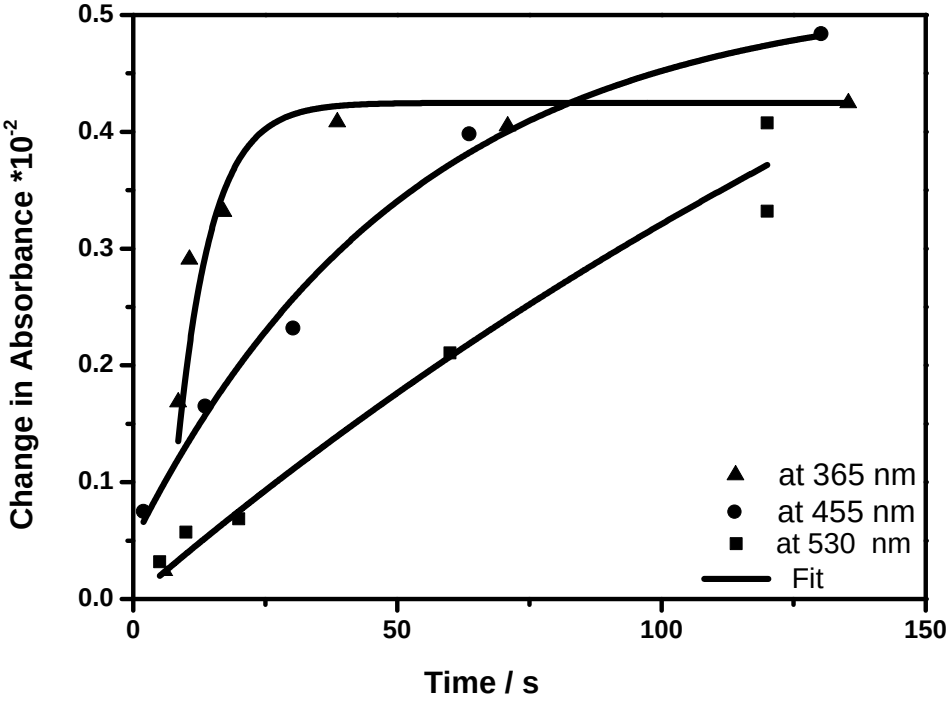

Fig. 4.23 *cis-trans* isomerization as function of time at different illumination wavelengths.

chain length of 11 carbons, the co-ligand with 10 and 12 carbons reach up to the benzene ring of the azo-moiety, whereas the co-ligand C16 reaches above the benzene unit. Therefore, it is expected that the dC16 co-ligand causes strong steric hindrance, whereas the mixed SAMs with 10 and 12 should switch more efficiently. As already mentioned, the SFG studies reveal that mixed monolayers with short chains show more pronounced switching effects as compared to the ones with long chain co-ligands (see Table 4.4 and Fig. 4.18). Steric hindrance within these monolayers is assumed to be the main reason of low switching with dC16 as co-ligand. UV-Vis analysis also depicts that the mixed monolayers with the short-chain co-ligands yield higher absorbance change opon irradiation. This is shown in Fig. 4.24. About the same change in absorbance was observed for pure monolayer and the mSAM with dC12 co-ligand. Whereas mSAM with short chain co-ligand (dC12S) exhibits more absorbance change on irradiation as compared to the mSAMs with the long chain co-ligand (dC16S).

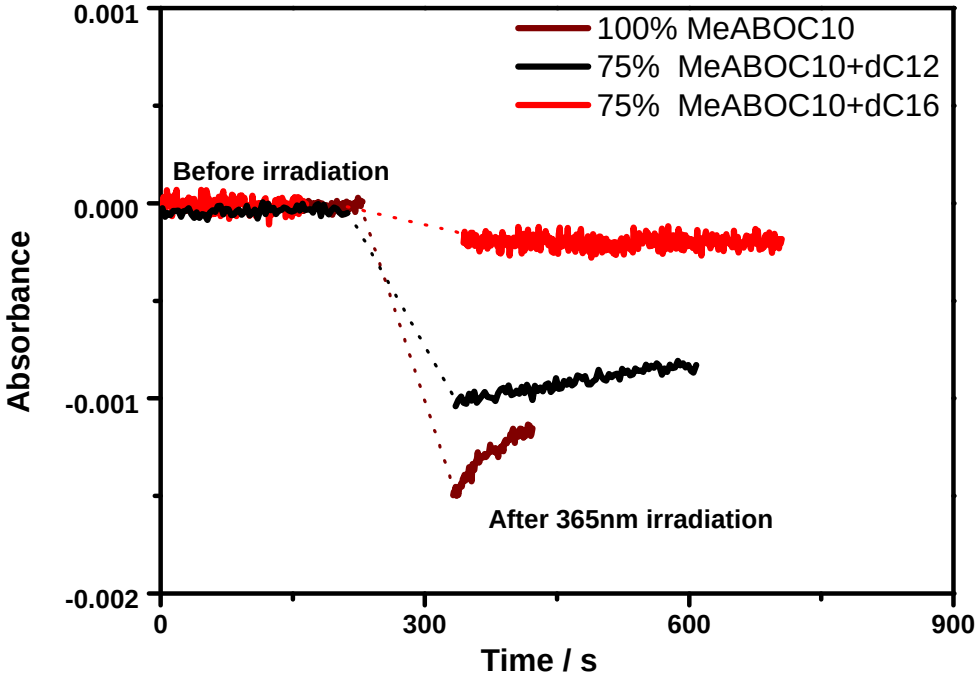

Fig. 4.24 Effect of the co-ligand on the photo switching properties of mixed monolayers. Whereas change in absorbance upon UV illumination is about the same for pure monolayer and the MeABC10/ dC12 layer, it is significantly reduced for the MeABC10/ dC16 monolayer.

4.5 Even-Odd effect

An even or odd number of methylene groups in the alkyl chain influences the orientation of end group in monolayer, this is called Even-Odd effect as discussed in section 2.2. Monolayers with sufficient packing density and molecular length form ordered structures whereas the backbones of the molecules are tilted in a certain direction. Consequently, the direction of the terminal methyl group of alkyl chain or SFG marker group for MeAB thiol tends to the surface normal or the surface parallel depending on the alkyl carbon number [227–230]. Porter *et al.* [230] found that the structure of SAMs is dependent on the length, short chains $(n < 12)$ exihibit a disordered structure and highly ordered structure for long chains $(n > 12)$. Using XRD, Fenter *et al.* [231] reported that the tilt angle for short alkanethiols $(10 \leq n \leq 14)$ was larger compared with long ones $(n \geq 14)$. They also reported that short molecules were tilted closer towards their nearest neighbor, whereas long ones were

closer towards their next nearest neighbor. W. Azzam [232] reported that Oligo-para-phenyl substituted alkanethiols with an odd number of methylene units achieved a higher packing density and a smaller inclination of the phenyl groups compared to thiols with an even number of methylene units. In other words, the orientation of the phenyl backbone in the former case was almost perpendicular to surface.

Even-Odd effects induce corresponding odd-even alternation in various chemical, physical, and interfacial properties of self-assembled monolayers. In order to see if an even-odd effect of azobenzene of variable alkyl chain length can be observed, the SFG spectrum of MeAB-OC10S and MeAB-OC11S have been monitored. Comparison of the intensities and the corresponding fitting parameters are given in Fig. 4.25 and in Table 2, respectively. The comparison of symmetric and antisymmetric vibration stretch of the methyl group shows that the amplitude of r^+ is slightly higher for MeAB-OC10S than for the amplitude of r^+ of MeAB-OC11S. Whereas the intensity of r^- mode in MeAB-OC11S is higher than MeAB-OC10. This feature is well known for the odd–even effect. Nishi *et al.* [189] studied the structure of self-assembled monolayers of n-alkanethiols using broad-band sum frequency generation spectroscopy and reported that intensities of r^+, r^+_{FR} mode are higher and intensities of r^- are lower for odd number of alkyl chain. As discussed before, the

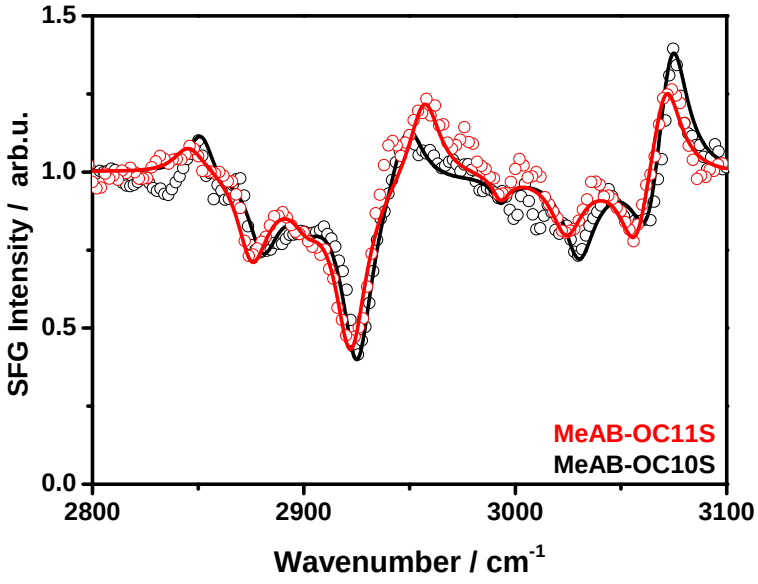

Fig. 4.25 SFG spectrum of MeAB functionalized SAM with 11 and 10 carbon chain.

photoisomerization of the azobenzene depends on the alignment. So, the photo-efficiency of SAMs with odd or even number of carbon chains is expected to be different. Actually,

only a little odd-even effect on the photoisomerization for azobenzene moiety with C10 and C11 on UV light illumination is observed. % average signal change are about same for pure monolayer shown in Table 4.4. However, electronic and steric effect of non-bonding electron of O-atom causes distortion from *trans* conformation. Due to this reason the prediction of conformation of azobenzene with O-atom is difficult [233].

4.6 Conclusion

Pure and mixed monolayers of azobenzene functionalized thiols of various fractions on 100 nm gold substrate have been probed by the SFG. Non-resonant SFG signal of the gold substrate interferes with the molecular resonances leading to positive or negative peaks in the spectra is a result of constructive or destructive interference. The SFG spectrum of decanethiol and AB SAM has been used as a reference for peak assignment of the probed methyl substituted azobenzene thiol.

The MeAB-OC11S spectrum on gold has negative and positive peaks predominantly correspond to CH_3 and CH of phenyl group of azobenzene. A strong negative peak at $2922\,cm^{-1}$ can be assigned to the symmetric stretch vibration of the CH_3 group of MeAB-OC11S indicating its more or less perpendicular orientation with respect to surface normal. The peaks at $2957\,cm^{-1}$ and $2993\,cm^{-1}$ correspond to out of plane and in plane antisymmetric stretch vibration of the methyl group. CH of phenyl group are represented by three peaks in the range of $3024-3071\,cm^{-1}$.

Slight shift in CH peak positions for mixed monolayer indicate the formation of well mixed monolayer instead of separate domains. The SFG spectrum of a 50 : 50 of decanethiol and MeAB-OC11S mixed monolayer exhibits peaks from decanethiol at $2853\,cm^{-1}$ (assigned to CH_2 symmetric stretch) and $2937\,cm^{-1}$ (assigned to CH_3 contribution). The peaks at $2917\,cm^{-1}$, $2941\,cm^{-1}$, and $2999\,cm^{-1}$ are considered as contribution of CH_3 from MeAB-OC11S and three peaks above $3000\,cm^{-1}$ are of aromatic character. A negative peak at $2880\,cm^{-1}$ in mixed monolayers arise from the contribution of CH_3 of both thiol. The SFG spectrum of a 50 : 50 of MeAB-OC11S with perdeuterated dC12 is less congested because the perdeuterated thiol dC12 yields contributions of CD_2 and CD_3 in the range of $2000-2250\,cm^{-1}$. Shift in peak position with dilution, however could not be clearly observed as seen in the mixed azobenzene thiol without deuteration. For dC12S a linear correlation of the signal intensities and the respective concentration in the immersion solution was found. In contrast,

the signal intensity trend is not linear for the MeAB moiety. CH $_3(r^+)$ and CH (aromatic) peak intensities of of MeAB decrease strongly with dilution. Even more rapid decrease in CH (aromatic) signal intensity with dilution may be due to loss of phenyl-phenyl interaction. Upon dilution the phenyl rings bent down which causes the loss of signal intensity. All these findings lead to the conclusion that at low surface concentrations of MeAB moiety loose its structural order in monolayers. The amplitude ratio of CH_3 and CH_2 (r^+/d^+) as well the ratio of intensities for symmetric and antisymmetric CH_3 stretches (r^+/r^-) increases with dilution of MeAB thiol in mixed monolayer. Change in signal intensity of the r^+ resonance vibration upon 365 nm reveals that the monolayer switches. Pure monolayers as well as mixed monolayer switch, whereas the dilution of the monolayer could not significantly enhances switching efficiency. The signal from MeAB moiety in the mixed monolayers is lost earlier upon dilution due to loosely packed disordered morphologies. For SAMs, initial back isomerization calculated from UV-Vis absorbance is fast, but the switching process is retarded as apparent from a second time constant which may indicate different domains. For solution, as expected, a single time constant is calculated. Due to steric hindrance the mixed monolayer with long chain alkyl co-ligand exhibit less UV absorbance change upon irradiation as compare to short chain co-ligand. Comparison of spacer of even and odd number of carbon chain shows that the intensities of symmetric vibration stretch of the methyl group (r^+) is slightly higher for MeAB-OC10S than amplitude of (r^+) of MeAB-OC11S. whereas the intensity of antisymmetric (r^-) mode in MeAB-OC11S is higher than MeAB-OC10. However, the expected higher switching contrast for even number carbon containing monolayer could not be observed. The signal change due to the photoisomerization for MeAB-OC10S is only slightly more efficient than for MeAB-OC11S, which may taken as an indication for a possible odd-even effect.

Chapter 5

Azobenzene derivative on quartz substrate

During the SFG measurements with gold, the metal surface turned out to be very sensitive to high-intensities of the laser beams. As discussed in chapter 4, the resulting surface damage as well as non-resonant background signals of gold turned out to be disadvantageous. Eventually, the gold substrate had been replaced by a quartz substrate to analyze the structural features and photochemical properties of azobenzene molecular switches. As quartz has neither electronic nor vibrational resonances in the visible and infrared region, the non-resonant susceptibility of fused quartz is insignificant in comparison to that of metals such as gold or silver. In this chapter azobenene functionalized monolayers deposited on quartz substrate has been analyzed and discussed.

5.1 Azobenzene-TATA

As discussed in chapter 3 the availability of free volume [90] is the main obstacle for photo isomerization. As an alternative to mixed monolayers large platform molecules triazatriangulene (TATA) can be used [118–120]. These platform units allow one to mount the functional groups as free standing units perpendicular to the surface. Well-ordered and stable monolayers of these azobenzene-functionalized platform on Au (111) surfaces have been reported in the literature [119, 120, 123, 124] and proved suitable for preparation of

self-assembled monolayers with controlled intermolecular distances [120, 124, 125]. So far, no SFG measurements on such systems have been reported in the literature. Here, molecular systems consisting of a triazatriangulenium unit with three octyl substituents at the three angular nitrogen atoms and an azobenzene unit attached to the central carbon atom of TATA molecule have been used as sample. Samples have been kindly provided by research group of Prof. Olaf Magnussen at the Institute for Experimental and Applied Physics, Kiel University. Molecular structure of TATA molecule is shown in Fig. 3.3 in chapter 3. In contrast to thiol layers on gold, immobilization of TATA molecule on quartz surfaces is supposed to be due to physical Van der Waals interaction in particular between π electron system of the TATA platform and the quartz.

This thesis presents spectroscopic evidence that TATA platform system can be deposited on quartz surface and such monolayers exhibit a high degree of structural order. Furthermore, photo isomerization experiments have also been performed.

5.2 Blank Quartz

Before investigating functionalized surfaces on quartz, it was necessary to acquire SFG spectra of the cleaned blank quartz samples. In the bulk, quartz is represented as a network of SiO_4 units while on the surface quartz may simply be considered as a SiO_2 network with neutral or charged silanol groups (SiO- or SiOH) [234, 235]. The SFG spectrum of blank quartz is shown in Fig. 5.1.

The peak at 3840 cm^{-1} is attributed to the Si-OH stretch mode [236], while the broad peak at $3200-3400$ cm^{-1} is assigned to hydrogen-bonded OH stretching modes [237, 238]. These OH bond SFG signals are broad due to the strong coupling between the vibrations of neighboring water molecules and/ or a Fermi resonance with the overtone of the H-OH bending mode [238–240]. The presence of water signals in the spectrum can readily be explained by the ambient humidity in the laboratory, which can actually affect the behavior of a substrate's surface [241]. Blank quartz samples exhibit small CH vibration signals as well around $2800-3000$ cm^{-1}. These peaks indicate a small amount of organic impurities on the sample's surface. Many attempts have been made (which were discussed in chapter 3) to remove these impurities but small signals in the CH stretch vibration region always remained. Interestingly, assignment of the most prominent peak at 2400 cm^{-1} is not yet clear. To the best of my knowledge, it has not been reported in the literature. It may be attributed

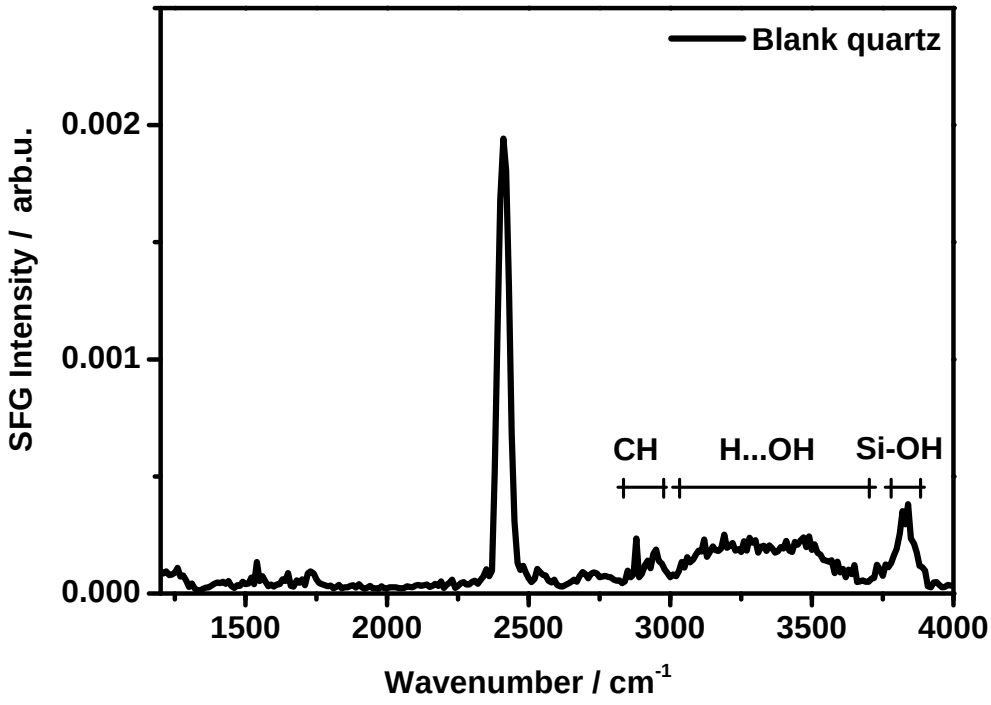

Fig. 5.1 SFG spectrum of a blank quartz measured in ssp polarization.

to a vibration peak of carbon dioxide adsorbed on the surfaces [242] or of course much less likely may be due to hydrogen bonded water having D_2O as contamination [243, 244]. In principle, this spectral region is typical for strong band of NH...N= for five membered hetrocyclic aromatic rings [245, 246]. Thus, the assignment of this peak is still debatable. To ensure that this peak is specific for quartz samples, the spectrum was compared with a reference OTS (octadecyltrichlorosilane) spectrum on glass (see Fig. 5.2). The 2400 cm^{-1} peak is absent in case of the glass substrate, which may indicate that peak, in fact arises from quartz substrate. Further investigation is necessary to clarify the origin of this prominent peak.

5.3 8-TATA

In this work, sum frequency generation spectroscopy has been employed to elucidate the structure of TATA adlayers on quartz. The structure of such molecules is represented by

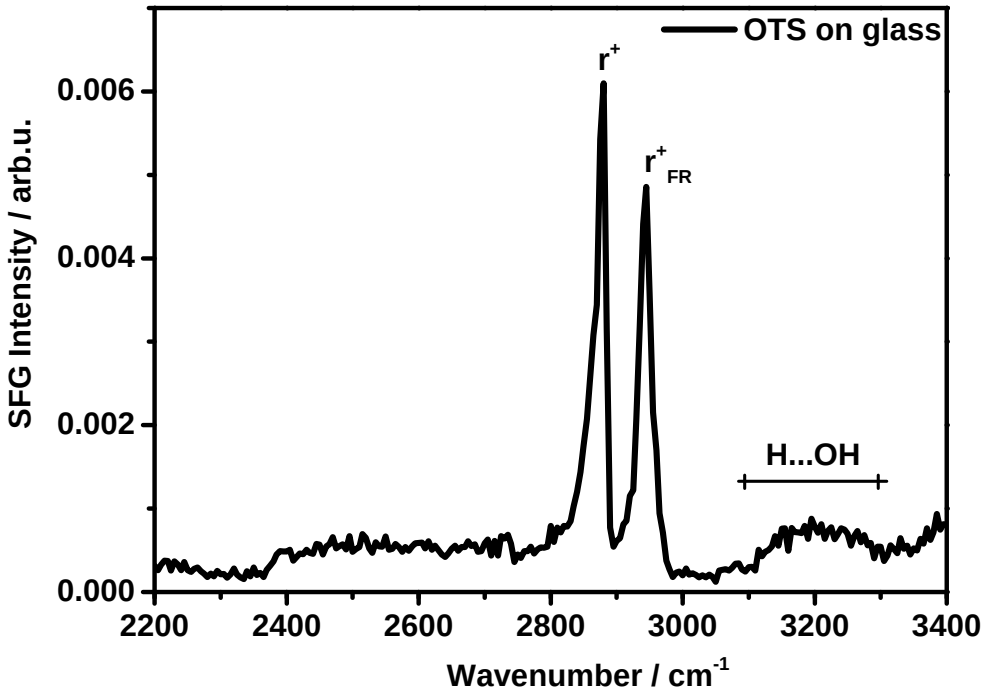

Fig. 5.2 SFG spectrum of OTS (octadecyltrichlorosilane) on glass substrate.

molecule A in Fig. 3.3. In order to analyze the SFG spectrum of TATA layers with attached azobenzene units the SFG spectrum of bare TATA platforms deposited on quartz needs to be recorded first. The occurrence of the SFG resonances that are not related to the quartz substrate, indicates the formation of a TATA adlayer. The SFG spectrum of a TATA adlayer is shown in Fig. 5.3 in direct comparison with corresponding quartz peak. The TATA spectrum is normalized with respect to 2400 cm^{-1}. It can be characterized as follow: (a) a broad peak at $2520-2650$ cm^{-1} which can be assigned to vibrations of the tertiary nitrogen present in the platform structure [120], (b) signals from CH arising from vibrations at $2840-2968$ cm^{-1}, (c) a broad peak at $3200-3400$ cm^{-1} assigned to H-bonded H-OH, and (d) peaks at 3787 cm^{-1} and 3858 cm^{-1}attributed to free H-OH and Si-OH. The signals present in the CH vibrational range are characteristics for terminal methyl (CH_3) and methylene (CH_2) vibration modes present in the TATA platform. The structure of CH region can be tentatively assigned as usual (see in set of Fig. 5.3 and chapter 4). Most likely, the two peaks at 2880 cm^{-1} and 2964 cm^{-1} correspond to the symmetric and antisymmetric CH_3 stretch mode, respectively [32, 160, 168, 202]. The resonance at 2945 cm^{-1} is attributed to the Fermi resonance of the CH_3 symmetric stretch vibrations and the peak at 2843 cm^{-1} is characteristic for the

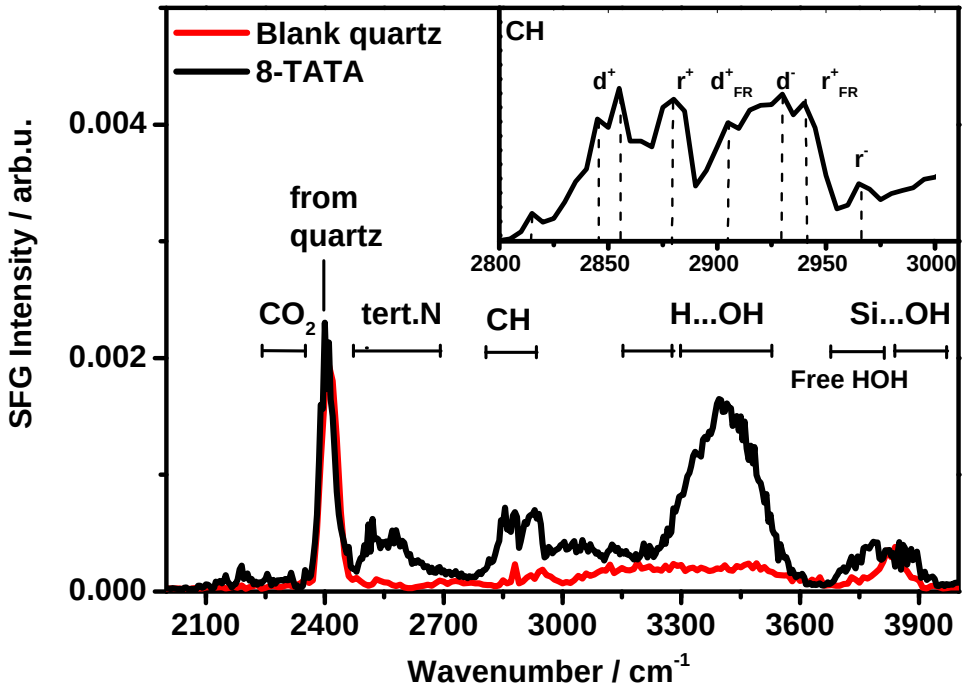

Fig. 5.3 SFG spectrum of TATA platform in ssp polarization setup. The inset shows the CH vibrational spectral range.

symmetric (d^+) stretch vibration of CH_2 (methylene) group [32, 160]. The methylene stretch vibrational modes appear with comparable intensity as the CH_3 resonances, serving as an indicator for gauche defects in the octyl chains. However, the fact that relatively strong CH_3 peaks can be observed, revealing that alkyl chains point away from the surface. No obvious contributions from aromatic CH vibration region ($3000-3100$ cm^{-1}) have been observed, which is consistent with the fact that the platforms lying flat on the surface. The free OH peak and the broad band from water are also present in spectra. It is tempting to assign the broad peak at $3300-3500$ cm^{-1} to free NH bond, however assuming as intact TATA platform unit, these should not be present in the spectrum. Therefore, it is more likely that this band arises from structured residual water as well. In Table 5.1, all mode assignments are summarized.

Table 5.1 SFG peak assignment for 8-TATA on quartz.

Wavenumber $\tilde{\nu}$ / cm $^{-1}$	**Peak assignment**
2400	from quartz
2520 – 2650	tertiary N
2843 – 2945	CH alkyl
3100 – 3500	H...OH
3787	free H-OH
3858	Si-OH

5.4 Me-Azo-8-TATA

Methyl substituted azobenzene unit is attached to TATA platform through C≡C bond in Me-Azo-8-TATA on quartz, the molecular structure has been shown in Fig. 3.3 (molecule I). For comparison with the 8-TATA in Fig. 5.4, the spectrum is normalized with respect to the peak at 2400 cm^{-1}. The spectrum shows two very prominent stretching resonances characteristic of CH_3 symmetric stretch vibration and its corresponding Fermi resonances at 2879 cm^{-1} and 2945 cm^{-1} [32, 160, 168, 202, 204–208]. The relative intensity of the CH_3 vibration peaks of Me-Azo-8-TATA shows up more than four times higher than that of bare TATA. This indicates that the observed signal is mainly from the CH_3 group located on the azobenzene unit instead of the resulting from the alkyl chains attached to the platform. Obviously, the overall orientation of this methyl group is more or less perpendicular to the surfaces, as it is expected for upright standing MeAB unit. A peak at 2850 cm^{-1} and a shoulder at 2915 cm^{-1} is assigned to symmetric stretch vibration of CH_2 groups [32, 160, 168, 202, 207]. They can only arise from the alkyl side chain of the platform, nevertheless theyare much more intense than for 8-TATA. The question arises if the normalization of the two spectra with respect to 2400 cm^{-1} peak is really valid. However, even if the spectra would be normalized to the intensity of the CH_2 bands, the CH_3 peaks would still be significantly enhanced in the Me-Azo-8-TATA spectrum. A small peak at 2190 cm^{-1} can be assigned to C≡C, while the broad peak in the spectral range $2520 - 2650$ cm^{-1} as for 8-TATA platform can be assigned to the tertiary nitrogen. The peak assignments are summarized in Table: 5.2.

Table 5.2 Peak assignment of Me-Azo-8-TATA

Wavenumber $\tilde{\nu}$ / cm $^{-1}$	**peak assignment**
2190	C≡C
2400	from quartz
2520 – 2650	tertiary N
2850	d^+
2880	r^+
2915	d^-
2945	r^+_{FR}
2964	r^-
3200 – 3400	H...OH
3787	free H-OH
3858	Si-OH

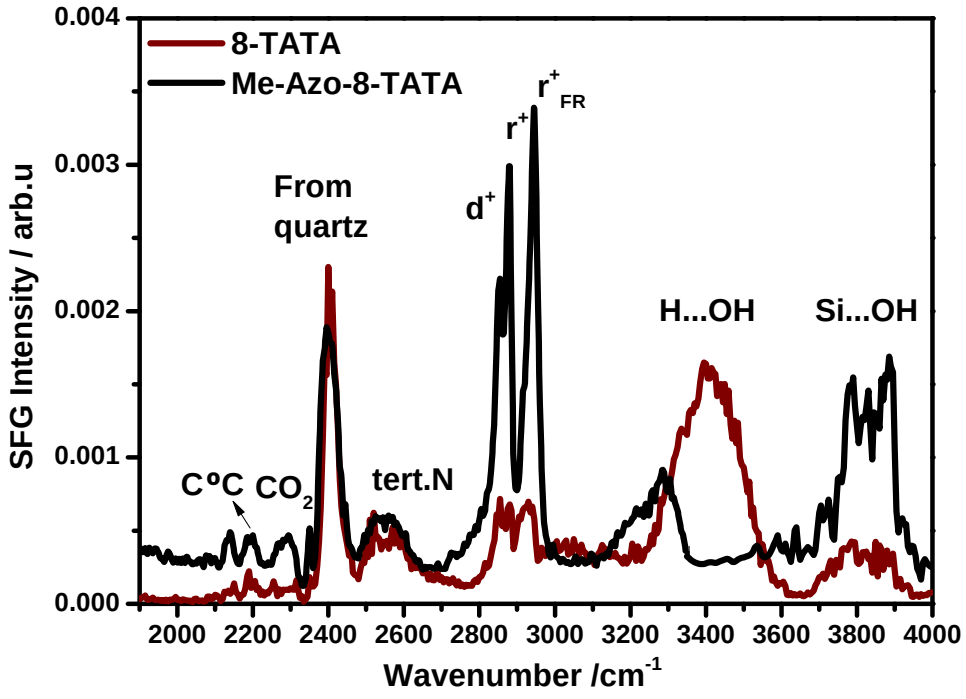

Fig. 5.4 SFG spectrum of CH_3-Azo-8-TATA with the methyl substituted azobenzene unit attached to TATA platform via C - C triple bond. The spectrum exhibits strong features of r^+, r^+_{FR} modes stemming of methyl group attached to azobenzene unit.

5.5 CN-Azo-8-TATA

A cyano group attached to azobenzene unit, serves as an alternative SFG marker. The molecular structure is shown in Fig. 3.3 (molecule II). The spectrum is shown in Fig. 5.5. In comparison with the Me-Azo-8-TATA spectrum (in Fig. 5.4) a new peak appears at 2200 cm^{-1} and the strong methyl stretch signals disappear. Consequently, the 2200 cm^{-1} peak can be assigned to the CN group [117, 247, 248]. Despite the fact that the cyano group is attached at the para position of the azobenzene ring and therefore, should be perpendicular to surface normal, the signal intensity remains low compared to the corresponding methyl group. Reasons for this comparable low intensity may be (a) a lower transition dipole moment of the CN group, (b) a less well aligned CN-AB moiety that can not be ruled out or, (c) a lower surface coverage of this particular sample. Some characteristic signals for CH stretch vibrations, tertiary nitrogen vibration, and the prominent quartz peak are similarly observed again, hence consistent with the other TATA functionalized surfaces. The peak assignments

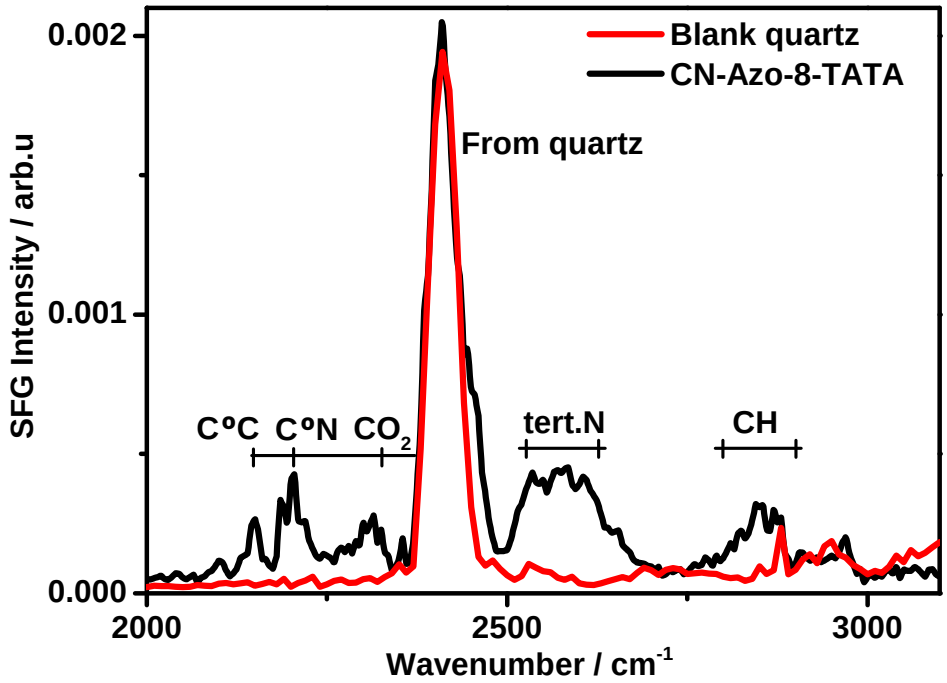

Fig. 5.5 SFG spectra of CN-Azo-8-TATA (octyl) on quartz.

are summarized in Table: 5.3.

Table 5.3 Peak assignment for CN-Azo-8-TATA on quartz

Wavenumber $\tilde{\nu}$ / cm $^{-1}$	**Peak Assignment**
2190	C≡C
2200	CN
2400	from quartz
2520-2650	tertiary N
2845-2945	alkyl CH

5.6 CN-Azo-8-TATA-propanol

Another modification of the Azo-8-TATA unit was studied to (i) investigate the source of residual CH signals and (ii) to elucidate the role of the TATA side chain on the overall structure and surface coverage of the adlayers. Octyl side chains of TATA platform were replaced by 1-hydroxypropyl in CN-Azo-8-TATA (propanol). The molecular structure is given in Fig. 3.3 molecule C. Since the OH functional group of the propanol side chains interacts with the quartz surface, these chains are expected to be no longer oriented perpendicular to the surface. This further reduces the SFG sensitivity of these groups in SFG spectroscopy. The Fig. 5.6 compares with other derivatives. All spectra are normalized with respect to the 2400 cm $^{-1}$ peak. For CN-Azo-8-TATA-propanol intensities of CH vibrational signals in Fig. 5.6 have been reduced to half of the intensity of the signals originating from TATA platforms functionalized with octyl side chains. This is consistent with the expected trend. Surprisingly, the peaks assigned to tertiary nitrogen are missing in the spectrum. If this is simply a spectrometer artifact or real effect, it is unclear. All peak assignments are summarized in Table: 5.4.

Table 5.4 Peak assignment for CN-Azo-8-TATA (propanol).

Wavenumber $\tilde{\nu}$ / cm $^{-1}$	**Peak assignment**
2190	C≡C
2200	CN
2400	from quartz
2520-2650	tertiary N
2856-2945	alkyl CH

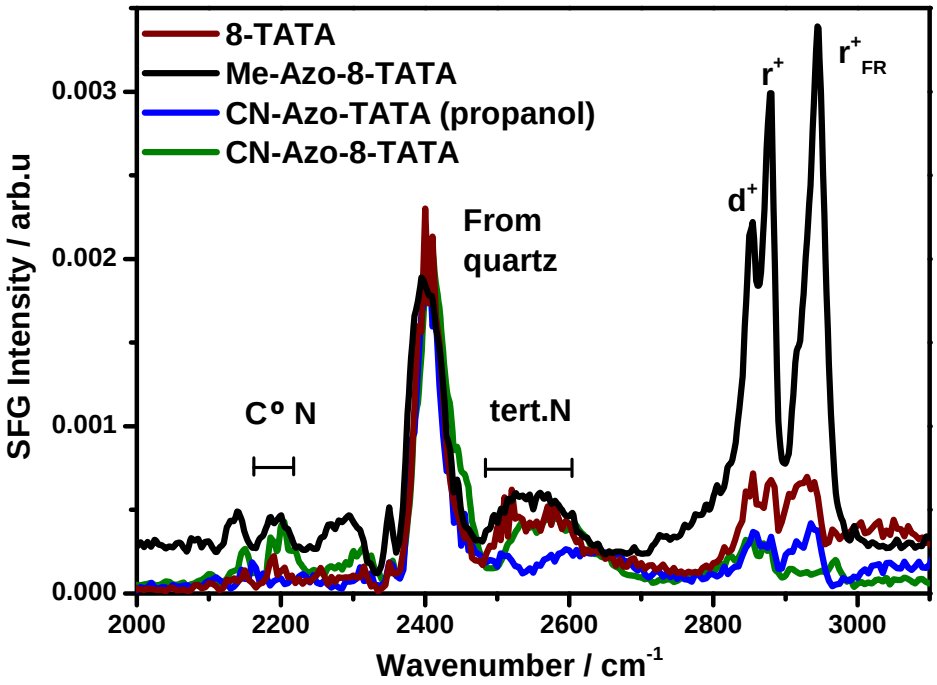

Fig. 5.6 SFG spectra of CN-Azo-8-TATA (1-hydroxy propyl) on quartz. In order to reduce contribution of side chain of octyl chain of TATA platform 1-hydroxy propyl is used as side chain of platform. The intensity of peaks in CH region has been reduced as compare to TATA platform carrying octyl side chain.

5.7 Summary for substituted Azobenzene-TATA molecule on quartz

A comparison of the results obtained for the substituted azobenzene TATA molecules with octyl side chain is given in Fig. 5.7. All samples showed a prominent peak at 2400 cm^{-1}. For comparison, all spectra have been normalized to the intensity of peak at 2400 cm^{-1}. As this study has been based on a limited number of samples, more comprehension and synthetic measurements are needed to support these findings. Several conclusions can be drawn from these preliminary studies.

1. SFG spectrum of TATA platform shows the contribution of methylene and methyl of octyl side chain, of tertiary nitrogen, a peak for H...OH and a peak for Si...OH.

2. TATA platform bonded to methyl or cyano substituted azobenzene show contribution of TATA platform as well as for methyl stretching in case of Me-Azo-8-TATA and for cyano in case of CN-Azo-8-TATA.

3. CH intensities in normalized spectra of CN-Azo-8-TATA-propanol (where octyl side chains are replaced by 1-hydroxypropyl chain) are reduced as compared to the other molecules.

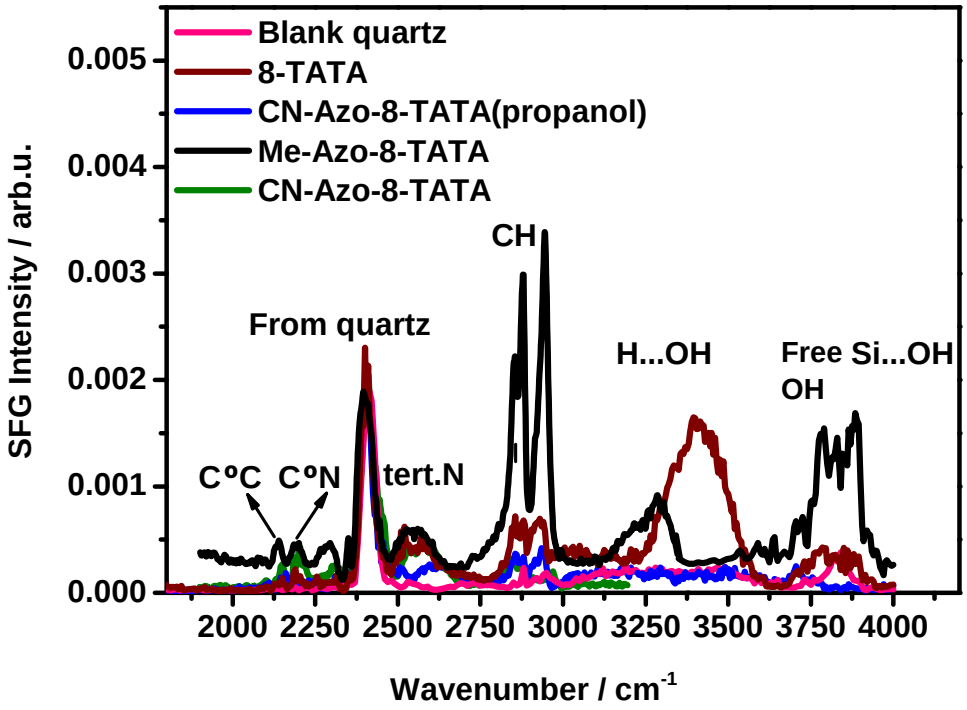

Fig. 5.7 Comparison of substituted Azobenzene-TATA molecule on quartz. Spectra was normalized with respect to the peak at 2400 cm^{-1}.

5.8 Switching of Azobenzene-TATA SAMs on quartz

Azobenzene derivatives represent a well investigated group of the photo-switchable SAM systems. These moieties display a *trans* $\rightarrow$ *cis* isomerization. The photo and thermally induced switching process of molecular arrays of free-standing azobenzene groups, formed by self-assembly of TATA functionalized on gold surfaces, have been studied by photo

electrochemical methods such as cyclic voltammetry, chronoamperometry as well surface plasma resonance spectroscopy and IRRAS [124, 126, 219, 249]. Here, such free standing molecular system has been adsorbed at quartz and probed by SFG for finite time. Possible changes in peak intensity of SFG marker groups (CN, CH_3) on illumination with UV and blue light have been investigated. Actually a change in signal was observed, but only for fresh samples and only for one switching cycle. The issue was comparable with the problems encountered with SAMs on gold substrate and can be attributed to an irreversible change in the structure of the monolayer or simply ablation effects induced by high-intensity laser light. In the light of these problems to reproduce the photo-switching effect, these data will not be discussed here further. Clearly, more measurements are needed to draw definite conclusions with regard to the photo-switching behavior of functionalized TATA on gold.

5.9 Sample aging

Photoswitching could not be observed as yet with older samples (i.e., 8 weeks sample kept at atmospheric condition). As an example, a comparison is drawn for relatively fresh (few days older) and 8 weeks old sample of CN-Azo-8-TATA in Fig. 5.8. There was a decrease in TATA-related signals as well of SFG marker CN band at 2205 cm^{-1}. On the other hand the signals corresponding to CH strongly increased. This may be explained by contamination of the sample with time or may be laser damage the structure of monolayer. A series of more systematic experiments are needed to further investigate the aging behavior. First of all, also samples should be analyzed directly after preparation as well.

5.10 AB on quartz

Flat quartz substrate were directly functionalized with azobenzene by click chemistry and were analyzed by SFG spectroscopy. Samples for this preliminary study were provided by research group of Prof. Friedrich Temps at the Institute of Physical Chemistry, Kiel University. The question arises as to what degree such monolayers are surface functionalized and if the formed adlayer is structurally ordered. Relying on the high quality spectra obtained for OTS on glass (see Fig. 5.2) it can be assumed that both criteria are fulfilled for AB layers as well. As seen in the spectrum shown in Fig. 5.9, interestingly other two strong peaks at

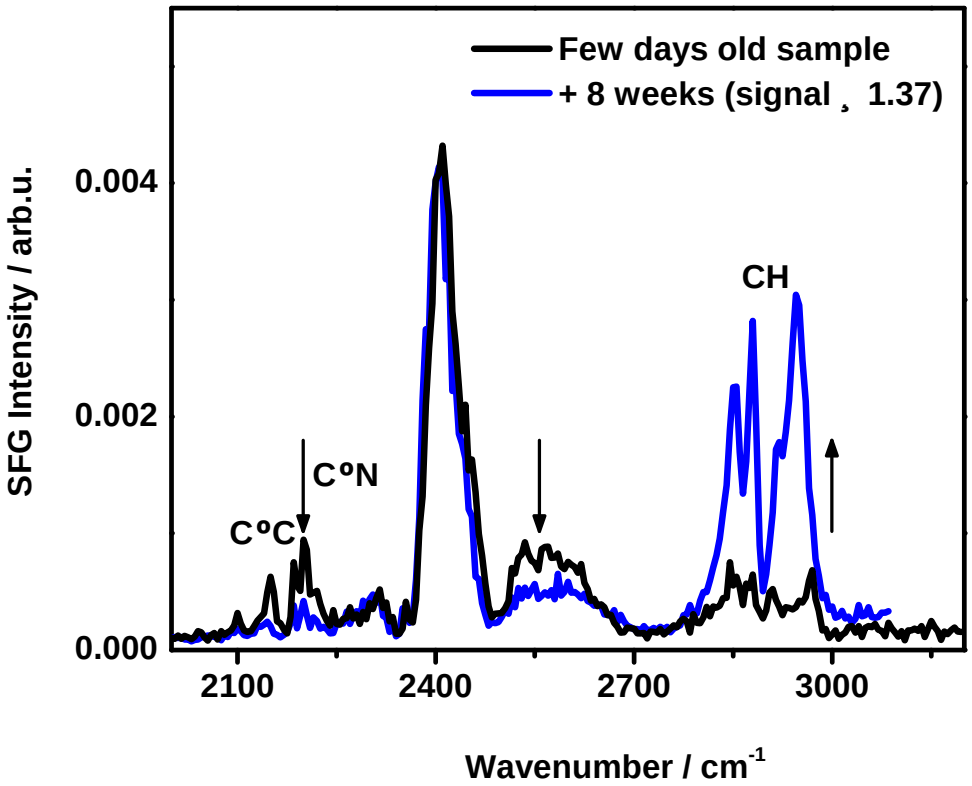

Fig. 5.8 Comparison of fresh and few weeks old sample.

2542- 2700 cm^{-1} show up. The assignment of these peaks remain unclear. Such monolayers show very intense and rich spectra, which in fact indicate both a high degree of surface functionalization and molecular order. The molecular structure is shown in Fig. 3.4. The SAMs spectra exhibit resonances for methylene and aromatic CH region $(2800-3100)\,cm^{-1}$, as well as characteristic hydrogen bonded OH, Si-OH and free water signals. Another peak appeared at 1600 cm^{-1} which probably can be assigned to N=N bond of azobenzene. The typical peak for the quartz substrate at 2400 cm^{-1} is also present in spectrum.

5.11 MeAB on quartz

Similarly methyl substituted azobenzene were synthesized by click chemistry and covalently bonded to quartz surfaces. As expected, the corresponding SFG spectra show much stronger

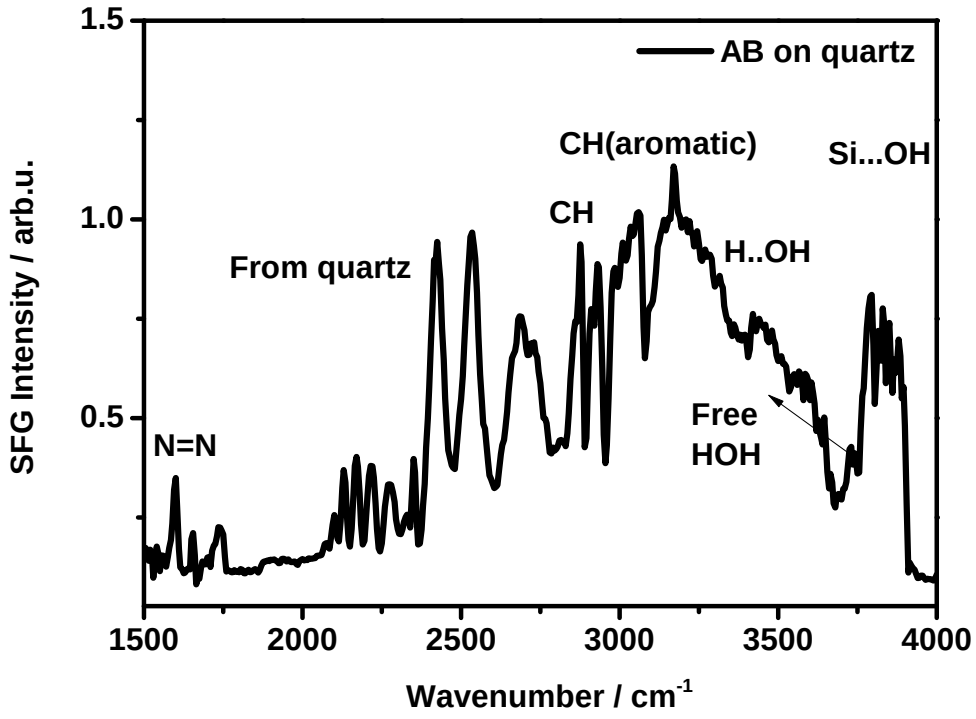

Fig. 5.9 Spectrum of AB on quartz surface. The azobenzene derivative was attached to quartz surface covalently via silanol bonds.

resonances of CH which particularly can be assigned to methylene and methyl group. The molecular structure is shown in Fig. 3.4. The symmetric stretch vibration (r^+) of methyl group attached to the phenyl group of azobenzene unit was assigned to peak at 2925 cm^{-1} [205, 206]. Also, the corresponding antisymmetric resonance (r^-) at 2979 cm^{-1} was observed (see Fig. 5.10). Signal for aromatic CH groups are in quite low intensity as compared to MeAB-OC11S. The two prominent resonances at 2554 and 2688 cm^{-1} were assigned to tertiary nitrogen from triazole ring. The typical peak of quartz substrate at 2400 cm^{-1} is clearly visible in the spectrum. The peak assignments are summarized in Table: 5.5 Monolayers with methyl group at para position have also been subjected to photoisomerization experiments. The signals of SFG marker group (methyl group) were monitored on irradiation with UV/blue light. The change of methyl signal intensity has been observed however reproducibility again proved to be a major issue. In all cases, the switching process could only be studied once.

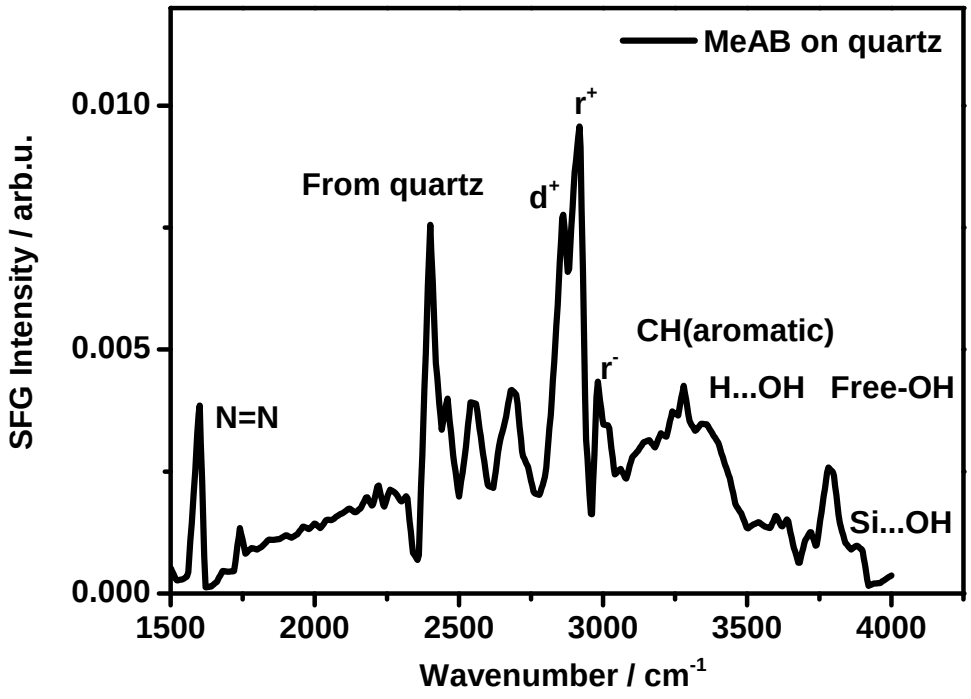

Fig. 5.10 Spectrum of MeAB on quartz surface. The azobenzene derivative was attached to quartz surface covalently via silanol bonds,see Fig. 3.4.

Table 5.5 Peak assignment for MeAB on Quartz

Wavenumber $\tilde{\nu}$ / cm $^{-1}$	**Peak assignment**
2100 – 2200	$Si-OSi$
2400	from quartz
2850	d^+
2925	r^+
2979	r^-
3152	CH(aromatic)
3400	H...OH
3740	Free H...OH
3858	Si...OH

5.12 Conclusion

As an alternative to mixed monolayers of AB functionalized thiol on gold, a preliminary SFG study of azobenzene-functionalized triazatriangulene (TATA) platform adlayers on quartz

has been performed for first time. In all cases, intense and spectrally rich SFG spectra have been observed, hence evidence of high degree of surface functionalization and surface order. in the SFG spectrum of the pure TATA platforms at quartz surfaces the signal of its alkyl side chains show up. Spectrum also shows the presence of H-bonded H-OH ($3200-3400\ \mathrm{cm}^{-1}$), free HOH ($3787\ \mathrm{cm}^{-1}$) as well as Si-OH ($3858\ \mathrm{cm}^{-1}$). It is not clear if either coverage is incomplete or strong water signals are due to the presence of some co-adsorption layer.

SAMs of TATA platforms functionalized with substituted azobenzene units show clear features of attached groups. For example, methyl substituted azobenzene TATA adlayer exhibits the stretching resonances of the terminal CH_3, the symmetric stretch vibrations of side alkyl-chains, and small peak for $C\equiv C$. Peaks for H-bonded H-OH, free H-OH and Si-OH and prominent peaks at $2400\ \mathrm{cm}^{-1}$ are also visible in spectrum. SFG spectrum of the cyano substituted azobenzene TATA adlayer reveals the resonances of the CN group. Another modified and substituted AB-TATA adlayer where octyl side chains of TATA platform were replaced by 1-hydroxypropyl in CN-Azo-8-TATA (propanol), elucidate the role of the TATA side chains, and unravel the source of CH signals in SFG spectrum. Intensities of CH vibrational signals attributed to the side chains of the TATA platform reduced to half the intensity of 1-hydroxypropyl in CN-Azo-8-TATA (propanol).

Attempts were also undertaken to study photoisomerizatin by monitoring the changes in peak intensity of the SFG marker groups (CN, CH_3) on illumination with UV and blue light. Typically signal changes were observed but only for fresh samples and only for one switching cycle. Reproducibility problems of these experiments were comparable with the problems encountered with SAMs on gold substrate. They can be attributed to irreversible changes in the structure of monolayer and ablation effects induced by the high-intensity laser light. Moreover, sample aging lead to a decrease of adlayer-related signals and show indication for increasing the contamination of the sample with time.

Finally flat quartz substrates functionalized with azobenzene and methyl AB by click chemistry showed very intense and rich spectra indicating high surface functionalization and molecular order. SAMs spectra show resonances for methyl, methylene and aromatic CH bonds $(2800-3100)\,\mathrm{cm}^{-1}$, but also characteristic hydrogen bonded OH, Si-OH and free water peak. Another peak appeared at $1600\,\mathrm{cm}^{-1}$ can be assigned to N=N group of azobenzene. A strong peak typically for quartz substrate at $2400\,\mathrm{cm}^{-1}$ is also present in all spectra.

Although in all cases prominent SFG peaks could be observed, much more work is needed to be able to draw clear conclusion. In particular, future experiments should be performed

with larger set of samples and SFG experiments should be performed directly after sample preparation. As the purpose of this Ph.D study was to assess the application of SFG spectroscopy in an explorative manner of all the different types of sample system would have been well beyond the possibilities. As a thorough analysis in laboratory future studies should concentrate on selected test system.

Chapter 6

Azobenzene derivative on the air-water interface

Azobenzene based lipids introduced into phospholipid monolayers help to investigate the characteristic properties of membranes. In this study, mixed monolayers of Azobenzene-Cholesterol-Dipalmitoylphosphatidylcholine (DPPC) (Azo-Chol/ DPPC) have been prepared. The structure of the molecular system of Azo-Chol/ DPPC is illustrated in Fig. 3.5. Addition of DPPC molecule can be assumed to affect the structural order of the monolayer of azobenzene based lipids. In order to test this hypothesis, the surface-selective vibrational spectroscopic technique (SFG) has been combined with a Langmuir film balance setup, allowing for reversible control of the surface pressure and the molecular ordering of the lipids in the monolayer. For example, it is reported in literature that cholesterol has marked effect on the phospholipid behavior [250–252]. Mischa Bonn *et al.* [250] studied the conformational and orientational order in the phospholipid as the function of surface pressure and cholesterol content by using SFG. They found an increase of molecular order upon addition of relatively small amounts of cholesterol. In addition to this structural effect, azobenzene functionalized cholesterol can undergo photo induced $trans - cis$ isomerization. The question arises to what extent the structural order of a mixed Azo-Chol/ DPPC monolayer can be modulated by switching the *trans* to *cis* isomer. The *cis* isomer is expected to exhibit a higher interfacial area, hence switching should induce an increase in surface pressure accompanied by a better structural order.

6.1 SFG spectra

When a surface active compound is deposited on a surface, it tends to spread out in order to increase the surface coverage and to decrease the surface pressure. One of the most intriguing features of binary mixtures of cholesterol with Dipalmitoylphosphatidylcholine (DPPC) is the formation of a presumably homogeneous phase [253]. However, small heterogeneities are also reported [254, 255]. In order to get the initial information of surface behavior of Azo-Chol/ DPPC mixed monolayers, SFG spectra at respective surface pressure and mixing ratio have been measured. The SFG spectrum of a mixed monolayer containing 5% Azobenzene-Cholesterol and 95% DPPC is shown in Fig. 6.1. Vibrational bands stemming from cholesterol are expected to be small and actually could not be observed because of the N^2 dependence of the SFG signal intensity. Vibrational peaks of CH_2 and CH_3 of DPPC are most prominent. The spectrum has the typical structure with a symmetric (r^+) and

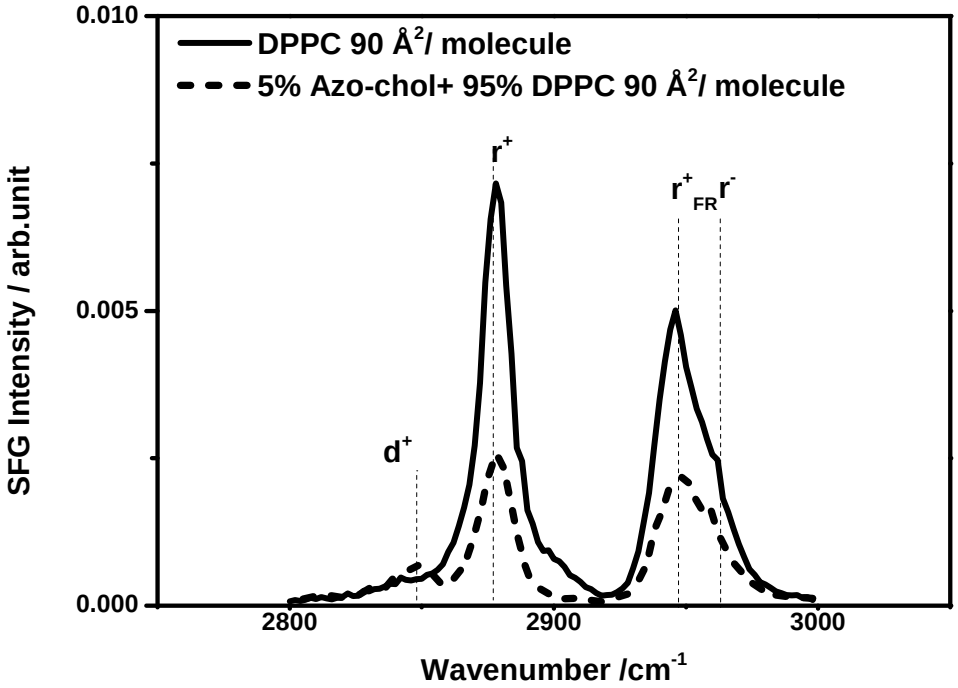

Fig. 6.1 Comparison of SFG spectrum for Azobenzene—cholesterol/DPPC in chloroform monolayer with pure DPPC spread in Teflon dish. Spectrum has vibrational peaks for DPPC molecule.

Fermi resonance (r^+_{FR}) at 2880 cm^{-1} and 2945 cm^{-1} of the terminal CH_3 group of DPPC.

The shoulder at 2850 cm^{-1} is due to (d^+) band [187, 256, 257] whereas, resonance of antsymmetric vibration of (r^-) appears with very small intensity. Compared with a pure DPPC spectrum, at the same surface concentration, the intensity of the CH_2 signal of the mixed monolayer is present, while it is absent in pure DPPC monolayer. Presence of CH_2 signal indicates a less-ordered alkyl chain, with gauche defects, where the ratio of CH_3 to CH_2 depends upon structural order of monolayer [258, 259]. Furthermore, the intensity of the CH_3 stretch vibration is higher when no cholesterol is present.

Actually the peak intensity difference is much more pronounced as it is expected from DPPC concentration ratio. Fig. 6.2 displays two SFG spectra of two different surface concentration of a mixed Azo-Chol/ DPPC monolayer. As expected, there is an increase in the CH_3 signal of the DPPC molecules with an increase in surface concentration.

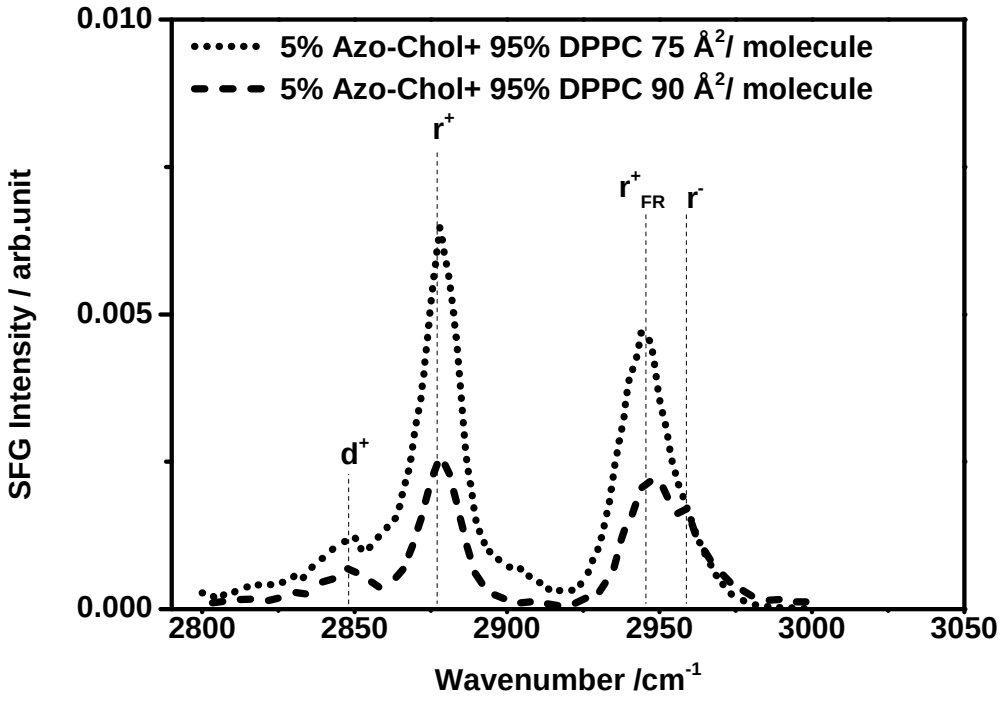

Fig. 6.2 SFG spectrum of Azobenzene-cholestrol-DPPC monolayer for different surface concentration. Addition of relatively small amounts of cholesterol, in DPPC monolayer is a witness of increase in CH_3 signals.

The ratio of CH_3 to CH_2 signal intensities for pure DPPC monolayer is higher as compared to mixed monolayer indicating that there is an expansion of the monolayer in the presence of cholesterol.

6.2 Two dimensional phase behavior

The two dimensional phase behavior of the mixed Azo-Cholesterol/DPPC monolayer has been studied in a Langmuir trough experiment. By compression (i.e., reduction of interfacial area) the monolayer undergoes transformation from its two dimensional gaseous to a liquid and then to solid state at high surface pressure. Typical spectra measured in such a Langmuir trough experiments are shown in Fig. 6.3. The peak assignment is given in Table 6.1

Table 6.1 Peak assignment of Azobenzene-cholesterol/DPPC in Langmuir trough experiment.

Vibrational mode	**Wavenumber $\tilde{\nu}$ / cm $^{-1}$**
d^+	2851
r^+	2879
d^-	2905
d^+_{FR}	2930
r^+_{FR}	2946
r^-	2962

At 2 mN/m surface pressure corresponding to an area per molecule of 100 Å^2 / molecule, the peaks from the methylene groups (CH_2) are clearly observed in spectra at 2850 cm^{-1} and 2930 cm^{-1}. As the surface area is compressed to 80 Å^2 / molecule, the surface pressure increased to 3 mN/m and the peak intensity of $CH_3(r^+)$ and $CH_3(r^+_{FR})$ increased. The intensity of the methylene stretching further decreases for 8 mN/m to 57 Å^2 / molecule, indicating the orientational order of monolayer. The SFG spectrum at 2 mN/m is dominated by CH_2 band near 2850 cm^{-1}, for a DPPC monolayer in the expanded liquid (LE) state with a conformationally disordered state containing gauche defects [165, 250]. The spectrum can be discussed in terms of a surface pressure isotherm as well. Fig. 6.4 illustrates the lateral surface pressure as function of molecular area (Π-A). Based on literature data, two dimensional phases are termed as gas-phase, liquid-expanded (LE), and liquid-condensed (LC) phases. Pressure–area isotherms of the mixed monolayer exhibits region of, liquid-condensed (LC) phase and liquid-expanded (LE) shown in Fig. 6.4 [260]. Liquid-condensed (LC) phase is dispersed in the less ordered liquid-expanded (LE) phase [260, 261]. Upon

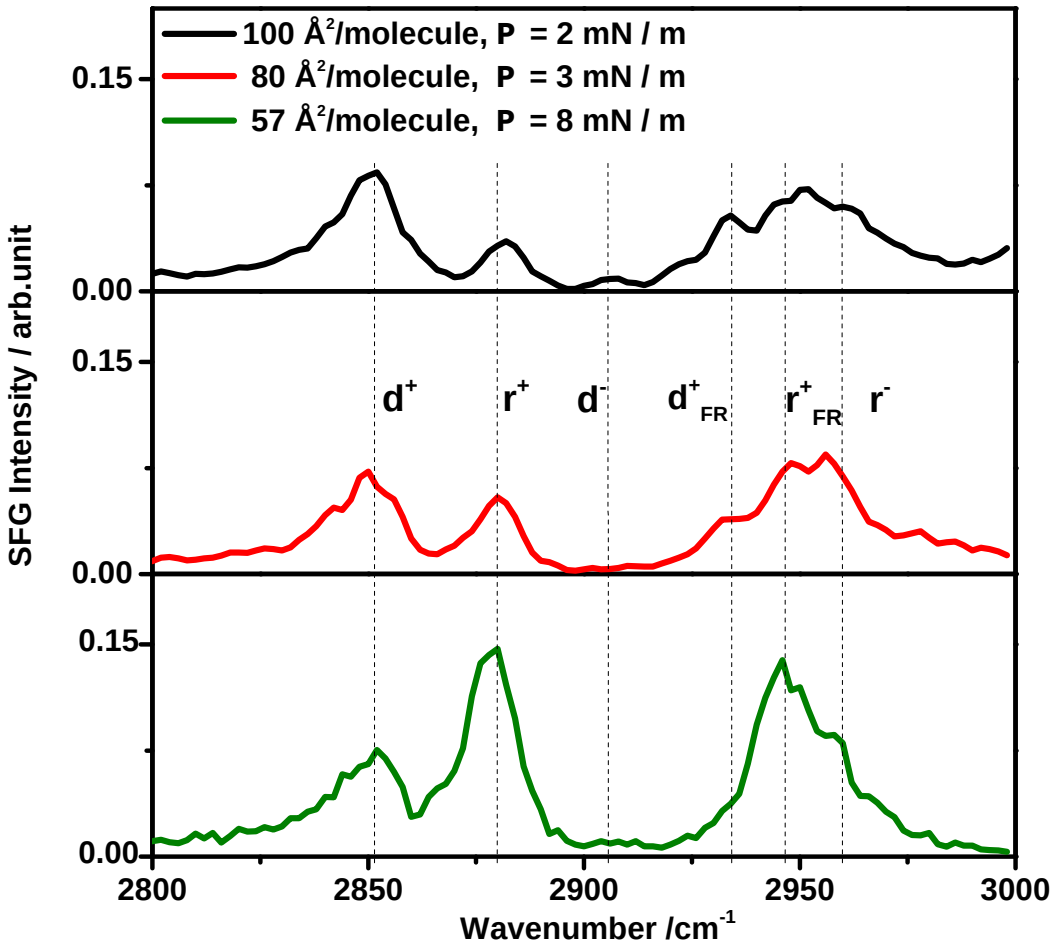

Fig. 6.3 SFG spectrum for Azobenzene-cholesterol/DPPC monolayer spread in a Langmuir trough.

compression of monolayer in its thermally stable *trans* state of AB unit, a transition from gaseous/ liquid expanded state to liquid expanded state occurs when the surface pressure becomes 40 Å^2 / molecule. At a density below 32 Å^2 / molecule, the monolayer collapses as shown in Fig. 6.4.

6.3 Photoisomerization

Morphological changes in the azobenzene within the surface films during photoisomerization have been investigated and reported in literature [170, 262–264]. Photoisomerisation of the

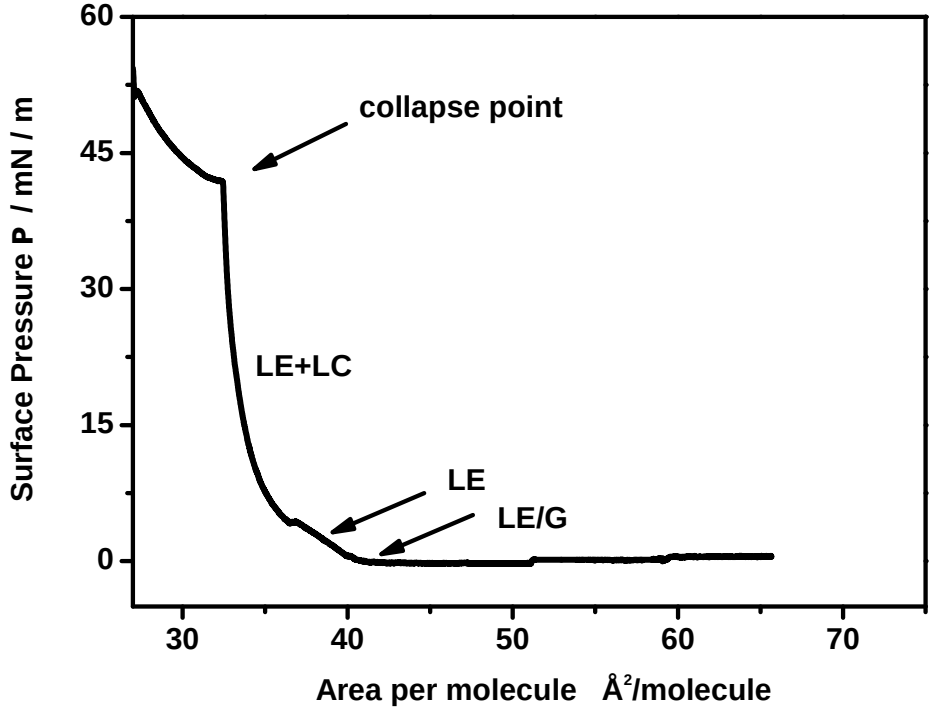

Fig. 6.4 Pressure–area isotherms for Azo-cholesterol-DPPC monolayer. The isotherm has gas (G), liquid expanded (LE), and condensed phases (LC). Assignment according to [260]

monolayers induced large changes in molecular surface pressure of monolayer [170, 261]. Ellen *et al.* [170] studied the molecular structures of mixtures of a photoswitchable lipid with the DPPC using SFG. They reported that the surface pressure and molecular ordering of DPPC can be influenced by switching the azobenzene-based lipid between its two states. As expected, the *cis* state corresponds to a higher surface pressure as compared to *trans*-state. The *cis* state, although exhibiting a higher surface pressure, showed lower structural order. This was explained by a direct interaction of the *cis*-molecule with the water-interface. Consequently, the order of the alkyl chains in the layer decreased. Photoisomerization experiments of Azo-chol in DPPC monolayers were performed by irradiating the monolayer with 365 nm LED for 30 minutes in order to switch the AB into its *cis* state [265]. This *cis*-solution, after spreading, was compressed to 35 mN/m and left for 1 hour to be relaxed and attained a stable surface pressure. Upon irradiation with 455 nm, the *cis*-state is switched to the *trans*-state, which has a lower spatial foot print. Fig. 6.5 illustrates the measured surface pressure as a function of time. Upon UV irradiation, a clear step towards lower surface pressure is observed. This change in surface pressure upon irradiation directly relates

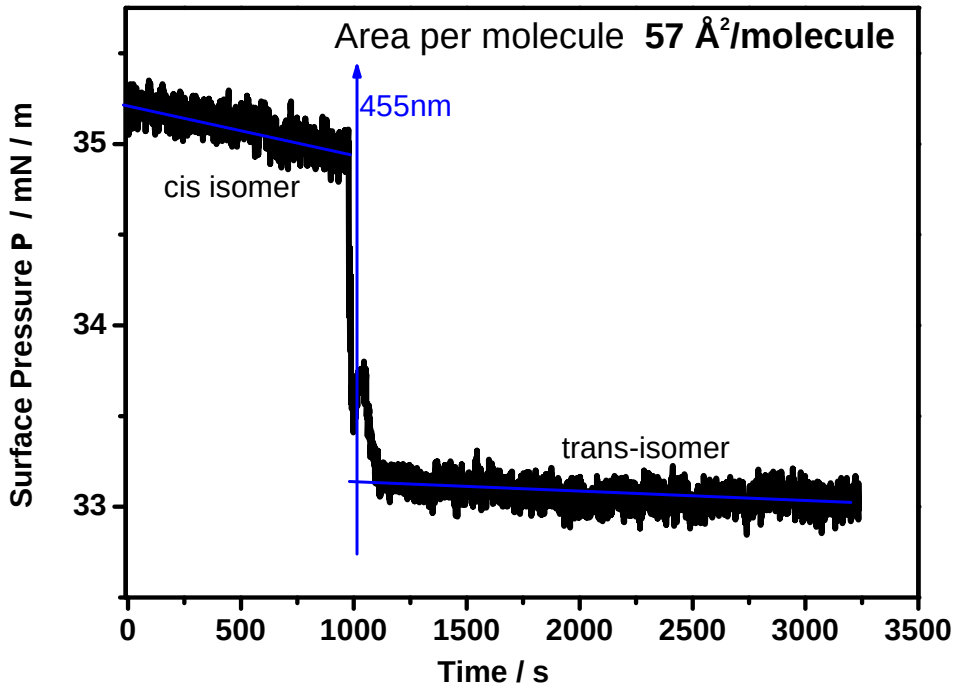

Fig. 6.5 Surface pressure change after illumination of *cis*-isomer with a 455 nm LED.

to the photoisomerization. Actually, it was possible to reversibly switch in-between the *cis* and *trans*-state. A corresponding surface-pressure is shown in Fig. 6.6.

Again, the $cis-trans$ isomerization is clearly observed. However, as the absolute change in surface pressure about 0.25 mN/m, was close to the sensitivity of the surface pressure measurements, the signal was somewhat noisy. Moreover, during repeated experiments it was observed that continuous exposure of the monolayer caused a slow drift in surface pressure.

Yet in another experiment the SFG spectra of a mixed monolayer following photoisomerization were measured. Figure 6.7 illustrates an experiment at a surface area of 57 $Å^2$ / molecule. Corresponding SFG spectra in the CH spectral range show an increase of CH_3 signal intensity with a surface pressure upon irradiation with 365 nm. Upon 450 nm illumination, the CH_3 intensity decreases again but did not reach to its original value.

The reproducibility of SFG signal intensity was low.

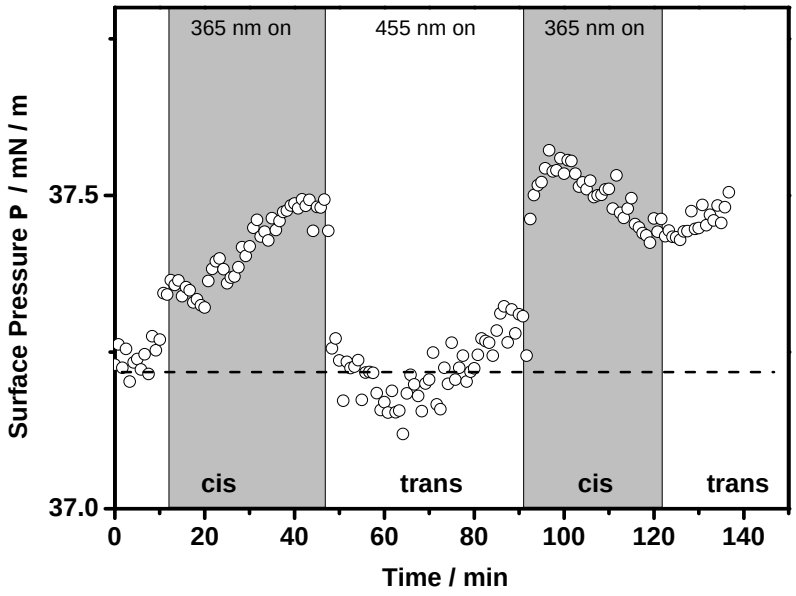

Fig. 6.6 Surface pressure modulation of a Azo-chol-DPPC monolayer 57 Å^2 / molecule upon 365/455 nm illumination are clearly observed.

6.4 Conclusion

SFG spectra of binary mixtures of Azobenzene-cholesterol-Dipalmitoylphosphatidylcholine (Azo-Chol-DPPC) shows the typical structure of a symmetric (r^+) and Fermi resonance ((r^+_{FR}) band of CH_3 stemming from DPPC. Due to the N^2 dependence of SFG intensity, vibrational bands attributed to cholesterol could not be observed. Compared with a pure DPPC spectra at the same surface pressure, the intensity of the CH_2 signal is somewhat more intense for the mixed monolayer, indicated that incorporation of cholesterol into the monolayers increases the conformational and orientational order of the alkyl chains of DPPC. By compressing monolayer from $2-8$ mN/m however, the ratio of CH_2/CH_3 decreases, which means that compression induces conversion of chains from the disordered state to a more or less ordered state. The surface pressure and molecular ordering of DPPC can be influenced by reversible switching of azobenzene-based lipid between its two states. Due to larger cross section area and dipole moment favors interaction with water, the *cis*-state corresponds to a higher surface pressure as compared to *trans*-state. Corresponding SFG spectra in CH spectral range show an increase of CH_3 signal intensity upon irradiation with

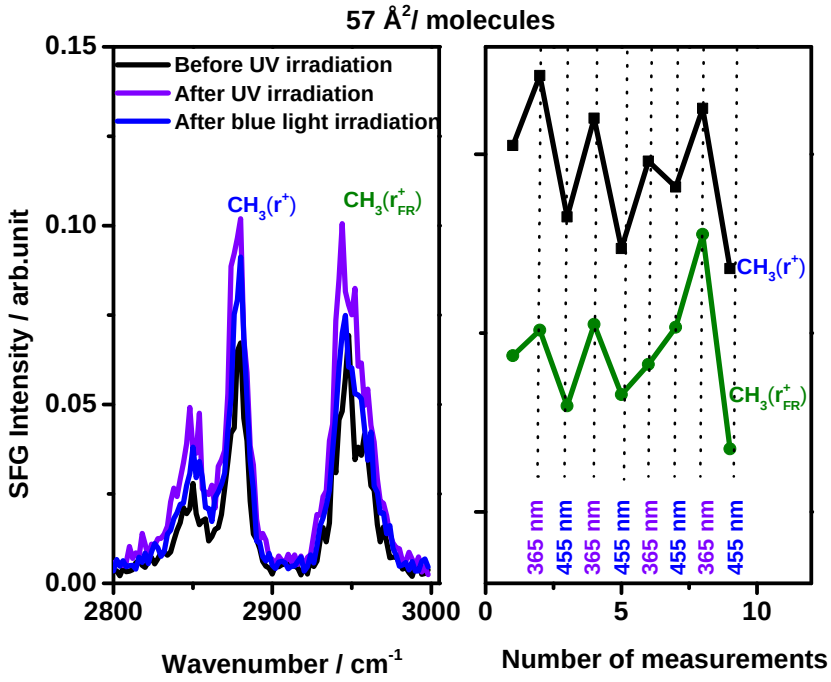

Fig. 6.7 Change in signal intensity of CH_3 peaks upon illumination of mixed azo-chol/ DPPC monolayer.

365 nm. Upon 450 nm illumination, the CH_3 intensity decreases again but didn't reach to its original value.

Appendix

Following tables depict the fitting parameter for SFG spectra

Table 1 Fitting parameters of MeAB-OC10S SAM on gold substrate.

SAMs	*Mode*	$\tilde{\nu}/\,cm^{-1}$	*A arb.u.*	*phase*	Γ */cm* $^{-1}$
MeABC10	d^+	2849	0.9	0	9
	d^+	2857	0.5	π	9
	$r^+/r^+_{FR} comb/overtone$	2880	1.2	π	9
	d^-	2901	0.5	π	9
	r^+	2925	3.3	π	9
	r^-_{op}	2949	1	0	9
	r^-	2969	1E-3	π	9
	r^-_{ip}	2993	0.2	π	9
	Ar	3030	1.3	π	9
	Ar	3063	1.4	π	9
	Ar	3074	2.2	0	9

Table 2 Fitting parameters of MeAB-OC11S SAM on gold substrate.

SAMs	*Mode*	$\tilde{\nu}/\,cm^{-1}$	*A arb.u.*	*phase*	Γ */cm* $^{-1}$
MeABC11	d^+	2845	0.4	0	9
	$r^+/r^+_{FR} comb/overtone$	2875	1.4	π	9
	d^-	2901	0.5	π	9
	r^+	2922	3.0	π	9
	r^-_{op}	2957	1.3	0	9
	r^-	2969	0.01	π	9
	r^-_{ip}	2993	0.2	π	9
	Ar	3024	0.9	π	9
	Ar	3057	1.3	π	9
	Ar	3071	1.5	0	9

Table 3 Fitting parameters of AB-OC11S SAM on gold substrate.

SAMs	*Mode*	$\tilde{\nu}/\,cm^{-1}$	*A arb.u.*	*phase*	Γ */cm* $^{-1}$
AB-C11	d^+	2849	0.4	0	9
	d^+	2857	0.2	π	9
	d^+	2868	0.9	0	9
	d^-	2900	0.5	π	9
	d^+_{FR}	2922	1.1	π	9
	Ar	3053	1.7	π	9
	Ar	371	1.5	π	9
	Ar	3079	1.0	0	9

Table 4 Fitting parameters of Decanethiol SAM on gold substrate.

SAMs	*Mode*	$\tilde{\nu}/\,cm^{-1}$	*A arb.u.*	*phase*	Γ */cm* $^{-1}$
C10S	d^+	2848	0.8	π	9
	d^+	2868	1.3	0	9
	r^+	2878	4.5	π	9
	d^-	2900	0.2	π	9
	r^+_{FR}	2938	2.8	π	9
	r^-_{op}	2950	1.0	π	9
	r^-_{ip}	2964	0.8	π	9

Table 5 Fitting parameters of Azobenzene functionalized SAMs on gold substrate with perdeuterated co-ligands dodecanethiol (dC12) in CH spectral range.

SAMs	*Mode*	$\tilde{\nu}/\,cm^{-1}$	*A arb.u.*	*phase*	Γ $/cm^{-1}$
$90\%MeABC_{11}+dC_{12}$	d^+	2845	0.3	0	9
	d^+	2870	0.3	π	9
	$r^+_{FR}comb/overtone$	2881	0.8	π	9
	d^-	2906	0.4	π	9
	r^+	2929	2.6	π	9
	r^-_{op}	2963	1.0	0	9
	r^-	2969	0.01	π	9
	r^-_{ip}	2999	0.01	π	9
	Ar	3032	0.06	π	9
	Ar	3060	0.7	π	9
	Ar	3078	0.9	0	9
$75\%MeABC_{11}+dC_{12}$	d^+	2845	0.05	0	9
	d^+	2858	0.7	π	9
	$r^+_{FR}comb/overtone$	2879	0.5	π	9
	d^-	2901	0.6	π	9
	r^+	2925	2.3	π	9
	r^-_{op}	2958	0.8	0	9
	r^-	2969	0.01	π	9
	r^-_{ip}	2993	0.5	π	9
	Ar	3030	0.9	π	9
	Ar	3058	1.1	π	9
	Ar	3079	0.5	0	9
$60\%MeABC_{11}+dC_{12}$	d^+	2852	0.1	0	9
	$r^+_{FR}comb/overtone$	2877	0.5	π	9
	d^-	2905	0.5	π	9
	r^+	2925	1.7	π	9
	r^-_{op}	2962	0.5	0	9
	r^-	2970	0.3	π	9
	r^-_{ip}	3007	0.5	π	9
	Ar	3034	0.3	π	9
	Ar	3054	0.5	π	9
	Ar	3066	0.2	0	9
$50\%MeABC_{11}+dC_{12}$	d^+	2845	1E-3	0	9
	$r^+_{FR}comb/overtone$	2879	0.3	π	9
	d^-	2903	0.09	π	9
	r^+	2920	1.3	π	9
	r^-_{ip}	2993	0.05	π	9
	Ar	3023	0.2	π	9
	Ar	3069	0.2	π	9
	Ar	3079	0.2	0	9

Table 6 Fitting parameters of Azobenzene functionalized SAMs on gold substrate with perdeuterated co-ligands dodecanethiol (dC16) in CH spectral range.

SAMs	*Mode*	$\tilde{\nu}/\,cm^{-1}$	*A arb.u.*	*phase*	Γ $/cm^{-1}$
$90\%MeABC_{11}+dC_{16}$	d^+	2853	0.2	0	9
	d^+	2870	1.1	π	9
	$r^+_{FR}comb/overtone$	2880	1.3	π	9
	d^-	2901	0.5	π	9
	r^+	2927	3.0	π	9
	r^-_{op}	2950	1.0	0	9
	r^-	2960	0.01	π	9
	r^-_{ip}	3003	0.7	π	9
	Ar	3029	1.0	π	9
	Ar	3060	1.0	π	9
	Ar	3078	1.7	0	9
$75\%MeABC_{11}+dC_{16}$	d^+	2849	0.1	0	9
	d^+	2860	1.0	π	9
	$r^+_{FR}comb/overtone$	2877	0.5	π	9
	d^-	2901	0.05	π	9
	r^+	2925	2.7	π	9
	r^-_{op}	2955	0.9	0	9
	r^-	2969	1E-3	π	9
	r^-_{ip}	2993	0.4	π	9
	Ar	3030	0.6	π	9
	Ar	3050	0.9	π	9
	Ar	3079	1.5	0	9
$60\%MeABC_{11}+dC_{16}$	d^+	2849	0.09	0	9
	d^+	2863	0.2	π	9
	$r^+_{FR}comb/overtone$	2874	0.1	π	9
	d^-	2901	0.02	π	9
	r^+	2925	2.0	π	9
	r^-_{op}	2955	0.4	0	9
	r^-	2970	1E-3	π	9
	r^-_{ip}	2993	0.3	π	9
	Ar	3028	0.5	π	9
	Ar	3057	0.5	π	9
	Ar	3077	1.5	0	9
$50\%MeABC_{11}+dC_{16}$	d^+	2848	0.005	0	9
	d^+	2865	0.5	π	9
	$r^+_{FR}comb/overtone$	2875	0.1	π	9
	d^-	2901	1E-3	π	9
	r^+	2922	1.5	π	9
	r^-_{op}	2955	0.6	0	9
	r^-	2969	0.01	π	9
	$r^{-]}ip$	3001	0.15	π	9
	Ar	3031	0.4	π	9
	Ar	3057	0.4	π	9
	Ar	3079	0.4	0	9

Table 7 Fitting parameters of Azobenzene functionalized SAMs on gold substrate with perdeuterated co-ligands decanethiol (dC10) in CH spectral range.

SAMs	*Mode*	$\tilde{\nu}/\,cm^{-1}$	*A arb.u.*	*phase*	Γ $/cm^{-1}$
$75\%MeABC_{11}+dC_{10}$	d^+	2853	0.6	π	10
	$r^+_{FR}comb/overtone$	2880	1.0	π	10
	d^+	2915	2.0	π	13
	r^+	2937	2.5	π	12
	r^-_{op}	2941	3.0	0	17
	r^-	2965	0.8	0	6
	r^-_{ip}	2999	0.5	π	20
	Ar	3020	0.2	π	5
	Ar	3065	0.2	π	5
	Ar	3078	0.3	0	7
$50\%MeABC_{11}+dC_{10}$	d^+	2852	0.9	π	10
	$r^+_{FR}comb/overtone$	2880	1.3	π	10
	d^+	2915	2.5	π	13
	r^+	2937	2.5	π	12
	r^-_{op}	2941	2.7	0	17
	r^-	2969	0.7	0	10
	r^-_{ip}	2999	0.5	π	20
	Ar	3020	0.2	π	5
	Ar	3055	0.2	π	5
	Ar	3071	0.2	0	7

Table 8 Fitting parameters of Azobenzene functionalized SAMs on gold substrate in CD spectral range for deuterated dodecanethiol

SAMs	*Mode*	$\tilde{\nu}/\,cm^{-1}$	*A arb.u.*	*phase*	Γ $/cm^{-1}$
100%dC_{12}	r^+	2079	3.0	π	9
	d^+	2100	0.3	π	9
	r^+_{FR}	2130	2.0	π	9
	dr^+_{FR}	2158	0.3	0	9
	r^-	2215	1.1	0	9
90%dC_{12}	r^+	2079	3.0	π	9
	d^+	2100	0.3	π	9
	r^+_{FR}	2130	1.8	π	9
	dr^+_{FR}	2158	0.3	0	9
	r^-	2215	1.1	0	9
75%dC_{12}	r^+	2079	3.0	π	9
	d^+	2100	0.3	π	9
	r^+_{FR}	2130	1.3	π	9
	dr^+_{FR}	2158	0.2	0	9
	r^-	2215	1.1	0	9
65%dC_{12}	r^+	2079	2.1	π	9
	d^+	2100	0.3	π	9
	r^+_{FR}	2130	0.8	π	9
	dr^+_{FR}	2158	0.1	0	9
	r^-	2215	0.3	0	9
50%dC_{12}	r^+	2079	2.1	π	9
	d^+	2100	0.2	π	9
	r^+_{FR}	2130	0.7	π	9
	dr^+_{FR}	2158	0.1	0	9
	r^-	2215	0.3	0	9

Table 9 Fitting parameters of Azobenzene functionalized SAMs on gold substrate in CD spectral range for deuterated hexadecanethiol.

SAMs	*Mode*	$\tilde{\nu}/\,cm^{-1}$	*A arb.u.*	*phase*	Γ $/cm^{-1}$
100%dC_{16}	r^+	2079	2.8	π	9
	d^+	2100	0.3	π	9
	r^+_{FR}	2130	1.3	π	9
	dr^+_{FR}	2158	0.2	0	9
	r^-	2224	0.5	0	9
90%dC_{16}	r^+	2079	2.5	π	9
	d^+	2105	5E-4	π	9
	r^+_{FR}	2131	2.1	π	9
	dr^+_{FR}	2162	0.5	0	9
	r^-	2223	0.3	0	9
75%dC_{16}	r^+	2080	2.5	π	9
	d^+	2100	1E-4	π	9
	r^+_{FR}	2130	1.3	π	9
	dr^+_{FR}	2158	0.8	0	9
	r^-	2220	0.2	0	9
65%dC_{16}	r^+	2074	1.4	π	9
	d^+	2109	0.2	π	9
	r^+_{FR}	2131	1.5	π	9
	dr^+_{FR}	2158	0.02	0	9
	r^-	2220	0.5	0	9
50%dC_{16}	r^+	2079	1.4	π	9
	d^+	2109	0.05	π	9
	r^+_{FR}	2131	0.4	π	9
	dr^+_{FR}	2158	0.1	0	9
	r^-	2218	0.7	0	9

Pure monolayer

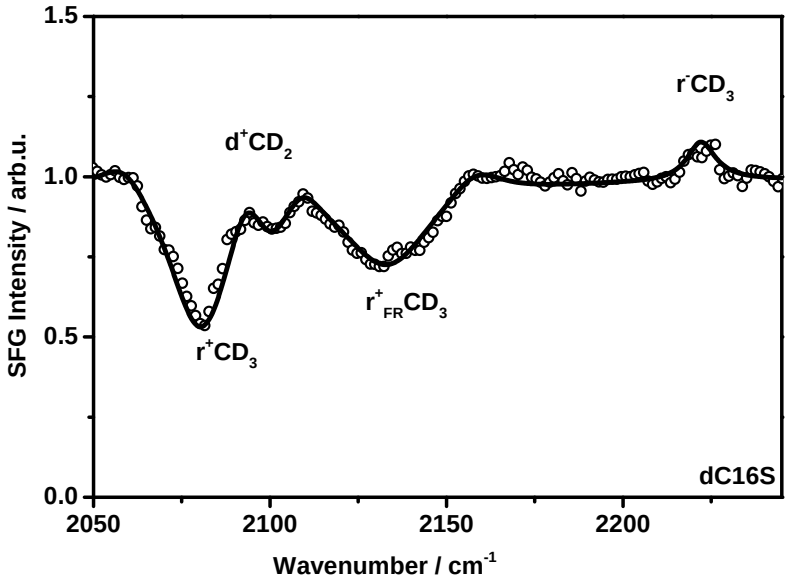

Fig. 1 SFG spectrum of a pure monolayer of dC16 on gold.

Concentration trend

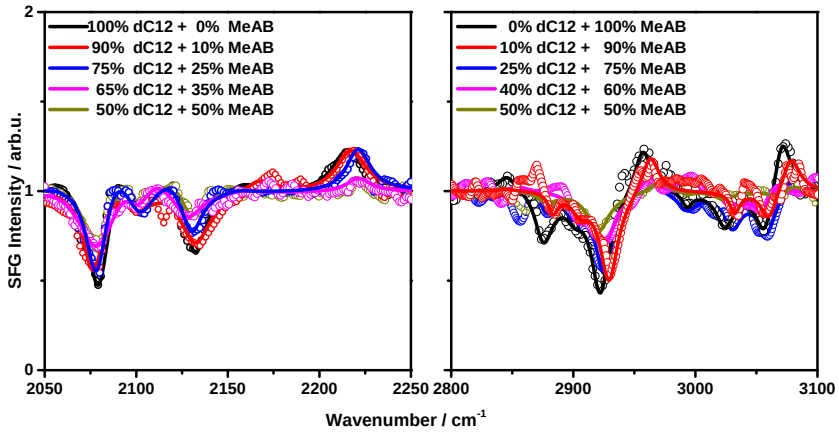

Fig. 2 SFG spectra of a pure and mixed thiol with dC12 as a co-ligand on gold. Peak intensities are decreasing with decreasing mole ratio of respective thiol in both CH and CD range.

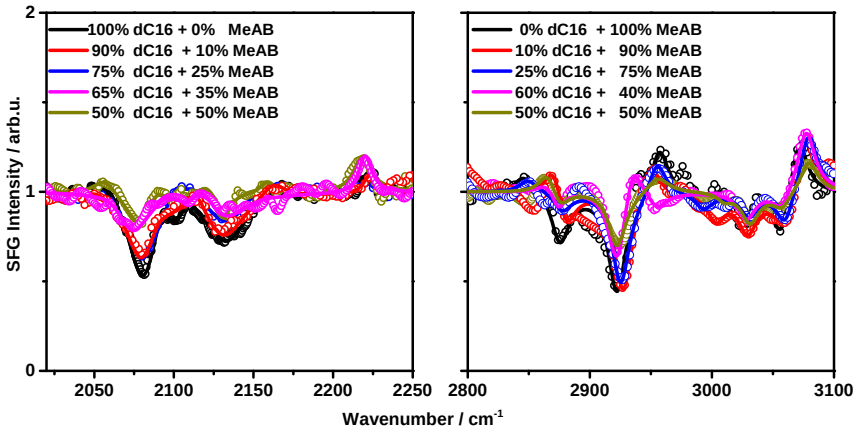

Fig. 3 SFG spectra of a pure and mixed AB thiol with dC16 as a co-ligand on gold. Peak intensities are decreasing with decreasing mole ratio of respective thiol in both CH and CD range.

References

[1] T. Seki, M. Sakuragi, Y. Kawanishi, T. Tamaki, R. Fukuda, K. Ichimura and Y. Suzuki. " Command surfaces" of Langmuir-Blodgett films. Photoregulations of liquid crystal alignment by molecularly tailored surface azobenzene layers. *Langmuir*, **1993**, 9(1), 211–218.

[2] A. Setaro, P. Bluemmel, C. Maity, S. Hecht and S. Reich. Non-Covalent Functionalization of Individual Nanotubes with Spiropyran-Based Molecular Switches. *Advanced Functional Materials*, **2012**, 22(11), 2425–2431.

[3] F. Pina, J. Parola, R. Gomes, M. Maestri and V. Balzani. Multistate/Multifunctional Molecular-Level Systems: Photochromic Flavylium Compounds. *Molecular Switches, Second Edition*, **2011**, pages 181–226. DOI: 10.1002/9783527634408.

[4] B. L. Feringa and W. R. Browne. Molecular Switches, volume 42. Wiley-VCH, **2001**.

[5] F. M. Raymo. Digital processing and communication with molecular switches. *Advanced Materials*, **2002**, 14(6), 401.

[6] W. R. Browne and B. L. Feringa. Making molecular machines work. *Nature Nanotechnology*, **2006**, 1(1), 25–35.

[7] E. R. Kay, D. A. Leigh and F. Zerbetto. Synthetic molecular motors and mechanical machines. *Angewandte Chemie International Edition*, **2007**, 46(1-2), 72–191.

[8] Z. Tian, W. Wu, W. Wan and A. D. Li. Single-chromophore-based photoswitchable nanoparticles enable dual-alternating-color fluorescence for unambiguous live cell imaging. *Journal of the American Chemical Society*, **2009**, 131(12), 4245–4252.

[9] R. Fishel. Mismatch repair, molecular switches, and signal transduction. *Genes & Development*, **1998**, 12(14), 2096–2101.

[10] P. Ducy. CBFA1: A molecular switch in osteoblast biology. *Developmental Dynamics*, **2000**, 219(4), 461–471.

[11] Y. Shi, W. H. Steier, L. Yu, M. Chen and L. R. Dalton. Large stable photoinduced refractive index change in a nonlinear optical polyester polymer with disperse red side groups. *Applied Physics Letters*, **1991**, 58(11), 1131–1133.

[12] R. Saito, M. Fujita, G. Dresselhaus and M. Dresselhaus. Electronic structure of chiral graphene tubules. *Applied physics letters*, **1992**, 60(18), 2204–2206.

[13] X.-M. Zhao, Y. Xia and G. M. Whitesides. Soft lithographic methods for nano-fabrication. *Journal of Materials Chemistry*, **1997**, 7(7), 1069–1074.

[14] R. Loucif-Saibi, K. Nakatani, J. Delaire, M. Dumont and Z. Sekkat. Photoisomerization and second harmonic generation in disperse red one-doped and-functionalized poly (methyl methacrylate) films. *Chemistry of Materials*, **1993**, 5(2), 229–236.

[15] T. A. Darwish, R. A. Evans and T. L. Hanley. Spiropyran, chromene and spirooxazine, mélange á trois: molecular logic systems through selective and reversible deactivation of photochromism mediated by CO_2 gas. *Dyes and Pigments*, **2012**, 92(2), 817–824.

[16] B. L. Feringa, W. F. Jager and B. de Lange. Organic materials for reversible optical data storage. *Tetrahedron*, **1993**, 49(37), 8267–8310.

[17] T. Ikeda and O. Tsutsumi. Optical switching and image storage by means of azobenzene liquid-crystal films. *Science*, **1995**, 268(5219), 1873–1875.

[18] G. Wang and J. Zhang. Photoresponsive molecular switches for biotechnology. *Journal of Photochemistry and Photobiology C: Photochemistry Reviews*, **2012**, 13(4), 299–309.

[19] X. Liang and J. Li. Biotechnology of Azobenzene-Modified DNA and RNA. In *Proceedings of the 2012 International Conference on Applied Biotechnology (ICAB 2012)*, pages 1317–1331. Springer, **2014**.

[20] M.-Q. Zhu, G.-F. Zhang, C. Li, M. P. Aldred, E. Chang, R. A. Drezek and A. D. Li. Reversible two-photon photoswitching and two-photon imaging of immunofunctionalized nanoparticles targeted to cancer cells. *Journal of the American Chemical Society*, **2010**, 133(2), 365–372.

[21] T. Shimoboji, E. Larenas, T. Fowler, S. Kulkarni, A. S. Hoffman and P. S. Stayton. Photoresponsive polymer–enzyme switches. *Proceedings of the National Academy of Sciences*, **2002**, 99(26), 16592–16596.

[22] G. Dormán and G. D. Prestwich. Using photolabile ligands in drug discovery and development. *Trends in biotechnology*, **2000**, 18(2), 64–77.

[23] B. W Laursen and F. C Krebs. Synthesis, structure, and properties of azatriangulenium salts. *Chemistry-A European Journal*, **2001**, 7(8), 1773–1783.

[24] J. Kubitschke, C. Näther and R. Herges. Synthesis of Functionalized Triazatriangulenes for Application in Photo-Switchable Self-Assembled Monolayers. *European Journal of Organic Chemistry*, **2010**, 2010(26), 5041–5055.

[25] A. Ulman. Formation and structure of self-assembled monolayers. *Chemical reviews*, **1996**, 96(4), 1533–1554.

[26] J. C. Love, L. A. Estroff, J. K. Kriebel, R. G. Nuzzo and G. M. Whitesides. Self-assembled monolayers of thiolates on metals as a form of nanotechnology. Apr. , (4), 1103–1169. ISSN 0009-2665. DOI: 10.1021/cr0300789.

[27] M. Zharnikov and M. Grunze. Spectroscopic characterization of thiol-derived self-assembling monolayers. *Journal of Physics: Condensed Matter*, **2001**, 13(49), 11333.

[28] C. D. Bain and G. M. Whitesides. Formation of monolayers by the coadsorption of thiols on gold: variation in the length of the alkyl chain. *Journal of the American Chemical Society*, **1989**, 111(18), 7164–7175.

[29] M. Hasan, D. Bethell and M. Brust. The fate of sulfur-bound hydrogen on formation of self-assembled thiol monolayers on gold: 1H NMR spectroscopic evidence from solutions of gold clusters. *Journal of the American Chemical Society*, **2002**, 124(7), 1132–1133.

[30] A. Ulman. An Introduction to Ultrathin Organic Films: From Langmuir–Blodgett to Self–Assembly. Academic press, **2013**.

[31] C. D. Bain, E. B. Troughton, Y. T. Tao, J. Evall, G. M. Whitesides and R. G. Nuzzo. Formation of monolayer films by the spontaneous assembly of organic thiols from solution onto gold. *Journal of the American Chemical Society*, **1989**, 111(1), 321–335.

[32] M. Himmelhaus, F. Eisert, M. Buck and M. Grunze. Self-assembly of n-alkanethiol monolayers. A study by IR-visible sum frequency spectroscopy (SFG). *Journal of Physical Chemistry B*, (3), 576–584.

[33] R. Yamada and K. Uosaki. In situ, real time monitoring of the self-assembly process of decanethiol on Au (111) in liquid phase. A scanning tunneling microscopy investigation. *Langmuir*, **1997**, 13(20), 5218–5221.

[34] G. Poirier and E. Pylant. The self-assembly mechanism of alkanethiols on Au (111). *Science*, **1996**, 272(5265), 1145–1148.

[35] S. Xu, S. J. Cruchon-Dupeyrat, J. C. Garno, G.-Y. Liu, G. Kane Jennings, T.-H. Yong and P. E. Laibinis. In situ studies of thiol self-assembly on gold from solution using atomic force microscopy. *Journal of Chemical Physics*, **1998**, 108, 5002–5012.

[36] M. Tachibana, K. Yoshizawa, A. Ogawa, H. Fujimoto and R. Hoffmann. Sulfur-gold orbital interactions which determine the structure of alkanethiolate/Au (111) self-assembled monolayer systems. *The Journal of Physical Chemistry B*, **2002**, 106(49), 12727–12736.

[37] C. A. Schlecht and J. A. Maurer. Functionalization of glass substrates: mechanistic insights into the surface reaction of trialkoxysilanes. *RSC Advances*, **2011**, 1(8), 1446–1448.

[38] N. A. LaFranzo. Use of Self-Assembled Monolayers to Tailor Surface Properties: From Lubrication to Neuronal Development. Washington university in St. Louis, **2013**.

[39] Y. Barness, O. Gershevitz, M. Sekar and C. N. Sukenik. Functionalized silanes for the preparation of siloxane-anchored monolayers. *Langmuir*, **2000**, 16(1), 247–251.

[40] G. J. Kluth, M. M. Sung and R. Maboudian. Thermal behavior of alkylsiloxane self-assembled monolayers on the oxidized Si (100) surface. *Langmuir*, **1997**, 13(14), 3775–3780.

[41] M. Mrksich and G. M. Whitesides. Using self-assembled monolayers to understand the interactions of man-made surfaces with proteins and cells. *Annual review of biophysics and biomolecular structure*, **1996**, 25(1), 55–78.

[42] A. Ulman. Formation and structure of self-assembled monolayers. *Chemical reviews*, **1996**, 96(4), 1533–1554.

[43] A. A. Beharry and G. A. Woolley. Azobenzene photoswitches for biomolecules. *Chemical Society Reviews*, **2011**, 40(8), 4422–4437.

[44] M. Banghart, K. Borges, E. Isacoff, D. Trauner and R. H. Kramer. Light-activated ion channels for remote control of neuronal firing. *Nature neuroscience*, **2004**, 7(12), 1381–1386.

[45] J.-P. Sauvage and V. Amendola. Molecular machines and motors, volume 99. Springer Science & Business Media, **2001**.

[46] A. Cembran, F. Bernardi, M. Garavelli, L. Gagliardi and G. Orlandi. On the Mechanism of the cis-trans Isomerization in the Lowest Electronic States of Azobenzene: S0, S1, and T1. *Journal of the American Chemical Society*, **2004**, 126(10), 3234–3243.

[47] J. Henzl, M. Mehlhorn, H. Gawronski, K.-H. Rieder and K. Morgenstern. Reversible cis–trans isomerization of a single azobenzene molecule. *Angewandte Chemie International Edition*, **2006**, 45(4), 603–606.

[48] M. Alemani, M. V. Peters, S. Hecht, K.-H. Rieder, F. Moresco and L. Grill. Electric field-induced isomerization of azobenzene by STM. *Journal of the American Chemical Society*, **2006**, 128(45), 14446–14447.

[49] W.-C. Chen, Y.-W. Lee and C.-T. Chen. Diastereoselective, synergistic dual-mode optical switch with integrated chirochromic helicene and photochromic bis-azobenzene moieties. *Organic letters*, **2010**, 12(7), 1472–1475.

[50] M. Akita. Photochromic Organometallics, A Stimuli-Responsive System: An Approach to Smart Chemical Systems. *Organometallics*, **2011**, 30(1), 43–51.

[51] A. Bannwarth, S. O. Schmidt, G. Peters, F. D. Sönnichsen, W. Thimm, R. Herges and F. Tuczek. FeIII Spin-Crossover Complexes with Photoisomerizable Ligands: Experimental and Theoretical Studies on the Ligand-Driven Light-Induced Spin Change Effect. *European Journal of Inorganic Chemistry*, **2012**, 2012(16), 2776–2783.

[52] S. Thies, H. Sell, C. Bornholdt, C. Schütt, F. Köhler, F. Tuczek and R. Herges. Light-Driven Coordination-Induced Spin-State Switching: Rational Design of Photodissociable Ligands. *Chemistry-A European Journal*, **2012**, 18(51), 16358–16368.

[53] P. Gütlich, A. B. Gaspar and Y. Garcia. Spin state switching in iron coordination compounds. *Beilstein journal of organic chemistry*, **2013**, 9(1), 342–391.

[54] P. Gütlich, Y. Garcia and T. Woike. Photoswitchable coordination compounds. *Coordination Chemistry Reviews*, **2001**, 219, 839–879. DOI: 10.1016/S0010-8545(01)00381-2.

[55] S. O. Schmidt, H. Naggert, A. Buchholz, H. Brandenburg, A. Bannwarth, W. Plass and F. Tuczek. Thermal and Light-Induced Spin Transitions of FeII Complexes with 4-and 5-(Phenylazo)-2, 2-bipyridine Ligands: Intra-vs. Intermolecular Effects. *European Journal of Inorganic Chemistry*, **2015**.

[56] S. Thies, H. Sell, C. Schutt, C. Bornholdt, C. Nather, F. Tuczek and R. Herges. Light-Induced spin change by photodissociable external ligands: A new principle for Magnetic Switching of Molecules. *Journal of the American Chemical Society*, **2011**, 133(40), 16243–16250. DOI: 10.1021/ja206812f.

[57] H. Rau. Photoisomerization of azobenzenes. *Photoreactive Organic Thin Films. Academic Press: San Diego*, **2002**.

[58] F. Lenci. Organic photochemistry and photobiology. CRC press, **2004**.

[59] G. S. Hartley. The cis-form of azobenzene and the velocity of the thermal cis→ trans-conversion of azobenzene and some derivatives. *Journal of the Chemical Society (Resumed)*, **1938**, pages 633–642.

[60] E. R. Talaty and J. C. Fargo. Thermal cis–trans-isomerization of substituted azobenzenes: a correction of the literature. *Chemical Communications (London)*, **1967**, (2), 65–66.

[61] C. Barrett, A. Natansohn and P. Rochon. Thermal cis-trans isomerization rates of azobenzenes bound in the side chain of some copolymers and blends. *Macromolecules*, **1994**, 27(17), 4781–4786.

[62] M. Sliwa, S. Létard, I. Malfant, M. Nierlich, P. G. Lacroix, T. Asahi, H. Masuhara, P. Yu and K. Nakatani. Design, synthesis, structural and nonlinear optical properties of photochromic crystals: Toward reversible molecular switches. *Chemistry of materials*, **2005**, 17(18), 4727–4735.

[63] V. Balzani, A. Credi and M. Venturi. Molecular devices and machines: concepts and perspectives for the nanoworld. John Wiley & Sons, **2008**.

[64] J. García-Amorós and D. Velasco. Recent advances towards azobenzene-based light-driven real-time information-transmitting materials. *Beilstein journal of organic chemistry*, **2012**, 8(1), 1003–1017.

[65] G. Berkovic, V. Krongauz and V. Weiss. Spiropyrans and spirooxazines for memories and switches. *Chemical reviews*, **2000**, 100(5), 1741–1754. DOI: 10.1021/cr9800715.

[66] H. D. Bandara and S. C. Burdette. Photoisomerization in different classes of azobenzene. *Chemical Society Reviews*, **2012**, 41(5), 1809–1825.

[67] P. Bortolus and S. Monti. Cis-trans photoisomerization of azobenzene. Solvent and triplet donors effects. *Journal of Physical Chemistry*, **1979**, 83(6), 648–652.

[68] L. Wang, W. Xu, C. Yi and X. Wang. Isomerization and electronic relaxation of azobenzene after being excited to higher electronic states. *Journal of Molecular Graphics and Modelling*, **2009**, 27(7), 792–796.

[69] E. Fischer, M. Frankel and R. Wolovsky. Wavelength dependence of photoisomerization equilibria in azocompounds. *The Journal of Chemical Physics*, **1955**, 23(7), 1367–1367.

[70] H. Rau and E. Lueddecke. On the rotation-inversion controversy on photoisomerization of azobenzenes. Experimental proof of inversion. *Journal of the American Chemical Society*, **1982**, 104(6), 1616–1620.

[71] D. Gegiou, K. Muszkat and E. Fischer. Temperature dependence of photoisomerization. VI. Viscosity effect. *Journal of the American Chemical Society*, **1968**, 90(1), 12–18.

[72] N. Siampiringue, G. Guyot, S. Monti and P. Bortolus. The cis→ trans photoisomerization of azobenzene: an experimental re-examination. *Journal of photochemistry*, **1987**, 37(1), 185–188.

[73] H. Dürr and H. Bouas-Laurent. Photochromism: molecules and systems: molecules and systems. Gulf Professional Publishing, **2003**.

[74] T. Asano, T. Yano and T. Okada. Mechanistic study of thermal ZE isomerization of azobenzenes by high-pressure kinetics. *Journal of the American Chemical Society*, **1982**, 104(18), 4900–4904.

[75] M. Robin, R. R. Hart and N. Kuebler. Electronic states of the azoalkanes. *Journal of the American Chemical Society*, **1967**, 89(7), 1564–1572.

[76] S. Ljunggren and G. Wettermark. A CNDO/2 Study of the Mechanism of Isomerization and. *Acta Chemica Scandinavica*, **1971**, 25(5), 1599–1606.

[77] J. L. Magee, W. Shand Jr and H. Eyring. Non-adiabatic Reactions. Rotation about the Double Bond. *Journal of the American Chemical Society*, **1941**, 63(3), 677–688.

[78] D. Y. Curtin, E. J. Grubbs and C. G. McCarty. Uncatalyzed syn-anti Isomerization of Imines, Oxime Ethers, and Haloimines1. *Journal of the American Chemical Society*, **1966**, 88(12), 2775–2786.

[79] T. Fujino, S. Y. Arzhantsev and T. Tahara. Femtosecond time-resolved fluorescence study of photoisomerization of trans-azobenzene. *The Journal of Physical Chemistry A*, **2001**, 105(35), 8123–8129.

[80] C.-W. Chang, Y.-C. Lu, T.-T. Wang and E. W.-G. Diau. Photoisomerization dynamics of azobenzene in solution with S–1 excitation: a femtosecond fluorescence anisotropy study. *Journal of the American Chemical Society*, **2004**, 126(32), 10109–10118.

[81] K. Nishiyama and M. Fujihira. cis–trans Reversible Photoisomerization of an Amphiphilic Azobenzene Derivative in Its Pure LB Film Prepared as Polyion Complexes with Polyallylamine. *Chemistry Letters*, **1988**, 17(8), 1257–1260.

[82] E. Benassi and S. Corni. Quenching of the Photoisomerization of Azobenzene Self-Assembled Monolayers by the Metal Substrate. *The Journal of Physical Chemistry C*, **2014**, 118(45), 25906–25917. DOI: dx.doi.org/10.1021/jp508246p.

[83] M. Piantek. Switchable molecules on metallic surfaces studied by core-level spectroscopies. *Dissertation*, Freie Universität Berlin. **2010**.

[84] M. J. Comstock, N. Levy, A. Kirakosian, J. Cho, F. Lauterwasser, J. H. Harvey, D. A. Strubbe, J. M. Fréchet, D. Trauner, S. G. Louie et al. Reversible photomechanical switching of individual engineered molecules at a metallic surface. *Physical review letters*, **2007**, 99(3), 038301.

[85] A. S. Kumar, T. Ye, T. Takami, B.-C. Yu, A. K. Flatt, J. M. Tour and P. S. Weiss. Reversible photo-switching of single azobenzene molecules in controlled nanoscale environments. *Nano letters*, **2008**, 8(6), 1644–1648.

[86] C. Bronner, M. Schulze, S. Hagen and P. Tegeder. The influence of the electronic structure of adsorbate–substrate complexes on photoisomerization ability. *New Journal of Physics*, **2012**, 14(4), 043023.

[87] M. Wolf and P. Tegeder. Reversible molecular switching at a metal surface: a case study of tetra-tert-butyl-azobenzene on Au (111). *Surface Science*, **2009**, 603(10), 1506–1517. DOI: 10.1016/j.susc.2008.11.049.

[88] S. Hagen, P. Kate, F. Leyssner, D. Nandi, M. Wolf and P. Tegeder. Excitation mechanism in the photoisomerization of a surface-bound azobenzene derivative: Role of the metallic substrate. *The Journal of chemical physics*, **2008**, 129(16), 164102. DOI: 10.1063/1.2997343.

[89] M. Muntwiler, C. Lindstrom and X.-Y. Zhu. Delocalized electron resonance at the alkanethiolate self-assembled monolayer/ Au (111) interface. *The Journal of chemical physics*, **2006**, 124(8), 081104.

[90] T. Weidner, F. Bretthauer, N. Ballav, H. Motschmann, H. Orendi, C. Bruhn, U. Siemeling and M. Zharnikov. Correlation between the molecular structure and photoresponse in aliphatic self-assembled monolayers with azobenzene tailgroups. *Langmuir*, Oct. , (20), 11691–11700. ISSN 0743-7463. DOI: 10.1021/la802454w.

[91] C. Gahl, R. Schmidt, D. Brete, E. R. McNellis, W. Freyer, R. Carley, K. Reuter and M. Weinelt. Structure and excitonic coupling in self-assembled monolayers of azobenzene-functionalized alkanethiols. *Journal of the American Chemical Society*, **2010**, 132(15), 1831–1838. ISSN 00027863. DOI: 10.1021/ja903636q.

[92] M. Utecht, T. Klamroth and P. Saalfrank. Optical absorption and excitonic coupling in azobenzenes forming self-assembled monolayers: a study based on density functional theory. *Physical Chemistry Chemical Physics*, **2011**, 13(48), 21608–21614.

[93] N. Heinemann, J. Grunau, T. Leissner, O. Andreyev, S. Kuhn, U. Jung, D. Zargarani, R. Herges, O. Magnussen and M. Bauer. Reversible switching in self-assembled monolayers of azobenzene thiolates on Au (111) probed by threshold photoemission. *Chemical Physics*, **2012**, 402, 22–28. ISSN 03010104. DOI: 10.1016/j.chemphys.2012.03.025.

[94] S. Evans, S. Johnson, H. Ringsdorf, L. Williams and H. Wolf. Photoswitching of azobenzene derivatives formed on planar and colloidal gold surfaces. *Langmuir*, **1998**, 14(22), 6436–6440.

[95] P. Ahonen, T. Laaksonen, D. J. Schiffrin and K. Kontturi. Photoswitching electron transport properties of an azobenzene containing thiol-SAM. *Physical Chemistry Chemical Physics*, **2007**, 9(35), 4898–4901.

[96] Y. B. Zheng, B. K. Pathem, J. N. Hohman, J. C. Thomas, M. Kim and P. S. Weiss. Photoresponsive Molecules in Well-Defined Nanoscale Environments. *Advanced Materials*, **2013**, 25(3), 302–312.

[97] R. Klajn. Immobilized azobenzenes for the construction of photoresponsive materials. *Pure and Applied Chemistry*, Jan. , (12), 2247–2279. ISSN 1365-3075. DOI: 10.1351/PAC-CON-10-09-04.

[98] J. G. Victor and J. M. Torkelson. On measuring the distribution of local free volume in glassy polymers by photochromic and fluorescence techniques. *Macromolecules*, **1987**, 20(9), 2241–2250.

[99] A. N. Shipway and I. Willner. Electronically transduced molecular mechanical and information functions on surfaces. *Accounts of chemical research*, **2001**, 34(6), 421–432.

[100] D. T. Valley, M. Onstott, S. Malyk and A. V. Benderskii. Steric hindrance of photoswitching in self-assembled monolayers of azobenzene and alkane thiols. *Langmuir*, **2013**, 29(37), 11623–11631. ISSN 1520-5827. DOI: 10.1021/la402144g.

[101] T. Moldt, D. Brete, D. Przyrembel, S. Das, J. R. Goldman, P. K. Kundu, C. Gahl, R. Klajn and M. Weinelt. Tailoring the Properties of Surface-Immobilized Azobenzenes by Monolayer Dilution and Surface Curvature. *Langmuir*, **2015**, 31, 1048–1057. DOI: 10.1021/la504291n.

[102] H. Yu, J. Zhao, Y. Wang, S. Cai and Z. Liu. Fabricating an azobenzene self-assembled monolayer via step-by-step surface modification of a cysteamine monolayer on gold. *Journal of Electroanalytical Chemistry*, **1997**, 438(1), 221–224.

[103] S. Yasuda, T. Nakamura, M. Matsumoto and H. Shigekawa. Phase Switching of a Single Isomeric Molecule and Associated Characteristic Rectification. *Journal of the American Chemical Society*, **2003**, 125(22), 16430–16433. ISSN 00027863. DOI: 10.1021/ja038233o.

[104] M. Ito, T. X. Wei, P.-L. Chen, H. Akiyama, M. Matsumoto, K. Tamada and Y. Yamamoto. A novel method for creation of free volume in a one-component self-assembled monolayer. Dramatic size effect of para-carborane. *Journal of Materials Chemistry*, (4), 478. ISSN 0959-9428. DOI: 10.1039/b411121d.

[105] U. Jung, O. Filinova, S. Kuhn, D. Zargarani, C. Bornholdt, R. Herges and O. Magnussen. Photoswitching behavior of azobenzene-containing alkanethiol self-assembled monolayers on Au surfaces. *Langmuir*, Sept. , (17), 13913–13923. ISSN 1520-5827. DOI: 10.1021/la1015109.

[106] K. Tamada, H. Akiyama, T.-X. Wei and S.-A. Kim. Photoisomerization reaction of unsymmetrical azobenzene disulfide self-assembled monolayers: modification of azobenzene dyes to improve thermal endurance for photoreaction. *Langmuir*, **2003**, 19(6), 2306–2312.

[107] R. K. Smith, S. M. Reed, P. A. Lewis, J. D. Monnell, R. S. Clegg, K. F. Kelly, L. A. Bumm, J. E. Hutchison and P. S. Weiss. Phase separation within a binary self-assembled monolayer on Au {111} driven by an amide-containing alkanethiol. *The Journal of Physical Chemistry*, pages 1119–1122. ISSN 1520-6106. DOI: 10.1021/jp0035129.

[108] B. Lüssem, L. Müller-Meskamp, S. Karthäuser, R. Waser, M. Homberger and U. Simon. STM study of mixed alkanethiol/biphenylthiol self-assembled monolayers on Au (111). *Langmuir*, **2006**, 22(7), 3021–3027.

[109] J. P. Folkers, P. E. Laibinis and G. M. Whitesides. Self-assembled monolayers of alkanethiols on gold: comparisons of monolayers containing mixtures of short-and long-chain constituents with methyl and hydroxymethyl terminal groups. *Langmuir*, **1992**, 8(5), 1330–1341.

[110] K. Tamada, M. Hara, H. Sasabe and W. Knoll. Surface phase behavior of n-alkanethiol self-assembled monolayers adsorbed on Au (111): An atomic force microscope study. *Langmuir*, **1997**, 13(6), 1558–1566.

[111] K. Tamada, H. Akiyama and T. X. Wei. Photoisomerization reaction of unsymmetrical azobenzene disulfide self-assembled monolayers studied by surface plasmon spectroscopy: Influences of side chain length and contacting medium. *Langmuir*, **2002**, 18 (13), 5239–5246.

[112] S. Stranick, A. Parikh, Y.-T. Tao, D. Allara and P. Weiss. Phase separation of mixed-composition self-assembled monolayers into nanometer scale molecular domains. *The Journal of Physical Chemistry*, **1994**, 98(31), 7636–7646.

[113] A. Köhntopp, A. Dabrowski, M. Malicki and F. Temps. Photoisomerisation and ligand-controlled reversible aggregation of azobenzene-functionalised gold nanoparticles. *Chemical Communications*, **2014**, 50(70), 10105–10107.

[114] H. Imahori, H. Norieda, Y. Nishimura, I. Yamazaki, K. Higuchi, N. Kato, T. Motohiro, H. Yamada, K. Tamaki, M. Arimura and Y. Sakata. Chain Length Effect on the Structure and Photoelectrochemical Properties of Self-Assembled Monolayers of Porphyrins on Gold Electrodes. *The Journal of Physical Chemistry B*, **2000**, 104(6), 1253–1260. DOI: 10.1021/jp992768f.

[115] M. Han, D. Ishikawa, T. Honda, E. Ito and M. Hara. Light-driven molecular switches in azobenzene self-assembled monolayers: effect of molecular structure on reversible photoisomerization and stable cis state. *Chemical communications*, May , (20), 3598–3600. ISSN 1364-548X. DOI: 10.1039/b921801g.

[116] H. Akiyama, K. Tamada, J. Nagasawa, K. Abe and T. Tamaki. Photoreactivity in self-assembled monolayers formed from asymmetric disulfides having para-substituted azobenzenes. *The Journal of Physical Chemistry B*, **2003**, 107(1), 130–135.

[117] S. Wagner, F. Leyssner, C. Kördel, S. Zarwell, R. Schmidt, M. Weinelt, K. Rück-Braun, M. Wolf and P. Tegeder. Reversible photoisomerization of an azobenzene-functionalized self-assembled monolayer probed by sum-frequency generation vibrational spectroscopy. *Physical Chemistry Chemical Physics*, **2009**, 11(29), 6242–6248. ISSN 1463-9076. DOI: 10.1039/b823330f.

[118] T. Kondo, T. Kanai and K. Uosaki. Control of the charge-transfer rate at a gold electrode modified with a self-assembled monolayer containing ferrocene and azobenzene by electro-and photochemical structural conversion of cis and trans forms of the azobenzene moiety. *Langmuir*, **2001**, 17(20), 6317–6324.

[119] U. Jung, C. Schütt, O. Filinova, J. Kubitschke, R. Herges and O. Magnussen. Photoswitching of Azobenzene-Functionalized Molecular Platforms on Au Surfaces. *The Journal of Physical Chemistry C*, Dec. , (49), 25943–25948. ISSN 1932-7447. DOI: 10.1021/jp310451c.

[120] H. Jacob, S. Ulrich, U. Jung, S. Lemke, T. Rusch, C. Schütt, F. Petersen, T. Strunskus, O. Magnussen, R. Herges and F. Tuczek. Monitoring the reversible photoisomerization of an azobenzene-functionalized molecular triazatriangulene platform on Au(111) by IRRAS. *Physical chemistry chemical physics : PCCP*, Sept. **2014**. ISSN 1463-9084. DOI: 10.1039/c4cp03438d. Webseite: http://www.ncbi.nlm.nih.gov/pubmed/25242068.

[121] B. Baisch, D. Raffa, U. Jung, O. M. Magnussen, C. Nicolas, J. Lacour, J. Kubitschke and R. Herges. Mounting freestanding molecular functions onto surfaces: The platform approach. *Journal of the American Chemical Society*, **2008**, 131(2), 442–443. DOI: 10.1021/ja807923f.

[122] C. Bronner, G. Schulze, K. J. Franke, J. I. Pascual and P. Tegeder. Switching ability of nitro-spiropyran on Au (111): electronic structure changes as a sensitive probe during a ring-opening reaction. *Journal of Physics: Condensed Matter*, **2011**, 23(48), 484005.

[123] S. Ulrich, U. Jung, T. Strunskus, C. Schutt, A. Bloedorn, S. Lemke, E. Ludwig, L. Kipp, F. Faupel, O. Magnussen and R. Herges. X-ray spectroscopy characterization of azobenzene-functionalized triazatriangulenium adlayers on Au(111) surfaces. *Phys. Chem. Chem. Phys.*, **2015**, 17, 17053–17062. DOI: 10.1039/C5CP01447F.

[124] U. Jung, J. Kubitschke, R. Herges and O. Magnussen. Studies of the molecular switching of azobenzene-functionalized platform adlayers on Au (111) by chronoamperometry. *Electrochimica Acta*, **2013**, 112, 869–880.

[125] N. Hauptmann, K. Scheil, T. G. Gopakumar, F. L. Otte, C. Schutt, R. Herges and R. Berndt. Surface control of alkyl chain conformations and 2D chiral amplification. *Journal of the American Chemical Society*, **2013**, 135(24), 8814–8817. DOI: dx.doi.org/10.1021/ja4036187.

[126] N. Krekiehn, M. Muller, U. Jung, S. Ulrich, R. Herges and O. Magnussen. UV/Vis Spectroscopy Studies of the Photoisomerization Kinetics in Self-Assembled Azobenzene-Containing Adlayers. *Langmuir*, **2015**, 31(30), 8362–8370.

[127] U. Jung, S. Kuhn, U. Cornelissen, F. Tuczek, T. Strunskus, V. Zaporojtchenko, J. Kubitschke, R. Herges and O. Magnussen. Azobenzene-containing triazatriangulenium adlayers on Au (111): Structural and spectroscopic characterization. *Langmuir*, **2011**, 27(10), 5899–5908.

[128] S. Sortino, S. Petralia, S. Conoci and S. Di Bella. Monitoring photoswitching of azobenzene-based self-assembled monolayers on ultrathin platinum films by UV/vis spectroscopy in the transmission mode. *Journal of Materials Chemistry*, **2004**, 14(5), 811–813.

[129] M. Elbing, A. Błaszczyk, C. von Hänisch, M. Mayor, V. Ferri, C. Grave, M. A. Rampi, G. Pace, P. Samorì, A. Shaporenko and M. Zharnikov. Single Component Self-Assembled Monolayers of Aromatic Azo-Biphenyl: Influence of the Packing Tightness on the SAM Structure and Light-Induced Molecular Movements. *Advanced Functional Materials*, 18(19). ISSN 1616-3028.

[130] T. Kawai, J. Umemura and T. Takenaka. UV absorption spectra of azobenzene-containing long-chain fatty acids and their barium salts in spread monolayers and Langmuir-Blodgett films. *Langmuir*, **1989**, 5(6), 1378–1383. DOI: 10.1021/la00090a020.

[131] P. Hamm, S. Ohline and W. Zinth. Vibrational cooling after ultrafast photoisomerization of azobenzene measured by femtosecond infrared spectroscopy. *The Journal of chemical physics*, **1997**, 106(2), 519–529.

[132] I. Lednev, T.-Q. Ye, P. Matousek, M. Towrie, P. Foggi, F. Neuwahl, S. Umapathy, R. Hester and J. N. Moore. Femtosecond time-resolved UV-visible absorption spectroscopy of trans-azobenzene: dependence on excitation wavelength. *Chemical Physics Letters*, **1998**, 290(1), 68–74.

[133] R. Alicante. Photoinduced Modifications of the Nonlinear Optical Response in Liquid Crystalline Azopolymers. Springer Science & Business Media, **2012**.

[134] C. Kouvatas, W. E. Baille, J. Ortíz-Palacios, E. Aguilar-Ortíz, E. Rivera and X. X. Zhu. Conformation of Novel Azo-Dyes Bearing End-Capped Oligo (ethylene glycol) Studied by UV–vis and NMR Spectroscopy. *The Journal of Physical Chemistry B*, **2015**, 119(37), 12318–12324.

[135] G. S. Kumar. Azo Functional Polymers: Functional Group Approach in Macromolec. CRC Press, **1992**.

[136] G. S. Kumar and D. Neckers. Photochemistry of azobenzene-containing polymers. *Chemical Reviews*, **1989**, 89(8), 1915–1925.

[137] Y. Zhao and T. Ikeda. Smart light-responsive materials: azobenzene-containing polymers and liquid crystals. John Wiley & Sons, **2009**.

[138] M. Davies. Dielectric and related molecular processes, volume 1. Royal Society of Chemistry, **1972**.

[139] W. Freyer, D. Brete, R. Schmidt, C. Gahl, R. Carley and M. Weinelt. Switching behavior and optical absorbance of azobenzene-functionalized alkanethiols in different environments. *Journal of Photochemistry and Photobiology A: Chemistry*, **2009**, 204 (2), 102–109.

[140] M. Han, T. Honda, D. Ishikawa, E. Ito, M. Hara and Y. Norikane. Realization of highly photoresponsive azobenzene-functionalized monolayers. *Journal of Materials Chemistry*, **2011**, 21(12), 4696–4702.

[141] K. Cimatu and S. Baldelli. Sum frequency generation microscopy of microcontact-printed mixed self-assembled monolayers. *The Journal of Physical Chemistry B*, **2006**, 110(4), 1807–1813.

[142] K. M. Bratlie, K. Komvopoulos and G. A. Somorjai. Sum Frequency Generation Vibrational Spectroscopy of Pyridine Hydrogenation on Platinum Nanoparticles. *The Journal of Physical Chemistry C*, **2008**, 112(31), 11865–11868.

[143] C. J. Kliewer, M. Bieri and G. A. Somorjai. Pyrrole hydrogenation over Rh (111) and Pt (111) single-crystal surfaces and hydrogenation promotion mediated by 1-methylpyrrole: A Kinetic and Sum-Frequency Generation Vibrational Spectroscopy Study. *The Journal of Physical Chemistry C*, **2008**, 112(30), 11373–11378.

[144] C. Chen, J. Wang, S. E. Woodcock and Z. Chen. Surface morphology and molecular chemical structure of poly (n-butyl methacrylate)/polystyrene blend studied by atomic force microscopy (AFM) and sum frequency generation (SFG) vibrational spectroscopy. *Langmuir*, **2002**, 18(4), 1302–1309.

[145] C.-y. Chen, M. A. Even, J. Wang and Z. Chen. Sum frequency generation vibrational Spectroscopy studies on molecular conformation of liquid polymers poly (ethylene glycol) and poly (propylene glycol) at different interfaces. *Macromolecules*, **2002**, 35 (24), 9130–9135.

[146] X. Chen, A. P. Boughton, J. J. Tesmer and Z. Chen. In situ investigation of heterotrimeric G protein $\beta\gamma$ subunit binding and orientation on membrane bilayers. *Journal of the American Chemical Society*, **2007**, 129(42), 12658–12659.

[147] X. Chen, J. Wang, Z. Paszti, F. Wang, J. N. Schrauben, V. V. Tarabara, A. H. Schmaier and Z. Chen. Ordered adsorption of coagulation factor XII on negatively charged polymer surfaces probed by sum frequency generation vibrational spectroscopy. *Analytical and bioanalytical chemistry*, **2007**, 388(1), 65–72.

[148] X. Chen and Z. Chen. SFG studies on interactions between antimicrobial peptides and supported lipid bilayers. *Biochimica et Biophysica Acta (BBA)-Biomembranes*, **2006**, 1758(9), 1257–1273.

[149] Y. Ishitsuka, L. Arnt, J. Majewski, S. Frey, M. Ratajczek, K. Kjaer, G. N. Tew and K. Y. C. Lee. Amphiphilic poly (phenyleneethynylene) s can mimic antimicrobial peptide membrane disordering effect by membrane insertion. *Journal of the American Chemical Society*, **2006**, 128(40), 13123–13129.

[150] G. Y. Stokes, J. M. Gibbs-Davis, F. C. Boman, B. R. Stepp, A. G. Condie, S. T. Nguyen and F. M. Geiger. Making "sense" of DNA. *Journal of the American Chemical Society*, **2007**, 129(24), 7492–7493.

[151] G. Ma and H. C. Allen. Condensing effect of palmitic acid on DPPC in mixed Langmuir monolayers. *Langmuir*, **2007**, 23(2), 589–597.

[152] G. Ma and H. C. Allen. New insights into lung surfactant monolayers using vibrational sum frequency generation spectroscopy. *Photochemistry and photobiology*, **2006**, 82 (6), 1517–1529.

[153] Y. Shen. Surface properties probed by second-harmonic and sum-frequency generation. *Nature*, **1989**, 337, 519–525.

[154] Y. Shen. Surfaces probed by nonlinear optics. *Surface Science*, **1994**, 299, 551–562.

[155] X. Zhu, H. Suhr and Y. Shen. Surface vibrational spectroscopy by infrared-visible sum frequency generation. *Physical Review B*, **1987**, 35(6), 3047.

[156] J. Hunt, P. Guyot-Sionnest and Y. Shen. Observation of CH stretch vibrations of monolayers of molecules optical sum-frequency generation. *Chemical physics letters*, **1987**, 133(3), 189–192.

[157] A. Harris, C. Chidsey, N. Levinos and D. Loiacono. Monolayer vibrational spectroscopy by infrared-visible sum generation at metal and semiconductor surfaces. *Chemical physics letters*, **1987**, 141(4), 350–356.

[158] S. Ye and M. Osawa. Molecular structures on solid substrates probed by sum frequency generation (SFG) vibration spectroscopy. *Chemistry Letters*, **2009**, 38(5), 386–391.

[159] Z. Chen, Y. Shen and G. A. Somorjai. Studies of polymer surfaces by sum frequency generation vibrational spectroscopy. *Annual review of physical chemistry*, **2002**, 53 (1), 437–465.

[160] C. D. Bain, P. B. Davies, T. H. Ong, N. W. Robert and M. A. Brown. Quantitative Analysis of Monolayer Composition. *Langmuir*, **1991**, 7, 1563–1566.

[161] E. A. Raymond and G. L. Richmond. Probing the molecular structure and bonding of the surface of aqueous salt solutions. *The Journal of Physical Chemistry B*, **2004**, 108 (16), 5051–5059.

[162] C. L. Loch, D. Ahn, C. Chen and Z. Chen. Polymer-silane interactions probed by sum frequency generation vibrational spectroscopy. *The Journal of Adhesion*, **2005**, 81 (3-4), 319–345.

[163] Y.-R. Shen. The principles of nonlinear optics. *New York, Wiley-Interscience, 1984, 575 p.*, **1984**.

[164] P. Guyot-Sionnest, R. Superfine, J. Hunt and Y. Shen. Vibrational spectroscopy of a silane monolayer at air/solid and liquid/solid interfaces using sum-frequency generation. *Chemical physics letters*, **1988**, 144(1), 1–5.

[165] P. Guyot-Sionnest, J. Hunt and Y. Shen. Sum-frequency vibrational spectroscopy of a Langmuir film: Study of molecular orientation of a two-dimensional system. *Physical review letters*, **1987**, 59(14), 1597.

[166] D. Zhang, J. Gutow and K. Eisenthal. "Vibrational spectra, orientations, and phase transitions in long-chain amphiphiles at the air/water interface: Probing the head and tail groups by sum frequency generation". *The Journal of Physical Chemistry*, **1994**, 98(51), 13729–13734.

[167] C. Hirose, H. Yamamoto, N. Akamatsu and K. Domen. Orientation analysis by simulation of vibrational sum frequency generation spectrum: CH stretching bands of the methyl group. *The Journal of Physical Chemistry*, **1993**, 97(39), 10064–10069.

[168] X. Chen, M. L. Clarke, J. Wang and Z. Chen. Sum frequency generation vibrational spectroscopy studies on molecular conformation and orientation of biological molecules at interfaces. *International Journal of Modern Physics B*, **2005**, 19(04), 691–713.

[169] Q. Du, E. Freysz and Y. R. Shen. Vibrational spectra of water molecules at quartz/water interfaces. *Physical Review Letters*, **1994**, 72(2), 238.

[170] E. H. Backus, J. M. Kuiper, J. B. Engberts, B. Poolman and M. Bonn. Reversible Optical Control of Monolayers on Water through Photoswitchable Lipids. *The Journal of Physical Chemistry B*, **2011**, 115(10), 2294–2302. DOI: 10.1021/jp1113619.

[171] T. A. Darwish, Y. Tong, M. James, T. L. Hanley, Q. Peng and S. Ye. Characterizing the photoinduced switching process of a nitrospiropyran self-assembled monolayer using in situ sum frequency generation spectroscopy. *Langmuir*, **2012**, 28(39), 13852–13860.

[172] J. Kubota and K. Domen. Study of the dynamics of surface molecules by time-resolved sum-frequency generation spectroscopy. *Analytical and bioanalytical chemistry*, **2007**, 388(1), 17–27.

[173] Y. Rao, N. J. Turro and K. B. Eisenthal. Solvation dynamics at the air/water interface with time-resolved sum-frequency generation. *The Journal of Physical Chemistry C*, **2010**, 114(41), 17703–17708.

[174] K. B. Eisenthal. Equilibrium and dynamic processes at interfaces by second harmonic and sum frequency generation. *Annual Review of Physical Chemistry*, **1992**, 43(1), 627–661.

[175] X. Zhuang, P. Miranda, D. Kim and Y. Shen. Mapping molecular orientation and conformation at interfaces by surface nonlinear optics. *Physical Review B*, May , (19), 12632–12640. ISSN 0163-1829. DOI: 10.1103/PhysRevB.59.12632.

[176] H.-F. Wang, W. Gan, R. Lu, Y. Rao and B.-H. Wu. Quantitative spectral and orientational analysis in surface sum frequency generation vibrational spectroscopy (SFG-VS). *International Reviews in Physical Chemistry*, **2005**, 24(2), 191–256.

[177] M. Che and J. C. Védrine. Characterization of solid materials and heterogeneous catalysts: From structure to surface reactivity. John Wiley & Sons, **2012**.

[178] A. G. Lambert, P. B. Davies and D. J. Neivandt. Implementing the Theory of Sum Frequency Generation Vibrational Spectroscopy: A Tutorial Review. *Applied Spectroscopy Reviews*, May **2005**, 40(2), 103–145. ISSN 0570-4928. DOI: 10.1081/ASR-200038326. Webseite: http://www.tandfonline.com/doi/abs/10.1081/ASR-200038326.

[179] M. Levenson and N. Bloembergen. Dispersion of the nonlinear optical susceptibility tensor in centrosymmetric media. *Physical Review B*, **1974**, 10(10), 4447.

[180] C. Hirose, N. Akamatsu and K. Domen. Formulas for the analysis of surface sum-frequency generation spectrum by CH stretching modes of methyl and methylene groups. *The Journal of Chemical Physics*, (2), 997. ISSN 00219606. DOI: 10.1063/1.462120.

[181] E. A. Raymond, T. L. Tarbuck, M. G. Brown and G. L. Richmond. Hydrogen-bonding interactions at the vapor/water interface investigated by vibrational sum-frequency spectroscopy of HOD/H2O/D2O mixtures and molecular dynamics simulations. *The Journal of Physical Chemistry B*, **2003**, 107(2), 546–556.

[182] A. M. Kuznetsov and G. A. Tsirlina. W. Ronald FawcettLiquids, Solutions, and Interfaces. From Classical Macroscopic Descriptions to Modern Microscopic Details2004Oxford University Pressp. 621. *Journal of Electroanalytical Chemistry*, **2005**, 578(1), 183.

[183] R. Snyder, S. Hsu and S. Krimm. Vibrational spectra in the CH stretching region and the structure of the polymethylene chain. *Spectrochimica Acta Part A: Molecular Spectroscopy*, **1978**, 34(4), 395–406.

[184] Y. Shen. Optical second harmonic generation at interfaces. *Annual Review of Physical Chemistry*, **1989**, 40(1), 327–350.

[185] Z. Wang, J. Chen, S. Oyola-Reynoso and M. Thuo. The Porter-Whitesides Discrepancy: Revisiting Odd-Even Effects in Wetting Properties of n-Alkanethiolate SAMs. *Coatings*, **2015**, 5(4), 1034–1055.

[186] J. Kleber. VSFG-spektroskopische Untersuchungen von organischen Filmen und ihrer Oxidationskinetik an der Luft-Wasser-Grenzfläche. *Dissertation*, Christian-Albrechts Universität Kiel. **2015**.

[187] S. Z. Can, C. F. Chang and R. A. Walker. Spontaneous formation of DPPC monolayers at aqueous/vapor interfaces and the impact of charged surfactants. *Biochimica et Biophysica Acta (BBA)-Biomembranes*, **2008**, 1778(10), 2368–2377.

[188] C. Ohe, H. Kamijo, M. Arai, M. Adachi, H. Miyazawa, K. Itoh and T. Seki. Sum frequency generation spectroscopic study on photoinduced isomerization of poly (vinyl alcohol) containing azobenzene side chain at the air-water interface. *The Journal of Physical Chemistry C*, **2008**, 112(1), 172–181.

[189] N. Nishi, D. Hobara, M. Yamamoto and T. Kakiuchi. Chain-length-dependent change in the structure of self-assembled monolayers of n-alkanethiols on Au(111) probed by broad-bandwidth sum frequency generation spectroscopy. *The Journal of Chemical Physics*, (4), 1904. ISSN 00219606. DOI: 10.1063/1.1531098.

[190] M. A. Hines, J. Todd and P. Guyot-Sionnest. Conformation of alkanethiols on Au, Ag (111), and Pt (111) electrodes: A vibrational spectroscopy study. *Langmuir*, **1995**, 11 (2), 493–497.

[191] F. Tao and S. L. Bernasek. Understanding odd-even effects in organic self-assembled monolayers. *Chemical reviews*, May , (5), 1408–53. ISSN 0009-2665. DOI: 10.1021/cr050258d.

[192] Y. T. Tao, M. T. Lee and S. C. Chang. Effect of biphenyl and naphthyl groups on the structure of self-assembled monolayers: packing, orientation, and wetting properties. *Journal of the American Chemical Society*, **1993**, 115(21), 9547–9555.

[193] K. Cimatu, H. J. Moore, T. R. Lee and S. Baldelli. Sum frequency generation imaging of microcontact-printed monolayers derived from aliphatic dithiocarboxylic acids: Contrast based on terminal-group orientation. *The Journal of Physical Chemistry C*, **2007**, 111(32), 11751–11755.

[194] L. Richardson, A. Riegel and E. Naeemi. Preparation of an Azobenzene Thiol for Use as a Light Driven Molecular Pump. *Journal of Undergraduate Research in Bioengineering*, **2008-2010**.

[195] W. B. Caldwell, D. J. Campbell, K. Chen, B. R. Herr, C. A. Mirkin, A. Malik, M. Durbin, P. Dutta and K. Huang. A highly ordered self-assembled monolayer film of an azobenzenealkanethiol on Au (111): Electrochemical properties and structural characterization by synchrotron in-plane X-ray diffraction, atomic force microscopy, and surface-enhanced Raman spectroscopy. *Journal of the American Chemical Society*, **1995**, 117(22), 6071–6082.

[196] R. E. Holmlin, X. Chen, R. G. Chapman, S. Takayama and G. M. Whitesides. Zwitterionic SAMs that resist nonspecific adsorption of protein from aqueous buffer. *Langmuir*, **2001**, 17(9), 2841–2850.

[197] J.-W. Zou, W.-N. Zhao, Z.-C. Shang, M.-L. Huang, M. Guo and Q.-S. Yu. A quantitative structure-property relationship analysis of logP for disubstituted benzenes. *The Journal of Physical Chemistry A*, **2002**, 106(47), 11550–11557.

[198] K. Laβ, J. Kleber and G. Friedrichs. Vibrational sum-frequency generation as a probe for composition, chemical reactivity, and film formation dynamics of the sea surface nanolayer. *Limnology and Oceanography: Methods*, **2010**, 8(5), 216–228.

[199] M. Watry, M. Brown and G. Richmond. Probing molecular structure at liquid surfaces with vibrational sum frequency spectroscopy. *Applied Spectroscopy*, **2001**, 55(10), 321A–321A.

[200] G. Richmond. Molecular bonding and interactions at aqueous surfaces as probed by vibrational sum frequency spectroscopy. *Chemical Reviews*, **2002**, 102(8), 2693–2724.

[201] R. Ward, P. Davies and C. Bain. Orientation of surfactants adsorbed on a hydrophobic surface. *The Journal of Physical Chemistry*, **1993**, 97(28), 7141–7143.

[202] D. Zhang, S. Dougal and M. Yeganeh. Effects of UV irradiation and plasma treatment on a polystyrene surface studied by IR-visible sum frequency generation spectroscopy. *Langmuir*, **2000**, 16(10), 4528–4532.

[203] D. Qu, B.-C. Kim, C.-W. J. Lee, M. Ito, H. Noguchi and K. Uosaki. 1, 6-Hexanedithiol self-assembled monolayers on Au (111) investigated by electrochemical, spectroscopic, and molecular mechanics methods. *The Journal of Physical Chemistry C*, **2009**, 114 (1), 497–505.

[204] A. Opdahl and G. A. Somorjai. Solvent vapor induced ordering and disordering of phenyl side branches at the air/polystyrene interface studied by SFG. *Langmuir*, **2002**, 18(24), 9409–9412. ISSN 07437463. DOI: 10.1021/la020537l.

[205] E. L. Hommel and H. C. Allen. The air-liquid interface of benzene, toluene, m-xylene, and mesitylene: a sum frequency, Raman, and infrared spectroscopic study. *The Analyst*, **2003**, 128(6), 750–755. ISSN 0003-2654. DOI: 10.1039/b301032p.

[206] J. L. Achtyl, A. M. Buchbinder and F. M. Geiger. Hydrocarbon on Carbon: Coherent Vibrational Spectroscopy of Toluene on Graphite. *The Journal of Physical Chemistry Letters*, Feb. , (3), 280–282. ISSN 1948-7185. DOI: 10.1021/jz2016796.

[207] J. Kleber, K. Laβ and G. Friedrichs. Quantitative Time-Resolved Vibrational Sum Frequency Generation Spectroscopy as a Tool for Thin Film Kinetic Studies: New Insights into Oleic Acid Monolayer Oxidation. *The Journal of Physical Chemistry A*, **2013**, 117(33), 7863–7875. DOI: 10.1021/jp404087s. Webseite: http://dx.doi.org/10.1021/jp404087s.

[208] K. Gautam, A. D. Schwab, A. Dhinojwala, D. Zhang, S. Dougal and M. Yeganeh. Molecular structure of polystyrene at air/polymer and solid/polymer interfaces. *Physical review letters*, **2000**, 85(18), 3854.

[209] O. Berg and D. Klenerman. Vibrational spectroscopy of mechanically compressed monolayers. *Journal of the American Chemical Society*, **2003**, 125(18), 5493–5500.

[210] H.-T. Rong, S. Frey, Y.-J. Yang, M. Zharnikov, M. Buck, M. Wühn, C. Wöll and G. Helmchen. On the importance of the headgroup substrate bond in thiol monolayers: a study of biphenyl-based thiols on gold and silver. *Langmuir*, **2001**, 17(5), 1582–1593. DOI: 10.1021/la0014050.

[211] J. C. Conboy, M. C. Messmer and G. L. Richmond. Investigation of surfactant conformation and order at the liquid-liquid interface by total internal reflection sum-frequency vibrational spectroscopy. *The Journal of Physical Chemistry*, **1996**, 100 (18), 7617–7622. DOI: 10.1021/jp953616x.

[212] B. C. Smith. Infrared spectral interpretation: a systematic approach. CRC press, **1998**.

[213] N. J. Brewer and G. J. Leggett. Chemical force microscopy of mixed self-assembled monolayers of alkanethiols on gold: evidence for phase separation. *Langmuir*, **2004**, 20(10), 4109–4115.

[214] C. S. Yang, L. J. Richter, J. C. Stephenson and K. A. Briggman. In Situ , Vibrationally Resonant Sum Frequency Spectroscopy Study of the Self-Assembly of Dioctadecyl Disulfide on Gold. *Langmuir*, **2002**, 18(27), 7549–7556.

[215] R. Klajn. Immobilized azobenzenes for the construction of photoresponsive materials. *Pure and Applied Chemistry*, **2010**, 82(12), 2247–2279. ISSN 0033-4545. DOI: 10.1351/PAC-CON-10-09-04.

[216] K. Heister, D. Allara, K. Bahnck, S. Frey, M. Zharnikov and M. Grunze. Deviations from 1: 1 compositions in self-assembled monolayers formed from adsorption of asymmetric dialkyl disulfides on gold. *Langmuir*, **1999**, 15(17), 5440–5443.

[217] Y. Shen. A few selected applications of surface nonlinear optical spectroscopy. *Proceedings of the National Academy of Sciences*, **1996**, 93(22), 12104–12111.

[218] C. D. Bain. Sum-frequency vibrational spectroscopy of the solid/liquid interface. *Journal of the Chemical Society, Faraday Transactions*, **1995**, 91(9), 1281–1296.

[219] J. D. C. Jacob, S. Rittikulsittichai, T. R. Lee and S. Baldelli. Characterization of SAMs Derived from Octadecyloxyphenylethanethiols by Sum Frequency Generation. *The Journal of Physical Chemistry C*, **2013**, 117(18), 9355–9365.

[220] H. Fujiwara. Molecular stochastic process on gold surface observed in broadband-infrared, background-suppressed, sum frequency generation spectroscopy: picosecond heat transfer to self-assembled monolayers. *arXiv preprint arXiv:1405.6533*, **2014**.

[221] Y. Zhang, G. L. Barnes, T. Yan and W. L. Hase. Model non-equilibrium molecular dynamics simulations of heat transfer from a hot gold surface to an alkylthiolate self-assembled monolayer. *Physical Chemistry Chemical Physics*, **2010**, 12(17), 4435–4445.

[222] P. S. Weiss. Functional molecules and assemblies in controlled environments: Formation and measurements. *Accounts of Chemical Research*, **2008**, 41(12), 1772–1781. ISSN 00014842. DOI: 10.1021/ar8001443.

[223] A. S. Kumar, T. Ye, T. Takami, B. C. Yu, A. K. Flatt, J. M. Tour and P. S. Weiss. Reversible photo-switching of single azobenzene molecules in controlled nanoscale environments. *Nano Letters*, **2008**, 8, 1644–1648. ISSN 15306984. DOI: 10.1021/nl080323+.

[224] H. Hinterwirth, S. Kappel, T. Waitz, T. Prohaska, W. Lindner and M. Lammerhofer. Quantifying thiol ligand density of self-assembled monolayers on gold nanoparticles by inductively coupled plasma–mass spectrometry. *ACS nano*, **2013**, 7(2), 1129–1136.

[225] V. Chechik, H. Schönherr, G. J. Vancso and C. J. Stirling. Self-assembled monolayers of branched thiols and disulfides on gold: Surface coverage, order and chain orientation. *Langmuir*, **1998**, 14(11), 3003–3010.

[226] W. Azzam. Self-Assembled Monolayers on Gold Made from Organothiols Containing an Oligophenyl-Backbone. *Physical Chemistry I*, **2003**.

[227] G. Heimel, L. Romaner, J. L. Bredas and E. Zojer. Odd - Even Effects in Self-Assembled Monolayers of ω - (Biphenyl-4-yl) alkanethiols : A First-Principles Study. *Langmuir*, **2008**, 24(34), 474–482.

[228] H. S. Kato, J. Noh, M. Hara and M. Kawai. An HREELS study of alkanethiol self-assembled monolayers on Au (111). *The Journal of Physical Chemistry B*, **2002**, 106 (37), 9655–9658.

[229] A. Shaporenko, M. Brunnbauer, A. Terfort, L. Johansson, M. Grunze and M. Zharnikov. Odd-even effects in photoemission from terphenyl-substituted alkanethiolate self-assembled monolayers. *Langmuir*, **2005**, 21(10), 4370–4375.

[230] M. D. Porter, T. B. Bright, D. L. Allara and C. E. Chidsey. Spontaneously organized molecular assemblies. 4. Structural characterization of n-alkyl thiol monolayers on gold by optical ellipsometry, infrared spectroscopy, and electrochemistry. *Journal of the American Chemical Society*, **1987**, 109(12), 3559–3568.

[231] P. Fenter, A. Eberhardt, K. Liang and P. Eisenberger. Epitaxy and chainlength dependent strain in self-assembled monolayers. *The Journal of chemical physics*, **1997**, 106 (4), 1600–1608.

[232] W. Azzam, A. Bashir, A. Terfort, T. Strunskus and C. Wöll. Combined STM and FTIR characterization of terphenylalkanethiol monolayers on Au (111): Effect of alkyl chain length and deposition temperature. *Langmuir*, **2006**, 22(8), 3647–3655.

[233] A. Terfort. Preparation of self-assembled monolayer with photoswitchable properties . *Australian Journal of Chemistry*, **2010**, 63, 303–314. DOI: http://dx.doi.org/10.1071/CH09308.

[234] M.-H. Du, A. Kolchin and H.-P. Cheng. Hydrolysis of a two-membered silica ring on the amorphous silica surface. *The Journal of chemical physics*, **2004**, 120(2), 1044–1054. DOI: dx.doi.org/10.1063/1.1630026.

[235] I. Li, J. Bandara and M. J. Shultz. Time evolution studies of the H2O/quartz interface using sum frequency generation, atomic force microscopy, and molecular dynamics. *Langmuir*, **2004**, 20(24), 10474–10480. DOI: dx.doi.org/10.1021/la048639u.

[236] P. F. McMillan and R. L. Remmele. Hydroxyl sites in SiO_2 glass: A note on infrared and Raman spectra. *American Mineralogist*, **1986**, 71(5-6), 772–778.

[237] Q. Du, R. Superfine, E. Freysz and Y. Shen. Vibrational spectroscopy of water at the vapor/water interface. *Physical Review Letters*, **1993**, 70(15), 2313.

[238] Y. R. Shen and V. Ostroverkhov. Sum-frequency vibrational spectroscopy on water interfaces: Polar orientation of water molecules at interfaces. *Chemical Reviews*, **2006**, 106(4), 1140–1154.

[239] H. Kitano. Characterization of polymer materials based on structure analyses of vicinal water. *Polymer Journal*, **2016**, 48(1), 15–24.

[240] S. Ye, S. Nihonyanagi and K. Uosaki. Sum frequency generation SFG study of the pH-dependent water structure on a fused quartz surface modified by an octadecyltrichlorosilane (OTS) monolayer. *Physical Chemistry Chemical Physics*, **2001**, 3(16), 3463–3469.

[241] K.-U. Goss and R. P. Schwarzenbach. Adsorption of a diverse set of organic vapors on quartz, CaCO 3, and α-Al 2 O 3 at different relative humidities. *Journal of colloid and interface science*, **2002**, 252(1), 31–41.

[242] P. Galhotra. Carbon dioxide adsorption on nanomaterials. *University of Iowa*, **2010**.

[243] M. Sovago, R. K. Campen, H. J. Bakker and M. Bonn. Hydrogen bonding strength of interfacial water determined with surface sum-frequency generation. *Chemical Physics Letters*, **2009**, 470(1), 7–12. DOI: 10.1016/j.cplett.2009.01.009.

[244] M. Sovago, R. K. Campen, G. W. Wurpel, M. Müller, H. J. Bakker and M. Bonn. Vibrational response of hydrogen-bonded interfacial water is dominated by intramolecular coupling. *Physical review letters*, **2008**, 100(17), 173901.

[245] N. Colthup. Introduction to infrared and Raman spectroscopy. Elsevier, **2012**.

[246] D. Lin-Vien, N. B. Colthup, W. G. Fateley and J. G. Grasselli. The handbook of infrared and Raman characteristic frequencies of organic molecules. Elsevier, **1991**.

[247] Z. Zhang, Y. Guo, Z. Lu, L. Velarde and H.-f. Wang. Resolving Two Closely Overlapping- CN Vibrations and Structure in the Langmuir Monolayer of the Long-Chain Nonadecanenitrile by Polarization Sum Frequency Generation Vibrational Spectroscopy. *The Journal of Physical Chemistry C*, **2012**, 116(4), 2976–2987. DOI: 10.1021/jp210138s.

[248] V. Spectra. Orientations, and Phase Transitions in Long-Chain Amphiphiles at the Air/Water Interface: Probing the Head and Tail Groups by Sum Frequency Generation Zhang, D.; Gutow, J.; Eisenthal. *Journal of Physical Chemistry*, **1994**, 98(51), 13729–34.

[249] U. Jung, C. Schutt, O. Filinova, J. Kubitschke, R. Herges and O. Magnussen. Photoswitching of azobenzene-functionalized molecular platforms on Au surfaces. *The Journal of Physical Chemistry C*, **2012**, 116(49), 25943–25948.

[250] M. Bonn, S. Roke, O. Berg, L. B. Juurlink, A. Stamouli and M. Müller. A molecular view of cholesterol-induced condensation in a lipid monolayer. *The Journal of Physical Chemistry B*, **2004**, 108(50), 19083–19085. DOI: 10.1021/jp0452249.

[251] D. M. Kamiński, G. Czernel, B. Murphy, B. Runge, O. M. Magnussen and M. Gagoś. Effect of cholesterol and ergosterol on the antibiotic amphotericin B interactions with dipalmitoylphosphatidylcholine monolayers: X-ray reflectivity study. *Biochimica et Biophysica Acta (BBA)-Biomembranes*, **2014**, 1838(11), 2947–2953. DOI: 10.1016/j.bbamem.2014.08.004.

[252] B. M. Murphy, M. Greve, B. Runge, C. T. Koops, A. Elsen, J. Stettner, O. H. Seeck and O. M. Magnussen. A novel X-ray diffractometer for studies of liquid–liquid interfaces. *Journal of synchrotron radiation*, **2014**, 21(1), 45–56. DOI: 10.1107/S1600577513026192.

[253] H. Reinl, T. Brumm and T. M. Bayerl. Changes of the physical properties of the liquid-ordered phase with temperature in binary mixtures of DPPC with cholesterol: A 2H-NMR, FT-IR, DSC, and neutron scattering study. *Biophysical journal*, **1992**, 61 (4), 1025.

[254] C. Yuan and L. Johnston. Phase evolution in cholesterol/DPPC monolayers: atomic force microscopy and near field scanning optical microscopy studies. *Journal of microscopy*, **2002**, 205(2), 136–146. DOI: 10.1046/j.0022-2720.2001.00982.x.

[255] R. M. Weis and H. M. McConnell. Cholesterol stabilizes the crystal-liquid interface in phospholipid monolayers. *The Journal of Physical Chemistry*, **1985**, 89(21), 4453–4459. DOI: 10.1021/j100267a011.

[256] R. A. Walker, J. A. Gruetzmacher and G. L. Richmond. Phosphatidylcholine monolayer structure at a liquid-liquid interface. *Journal of the American Chemical Society*, **1998**, 120(28), 6991–7003.

[257] J. Liu and J. C. Conboy. Structure of a gel phase lipid bilayer prepared by the Langmuir-Blodgett/Langmuir-Schaefer method characterized by sum-frequency vibrational spectroscopy. *Langmuir*, **2005**, 21(20), 9091–9097.

[258] J. D. C. Jacob, S. Rittikulsittichai, T. R. Lee and S. Baldelli. Characterization of SAMs Derived from Octadecyloxyphenylethanethiols by Sum Frequency Generation. *The Journal of Physical Chemistry C*, May **2013**, 117(18), 9355–9365. ISSN 1932-7447. DOI: 10.1021/jp402311g. Webseite: http://pubs.acs.org/doi/abs/10.1021/jp402311g.

[259] T. M. Uehara, H. B. de Aguiar, K. Bergamaski and P. B. Miranda. Adsorption of Alkylthiol Self-Assembled Monolayers on Gold and the Effect of Substrate Roughness: A Comparative Study Using Scanning Tunneling Microscopy, Cyclic Voltammetry, Second-Harmonic Generation, and Sum-Frequency Generation. *The Journal of Physical Chemistry C*, **2014**, 118(35), 20374–20382.

[260] K. Klopfer and T. Vanderlick. Isotherms of dipalmitoylphosphatidylcholine (DPPC) monolayers: features revealed and features obscured. *Journal of colloid and interface science*, **1996**, 182(1), 220–229. DOI: 10.1006/jcis.1996.0454.

[261] C. Ohe, M. Arai, H. Kamijo, M. Adachi, H. Miyazawa, K. Itoh and T. Seki. Interaction between a liquid crystalline molecule (4'-pentyl-4-cyanobiphenyl) and a poly (vinyl alcohol) derivative containing an azobenzene group at the air-water interface: Sum frequency generation spectroscopic study. *The Journal of Physical Chemistry C*, **2008**, 112(16), 6359–6365. DOI: 10.1021/jp076223u.

[262] M. Velez, S. Mukhopadhyay, I. Muzikante, G. Matisova and S. Vieira. Atomic force microscopy studies of photoisomerization of an azobenzene derivative on Langmuir-Blodgett monolayers. *Langmuir*, **1997**, 13(4), 870–872.

[263] T. Seki, J.-y. Kojima and K. Ichimura. Light-driven dot films consisting of single polymer chain. *The Journal of Physical Chemistry B*, **1999**, 103(47), 10338–10340. DOI: 10.1021/jp992062l.

[264] T. Seki, J.-y. Kojima and K. Ichimura. Multifarious photoinduced morphologies in monomolecular films of azobenzene side chain polymer on mica. *Macromolecules*, **2000**, 33(7), 2709–2717. DOI: 10.1021/ma991439i.

[265] I. Kim, J. F. Rabolt and P. Stroeve. Dynamic monolayer behavior of a photo-responsive azobenzene surfactant. *Colloids and Surfaces A: Physicochemical and Engineering Aspects*, **2000**, 171(1), 167–174.